UNIVERSITY OF CALIFORNIA SAN DIEGO

Decoding a Tumor-suppressive Gatekeeper Function of Pro-oncogenic Ras/MAPK and NF-κB Pathways in the Liver

A dissertation submitted in partial satisfaction of the requirements for the degree
Doctor of Philosophy

in

Biology

by

Kaisa Leigh Hanley

Committee in Charge

Professor Gen-Sheng Feng, Chair
Professor David Cheresh
Professor Shannon Lauberth
Professor Lorraine Pillus
Professor Jean Wang

2020

The dissertation of Kaisa Leigh Hanley is approved, and it is acceptable in quality and form for publication on microfilm and electronically:

_____

_____

_____

_____

_____
Chair

University of California San Diego

2020

TABLE OF CONTENTS

LIST OF FIGURES

LIST OF SCHEMA

LIST OF TABLES

LIST OF ABBREVIATIONS

Aacs: acetoacetyl-CoA synthetase

ALT: alanine transaminase

AFP: alpha fetoprotein

ANOVA: analysis of variance

AST: aspartate transaminase

Akt: protein kinase B

BA: bile acid

Bmal1: brain and muscle ARNT-like

BHLHE40: basic helix-loop-helix family member E40/DEC1

BHLHE41: basic helix-loop-helix family member E41/DEC2

CCG: clock-controlled gene

CCL: chemokine ligand

CCR: chemokine receptor

Clock: circadian locomoter output cycles kaput

Cre: Cre recombinase

Cry: cryptochrome

Ct: cycle threshold

Dbp: D-Box binding PAR BZIP transcription factor

DEN: diethylnitrosamine

DKO: hepatocyte-specific Ikkβ and Shp2 double knockout

ERK: mitogen-activated protein kinase 1

Fabp1: fatty acid binding protein 1

FBS: fetal bovine serum

FGF: fibroblast growth factor

Gab1: Grb2-associated-binding protein

GAP: GTPase-activating protein

Gapdh: glyceraldehyde 3-phosphate dehydrogenase

GDP: guanosine diphosphate

GEF: guanine nucleotide exchange factor

GO: gene ontology

Gp130: glycoprotein 130

Grb2: growth factor receptor-bound protein 2

GSEA: gene set enrichment analysis

GTP: guanosine triphosphate

HCA: hepatocellular adenoma

HBSS: Hank's balanced salt solution

HCC: hepatocellular carcinoma

HEPES: 4-(2-hydroxyethyl)-1-piperazineethanesulfonic acid

HGF: hepatocyte growth factor

HNF: hepatocyte nuclear factor

IARC: International Agency for Research on Cancer

Igf2: insulin-like growth factor 2

IκB: I kappa B kinase

IKK: inhibitor of kappa-B kinase

IKO: hepatocyte-specific Ikkβ knockout

IL: interleukin

IRS-1: insulin receptor substrate 1

JMML: juvenile myelomonocytic leukemia

Jnk: cJun N-terminal kinase

KO: knockout

MAPK: mitogen-activated protein kinase

MEK: mitogen-activated protein kinase kinase 1

Mdr2: multidrug resistance 2/Abcb4

NAFLD: non-alcoholic fatty liver disease

NASH: non-alcoholic steatohepatitis

NF-κB: nuclear factor kappa-B

NPC: nonparenchymal cell

PBS: phosphate-buffered saline

PDGF: platelet-derived growth factor

Per: period

PI3K: phosphatidylinositol 3-kinase

PLC: phospholipase C

Pten: phosphatase and tensin homolog

Ptpn11: tyrosine-protein phosphatase non-receptor type 11/Shp2

RTK: receptor tyrosine kinase

SCN: suprachiasmatic nucleus

SD: standard deviation

SDS-PAGE: sodium dodecyl sulfate-polyacrylamide gel electrophoresis

SFK: Src family kinase

SH2: Src homology region 2

Shp2: Src homology region 2 domain-containing phosphatase-2

SKO: hepatocyte-specific Shp2 knockout

Sos: son of sevenless

STAT: signal transducer and activator of transcription

TCGA: The Cancer Genome Atlas

TNF: tumor necrosis factor

VEGFR: vascular endothelial growth factor receptor

WT: wild type

ZT: Zeitgeiber time

ACKNOWLEDGEMENTS

This work was guided from its conception by my advisor, Dr. Gen-Sheng Feng. I am immensely grateful for his support throughout my doctoral training, and his dedication to furthering my professional development and scientific thinking. It has been an honor to learn from such a creative and rigorous scientist.

Sincere thanks to my committee members, who have helped challenge and refine my ideas throughout my predoctoral career. Drs. Jean Wang, David Cheresh, Shannon Lauberth, and Lorraine Pillus have provided many hours of stimulating discussion and debate, and have helped focus the scope of this project.

My path towards graduate studies were guided by exceptional undergraduate mentors: Dr. James Doohan and Blake Barron from Santa Barbara City College, and Dr. John Lew from University of California, Santa Barbara. They nurtured my love of biology and provided incredible opportunities for learning and development.

Throughout course of my doctoral studies, I have been sustained by the love and support of so many friends and family. My parents, Bruce and Mary Ann, have given a lifetime of love and encouragement; they and my brother Max have been my most unwavering cheerleaders for my nerdiest pursuits, and continue to be irrationally proud of me even (especially) when I struggle. My husband, Alberto Carreno, has been a weird and wonderful companion as we've both journeyed through graduate school. I owe him infinite gratitude for reminding me to eat, for tolerating the inevitable sleep disruptions intrinsic to circadian experiments, and for providing perspective and balance during the most difficult phases of this project. My cherished friends and fellow students Hannah Grunwald and Eileen Moreno have

been my emotional support humans and scientific sounding boards. Robin Carpenter has kept us all well-fed and as sane as can be reasonably expected. Other mammalian support came from Charlie, my beloved jogging partner and fellow mouse enthusiast.

Funding and training opportunities were provided by the NIH Cellular and Molecular Genetics Training Grant, as well as an individual Ruth L. Kirschstein individual predoctoral fellowship.

Chapters 1 and 2 are adapted from material that has been submitted for publication: Hanley, Kaisa L.; Lin, Xiaoxue; Liang, Yan; Yang, Meixiang; Karin, Michael; Fu, Wenxian; and Feng, Gen-Sheng. “Concurrent Disruption of Ras/MAPK and NF-kB Pathways Induces Circadian Deregulation and Hepatocarcinogenesis”. The dissertation author was the primary investigator and author of this paper.

VITA

2010 Tutor and grader, Santa Barbara City College

2010-2011 Research Assistant, Santa Barbara City College

2012-2013 Research Assistant, University of California Santa Barbara

2013 Bachelor of Sciences, University of California Santa Barbara

2015-2018 Instructional Assistant, University of California San Diego

2014-2020 Graduate Student Researcher, University of California San Diego

2020 Doctor of Philosophy, University of California San Diego

PUBLICATIONS

Hanley, K.L. and Feng, G.S. A new VETC in hepatocellular carcinoma metastasis. *Hepatology* **62(2)**:343-5(2015).

Luo, X., Liao, R., **Hanley, K.L**., Zhu, H.H., Malo, K.N., Hernandez, C., Wei, X., Varki, N.M., Alderson, N., Chu, C., Li, S., Fan, J., Loomba, R., Qiu, S., and Feng, G.S. Dual Shp2 and Pten Deficiencies Promote Non-alcoholic Steatohepatitis and Genesis of Liver Tumor-Initiating Cells. *Cell Reports* **17,** 2979–2993 (2016).

Feng, G. S., **Hanley, K. L**., Liang, Y., & Lin, X. Improving the Efficacy of Liver Cancer Immunotherapy: the Power of Combined Preclinical and Clinical Studies. *Hepatology* doi:10.1002/hep.31479 (2020).

Hanley, K. L.; Lin, X.; Liang, Y.; Yang, M.; Karin, M.; Fu, W.; and Feng, G. S. Concurrent Disruption of Ras/MAPK and NF-κB Pathways Induces Circadian Deregulation and Hepatocarcinogenesis. *Submitted* (2020).

FIELD OF STUDY

Major Field: Biological Sciences

Studies in Molecular Biology

Professor Gen-Sheng Feng

ABSTRACT OF THE DISSERTATION

Decoding a Tumor-suppressive Gatekeeper Function of Pro-oncogenic Ras/MAPK and NF-κB Pathways in the Liver

by

Kaisa Leigh Hanley

Doctor of Philosophy in Biology

University of California San Diego, 2020

Professor Gen-Sheng Feng, Chair

Despite ever-rising mortality due to hepatocellular carcinoma (HCC), efforts to identify effective chemotherapeutics have languished. A major source of this difficulty may be the underappreciated complexity of oncogenic signaling mechanisms that drive liver tumorigenesis. The Ras/ERK and NF-κB pathways have received extensive attention in the cell signaling and cancer research fields in the past few decades. These pathways play critical roles in cell survival and proliferation, and have been demonstrated to drive oncogenesis when excessively or constitutively activated. However, studies in animal models have revealed tumor-suppressive functions in the liver, as deleting Shp2 or Ikkβ in hepatocytes, which promote

Ras/ERK and NF-κB signaling, respectively, ironically aggravated HCC development induced by the chemical carcinogen diethylnitrosamine (DEN). Since parallel pathways might work antagonistically or cooperatively, our lab has been interested in taking a genetic approach to generate compound mutant mouse lines, which often yield unanticipated results and provide a fresh view on pathway cross-talk. The goal of my dissertation work was to dissect molecular and cellular mechanisms of hepatocarcinogenesis by creating a mutant mouse model with both Shp2 and Ikkβ deleted in hepatocytes. This allowed us to examine the functional interaction of these pathways in stressed and unstressed livers. My experimental results showed that dual Shp2 and Ikkβ deletion (DKO) dramatically accelerated DEN-induced tumorigenesis in the liver compared to either single knockout, evidently due to more extensive liver damages and metabolic disorders. More surprisingly, this dual deletion resulted in spontaneous development of HCC. Although multiple hepatic factors contributed to the pathogenic process, Shp2- and Ikkβ- deficient hepatocytes were characterized by disrupted expression of circadian clock genes. Circadian disruption has been linked to liver tumorigenesis in humans and in mice, suggesting a mechanism underlying spontaneous hepatocarcinogenesis in the DKO livers. In support of this mechanism, human HCCs with dysregulated circadian gene expression displayed downregulation of Ras/ERK and NF-κB signaling and poor prognosis. These data indicate that the ground state of the two central signaling pathways, previously known to mediate proliferative and oncogenic signaling, sustains tumor suppressive circadian homeostasis in the mammalian liver. Disruption of this signaling network results in spontaneous hepatocarcinogenesis.

Introduction

Natural history and treatment of hepatocellular carcinoma

Hepatocellular carcinoma (HCC), the most common form of liver cancer, is a rising cause of cancer mortality worldwide (Stewart and Wild, 2014). Globally, HCC is the fourth leading cause of cancer mortality in both sexes, and the second leading cause of cancer deaths for men (Bray et al., 2018). While the most common etiologies of HCC remain chronic Hepatitis B and C viral infection, obesity-related liver diseases such as non-alcoholic steatohepatitis (NASH) and its more advanced form, nonalcoholic fatty liver disease (NAFLD), are becoming an increasingly prevalent risk factor (Kulik and El-Serag, 2019). Other sources of liver damage, such as environmental hepatotoxins like aflatoxin, and excessive alcohol consumption, also substantially elevate risk of developing HCC (Stewart and Wild, 2014). The vast majority of HCC cases develop in a background of progressive liver injury caused by the aforementioned factors, with most cases occurring in patients with cirrhosis (Kulik and El-Serag, 2019). While resection and ablative treatments such as chemo- or radio-embolization remain the favored intervention at early stages, the severity of underlying liver disease and advanced tumor stage at time of diagnosis can preclude these treatment options. In advanced HCC patients, chemotherapeutic approaches must be used; however, very few drugs have shown clinical efficacy in treating nonresectable HCC. Of these, the standard-of-care multi-kinase inhibitor Sorafenib only offers a few months increased survival (Llovet et al., 2008). Recently, the

receptor tyrosine kinase (RTK) inhibitor Regorafenib was FDA-approved to treat advanced HCC, but it also provides very modest survival benefit (Bruix et al., 2017).

The limited therapeutic benefit of the multi-kinase inhibitors, which block the classic carcinogenic Raf and VEGFR signaling, underscores the complexity of signaling underlying liver tumorigenesis (Feng, 2012). Indeed, large scale genomic and molecular analyses of HCC specimens suggest the involvement of a heterogenous collection of tumor initiating oncogenic pathways (Ally et al., 2017; Zucman-Rossi et al., 2015). It is clear that development of effective HCC treatments will require a more thorough and comprehensive understanding of the molecular mechanisms in liver tumorigenesis.

Shp2 and Ras/MAPK signaling in cancer

Signaling from receptor tyrosine kinases to activate the Ras/MAPK cascade has long been implicated in carcinogenesis. Ras mutants were some of the first identified proto-oncogenes: the transforming viruses Harvey mutant sarcoma virus and Kirsten mutant sarcoma virus, first described in the 1960s, were later found to harbor *HRAS* and *KRAS*, respectively (Cox and Der, 2010). Ras mutations exert their oncogenic effects by enhancing signaling from receptor tyrosine kinases to hyperactivate the Raf/MAP kinase cascade.

Upon ligand binding to receptor tyrosine kinases, autophosphorylation and induces recruitment of factors such as phosphoinositide 3-kiase (PI3K), phospholipase Cγ (PLCγ), and Grb2, which bind phosphotyrosine motifs via their SH2 domains (Gu and Neel, 2003; Koch et al., 1991; Pawson, 1995). These SH2-

containing partners tether molecules such as the Ras-GEF Sos in proximity to Ras, increasing Ras activity. Ras guanine nucleotide exchange factors (GEFs) stimulate release of GDP; Ras then binds GTP, which causes it to adopt its active conformation. Ras's intrinsic GTPase activity is stimulated by GTPase-activating proteins (GAPs); hydrolysis of GTP to GDP returns Ras to its inactive conformation (Bos et al., 2007). Active Ras initiates the Raf/MAPK kinase cascade. The culmination of this cascade yields activated ERK, whose myriad targets effect such processes as cell survival and proliferation, differentiation, and migration, among others (Dhillon et al., 2007). In parallel to, and also highly interactive with, the Ras pathway is the PI3K/Akt pathway, which is highly implicated in cell proliferation and tumorigenesis.

The three Ras oncogenes constitute the most frequently mutated gene family in human cancer (Karnoub and Weinberg, 2008; Papke and Der, 2017; Simanshu, Dhirendra K., Nissley, Dwight. V., McCormick, 2017). Ras mutations are particularly common in certain cancers: 60% of pancreatic ductal adenocarcinomas and over 30% of large intestinal tumors and biliary tract malignancies harbor KRas mutations (Karnoub and Weinberg, 2008). In addition to the high mutation rate detected in established tumors, RASopathies represent a group of developmental disorders driven by aberrant Ras/MAPK signaling (Simanshu, Dhirendra K., Nissley, Dwight. V., McCormick, 2017) that are frequently associated with increased risk of cancer.

Shp2 is an SH2-containing cytoplasmic tyrosine phosphatase encoded by *Ptpn11* that promotes signaling from receptor tyrosine kinases to the Ras/MAPK pathway (Chan and Feng, 2007; Qu et al., 1999). Shp2 maintains an autoinhibitory

conformation until it interacts with phosphorylated binding partners. Upon binding to phosphotyrosine motifs on upstream signaling components such as Gab1 and IRS-1 via its SH2 domain, Shp2 adopts an active conformation (Cunnick et al., 2001). This association and activation at RTKs promotes downstream signaling.

Several mechanisms have been suggested to explain Shp2's ability to promote Ras/MAPK activation (Dance et al., 2008). Shp2 has been reported to dephosphorylate Gab1, which disrupts Gab1-RasGAP interactions and thereby enhances Ras activity (Montagner et al., 2005). Consistent with this, membrane-associated RasGAP levels were elevated in Shp2-deficient proliferating hepatocytes, and this localization was Gab1-dependent (Bard-Chapeau et al., 2006). It has also been implicated in regulation of Sprouty, which had been previously identified as a negative regulator of RTK signaling. Tyrosine phosphorylation of Sprouty prevented Shp2-Grb2-Sos binding and suppressed ERK activation in response to FGF (Hanafusa et al., 2002); it was later shown that Shp2 could dephosphorylate Sprouty and restore ERK activation (Hanafusa et al., 2004). Another view is that Shp2 acts as a scaffolding protein to recruit Grb2-Sos into proximity to the receptor (Bennett et al., 1994). However, this model was challenged by the finding that Shp2 mutants that retained Grb2 binding were unable to activate ERK (Araki et al., 2003). Another Ras-regulatory role for Shp2 was reported involving Src family kinases (SFKs), which themselves promote Ras pathway activity; decreased SFK activation was found in Shp2-deficient cells, and was accompanied by decreased MAPK phosphorylation (Furcht et al., 2015). Interestingly, Src family kinases have themselves been implicating in modulating RTK signal strength by sequestering Shp2/Gab1 complexes

away from RTKs (Furcht et al., 2015). More recently, Shp2 was reported to directly bind and dephosphorylate Ras in glioblastoma cells (Bunda et al., 2015). Through any of these mechanisms, it is clear that Shp2 is an important promoter of Ras/MAPK activity.

Consistent with this activity, Shp2 was the first tyrosine phosphatase identified as an oncogene. Dominant active mutations in PTPN11/Shp2 led to upregulated Ras/MAPK signaling in inherited Noonan syndrome patients; among the other developmental manifestations of Noonan syndrome, these patients have elevated risk of developing juvenile myelomonocytic leukemia (JMML) (Chan and Feng, 2007; Tartaglia et al., 2001). Subsequent analysis of juvenile myeloproliferative disorders identified gain-of-function Shp2 mutations in JMML, myelodysplastic syndrome, and acute myeloid leukemia (Tartaglia et al., 2003). Shp2 overexpession or overactivation has also been detected in adult leukemias and solid tumors (Bunda et al., 2015).

However, other signaling roles for Shp2 complicate its image as a tumor-promoter. Shp2 also regulates activation of STAT3 in response to IL-6 via the gp130 receptor (Ohtani et al., 2000). Shp2 and STAT3 were found to have opposing roles in mediating signaling from the receptor gp130, with prevention of Shp2 binding effectively blocking ERK activation, but enhancing STAT3 phosphorylation (Ohtani et al., 2000). STAT3 signaling is generally considered tumor-promoting due to its role in promoting sustained inflammation (He and Karin, 2011). Indeed, deletion of STAT3 from hepatocytes reduced chemically-induced tumor formation in mice (He et al., 2010), as well as ameliorating tumor burden in Shp2-deficient DEN-induced HCCs (Bard-Chapeau et al., 2011). In colorectal cancer, Shp2 levels and STAT3

phosphorylation and nuclear localization were inversely correlated, with higher Shp2 levels associated with better prognosis (Huang et al., 2017). Therefore, Shp2 activity may also exert a tumor-suppressive function at least in part by preventing overactivation of STAT3.

Despite this involvement in potentially tumor-suppressive signaling, its clear role in promoting Ras/MAPK signals has spurred active pursuit of Shp2 inhibition as a new cancer chemotherapy. Recently, Shp2 inhibitors were demonstrated to effectively curb the growth of RTK-driven cancer cells and xenografts, and concurrent inhibition of Shp2 and other components in the Ras pathway was shown to be better than monotherapy in a variety of solid tumors (Ahmed et al., 2019; Lamarche et al., 2016; Ruess et al., 2018). These preclinical results have generated substantial enthusiasm in pursuing Shp2 as a pharmaceutical target for inhibition of RTK-driven tumors, with several clinical trials ongoing.

NF-κB signaling in cancer

Since its identification as an immune-regulatory transcription factor in 1986 (Sen and Baltimore, 1986), innumerable studies have identified a wide range of functions for nuclear factor kappa-B (NF-κB) signaling (Hayden and Ghosh, 2012). The NF-κB family consists of five DNA-binding proteins (RelA, RelB, c-Rel, NF-κB1, NF-κB2) in homo- or heterodimers (Taniguchi and Karin, 2018). NF-κB1 and NF-κB2 are produced as precursors, which must be processed to become active. In the absence of a stimulus, the inactive dimers are retained in the cytoplasm by binding to the IκB inhibitor. In canonical NF-κB signaling, activation via Toll-like receptors, T-cell

receptors, and TNF receptor, among others, initiates a series of events that liberate these dimers. The catalytic subunits Ikkα and Ikkβ, and the regulatory subunit Ikkγ/NEMO make up the inhibitor of IκB kinase (IKK) complex, which mediates phosphorylation and degradation of IκB, leading to nuclear translocation and activation of NF-κB dimers (Liu et al., 2017; Vallabhapurapu and Karin, 2009). The variety of IκB regulatory subunits, and of NF-κB dimer combinations, allow for highly context-specific regulation and output (Hayden and Ghosh, 2012). Additionally, noncanonical NF-κB signaling can occur in response to ligands including CD40L. Noncanonical NF-κB activation occurs via the NF-κB inducing kinase (NIK), which activates Ikkα and promotes p100 processing to its active form; this bypasses the need for IκB degradation (Sun, 2012; Vallabhapurapu and Karin, 2009), This complex system of regulation allows for a diversity of context-specific outputs. NF-κB target genes include mediators of such diverse processes as immunity, inflammation, cellular proliferation, and resistance to apoptosis.

Since Virchow's renowned observations, which linked inflammation and cancer as early as 1863, and the subsequent characterization of cancer as "the wound that does not heal", inflammation has consistently been implicated in the process of tumor formation (Dvorak, 1986). As an important mediator of inflammatory processes, NF-κB signaling has been a topic of great interest in cancer research. Overactivation of NF-κB leads to pleiotropic oncogenic processes (Taniguchi and Karin, 2018), including prolonged inflammation, escape from apoptosis, cancer cell proliferation, and epithelial-to-mesenchymal transition. Consistent with its role in promoting most of the hallmarks of cancer (Hanahan and Weinberg, 2011, 2000),

NF-κB is constitutively active in many types of cancer (Taniguchi and Karin, 2018). In particular, higher levels of NF-κB activity has been reported in many types of inflammation-related cancers, such as lung cancer (Tang et al., 2006), pancreatic ductal adenocarcinoma (Wang et al., 1999), and colorectal cancer (Slattery et al., 2018).

The association between NF-κB signaling and cancer has been further reinforced by numerous mouse models of cancer. In keeping with its well-established oncogenic role, disrupting the pathway has been shown to suppress tumor progression in a mouse HCC model (Pikarsky et al., 2004). In a colitis-associated colorectal cancer model, deletion of Ikkβ from intestinal epithelial cells and myeloid cells reduced tumor number and size, respectively, suggesting cell-type specific roles of NF-κB in promoting tumor initiation and progression (Greten et al., 2004). In a mouse model of progressive lung metastases, inflammation-driven tumor progression was reversed by inhibition of NF-κB in tumor cells using an IκB super-repressor (Luo et al., 2004). Growth of lung adenocarcinomas driven by mutant KRas and loss of p53 were effectively slowed by NF-κB inhibition, even when such inhibition was initiated in established tumors (Meylan et al., 2009).

In addition to its direct role in promoting carcinogenesis, as evidenced by the animal models and human data, NF-κB signaling has been reported to interact with other cancer-implicated pathways, including MAPK, Wnt/β-catenin, STAT3, and p53 (Hoesel and Schmid, 2013; Taniguchi and Karin, 2018). Due to its roles in mediating many of the hallmarks of cancer, NF-κB is an attractive target for cancer therapeutics, particularly in combinatorial approaches. However, due to the cell-type-

and context-specific activities of this pathway, and the difficulty in identifying sufficiently specific inhibitors, this is a challenging task that will require careful assessment of specific microenvironmental and tumor-intrinsic features to avoid unintended negative effects.

Tumor-suppressive roles of oncogenes in the liver

Despite the well-documented roles of Ras/MAPK and NF-κB pathways in carcinogenesis, mouse models have surprisingly revealed that inhibiting the individual pathway in hepatocytes has shown a tumor-promoting effect in the liver (Bard-Chapeau et al., 2011; Feng, 2012; Maeda et al., 2005). Ablating either Shp2 or Ikkβ in hepatocytes unexpectedly aggravates HCC development induced by a chemical carcinogen (Bard-Chapeau et al., 2011; Maeda et al., 2005). Several other pro-oncogenic molecules have also been found to protect against liver cancer (Feng, 2012), including β-catenin (Zhang et al., 2010), Jnk (Das et al., 2011) and Akt (Wang et al., 2016). A general mechanism has been proposed in which loss of growth and survival signaling causes chronic hepatic damage, creating prolonged inflammatory signaling and spurring compensatory proliferation of hepatocytes, which eventually enhances HCC development (Feng, 2012). While the precise mechanisms of these surprising phenotypes are still being elucidated, both hepatocyte-intrinsic processes and microenvironmental causes must be considered. Specifically, enhanced tumorigenesis could be due to forced upregulation of a parallel pathway upon suppressing one oncogenic pathway and/or generation of tumor-promoting microenvironment due to increased hepatic damages and inflammation. The use of

mouse models has begun to unravel the mechanisms of tumorigenesis enhanced by deletion of these erstwhile oncogenes. Further, compound mutant models have provided key insight into the functional interactions between oncogenic pathways in the liver.

Mechanistic insights from mouse models of HCC

After the surprising identification of multiple oncogenic pathways exhibiting tumor suppressive roles in the liver, compound mutant mouse models have been utilized to dissect the molecular and pathological mechanisms of these unexpected tumorigenic phenotypes. Recent work from our lab demonstrated an interesting cooperativity of Shp2 with the classic tumor suppressor Pten, where deletion of both Shp2 and Pten aggravated development of non-alcoholic steatohepatitis (NASH) and liver cancer (Luo et al., 2016). This stands in contrast to the neutralizing interaction of Shp2 and Pten knockouts in myeloproliferation and leukemogenesis (Zhu et al., 2015). In a different pattern of interaction, while deletion of either Shp2 or Stat3 alone enhanced DEN-induced HCC, additional deletion of Stat3 in Shp2-deficient hepatocytes partially neutralized the tumor-promoting effect (Bard-Chapeau et al., 2011). While Shp2-knockout livers are more susceptible to Myc-induced HCC (Liu et al., 2018), the additional deletion of β-catenin, itself tumor-promoting in the DEN model (Zhang et al., 2010), also prevented Myc-driven hepatocarcinogenesis in Shp2-deficient livers (unpublished data).

Likewise, overactivation of NF-κB is usually considered to mediate myriad oncogenic processes (Taniguchi and Karin, 2018), including cell survival, growth, and

inflammation. In contrast to this well-documented tumor-promoting role, suppression of NF-κB via ablation of IKKβ from otherwise WT hepatocytes was previously shown to enhance DEN-induced HCC, and to enhance the growth of established HCC cells (He et al., 2010; Koch et al., 2009; Maeda et al., 2005). However, the role of NF-κB signaling in other HCC models has been ambiguous. Although hepatocyte-specific loss of NF-κB signaling has been demonstrated to cause apoptosis of transformed hepatocytes and inhibit HCC formation, it did not affect early hepatocyte transformation and was actually required for tumor progression in one Mdr2-KO model (Pikarsky et al., 2004). In another report, Ikkβ deletion in a different strain of Mdr2-deficient mice exacerbated cholestatic liver damage and caused liver failure without inducing tumorigenesis (Ehlken et al., 2011). While Ikkα and Ikkβ exhibited redundant roles in protecting against LPS-induced liver injury, combined deletion of Ikkα and Ikkβ in liver parenchymal cells (hepatocytes and hepatic biliary cells), unexpectedly caused severe biliary disease, seemingly due to an Ikkα-specific role in maintaining the integrity of the biliary epithelial barrier (Luedde et al., 2008). Additionally, in contrast to the relatively mild phenotypes of Ikkβ deletion (Maeda et al., 2005), ablation of Ikkγ/NEMO in liver parenchymal cells induced steatosis and spontaneous HCC (Luedde et al., 2007). Clearly, the role of NF-κB in cholestatic/inflammation-induced HCCs and in liver damage in general is highly context-specific, and may depend on multiple factors, including the precise nature of liver damage, both canonical and non-canonical activities of various NF-κB components, the cell types in which NF-κB activity is altered, and the degree of NF-κB pathway inhibition.

Circadian clock in homeostasis and cancer

Circadian rhythms of gene expression control the timing of activity level, food intake, metabolism, and a variety of other physiological processes. Feedback loops of both transcriptional and translational control maintain rhythmic expression of clock genes and their targets: the core mammalian clock consists of the effectors Clock and Bmal, which drive expression of various target genes as well as their own repressors. These proteins, consisting of Period and Cryptochrome family members (Per1, 2, 3, and Cry 1,2), then repress the activity of Clock and Bmal, thereby suppressing their own transcription (Takahashi, 2017). Additional complexity in clock regulation comes from further interlocking feedback loops. The nuclear receptors and transcriptional repressors REV-ERBα and β also inhibit Clock/Bmal activity, and are themselves target genes of these clock effectors (Takahashi, 2017). Clock/Bmal target genes BHLHE40/DEC1 and BHLHE41/DEC2 form an additional feedback loop by inhibiting Clock/Bmal transcriptional activity, thus preventing their own expression; they can also repress Per expression (Kawamoto et al., 2004). This pattern of feedback creates robust oscillations of both clock genes and clock-controlled processes. Clock-controlled genes (CCGs) therefore exhibit periodic expression, with timing and amplitude controlled by Zeitgeibers (“time-givers”) such as light exposure, feeding, and physical activity. CCGs vary based on tissue type, but include genes implicated in locomotor activity, neurotransmitters, multiple metabolic pathways, and genes controlling cellular proliferation (Matsuo et al., 2003; Miller et al., 2007; Panda et al., 2002). Thus, among other functions, the circadian clock gates cell cycle progression, and clock disruption can produce uncontrolled proliferation. While the

“central pacemaker” for the circadian clock resides in the suprachiasmatic nucleus (SCN) of the brain, peripheral organs also experience rhythmic gene expression patterns, which can be independent, both in timing and in the identity of genes under circadian control, of the central clock (Panda et al., 2002).

The liver is one such organ with a peripheral clock. Multiple metabolic processes in the liver exhibit circadian activity patterns, including metabolism of glucose, fatty acids, cholesterol, bile acids, and xenobiotics (Tahara and Shibata, 2016). Some inflammatory and coagulation processes also appear to be under circadian control (Panda et al., 2002). Disruption of the circadian clock by ablation of Per1 and Per2 in mouse models caused elevated bile acid synthesis and cholestasis (Ma et al., 2009). Clock disruption has also been linked to steatosis (Marbach-Breitrück et al., 2019) in mouse models, further evidence of crosstalk between metabolic processes and circadian clock function.

Epidemiological studies have shown correlation between chronic circadian disruption and increased cancer risk, such as elevated levels of breast and prostate cancers in shift workers (Masri and Sassone-Corsi, 2018). Studies in cell lines and mice have further cemented this link; in a breast cancer model, chronic jet lag accelerated primary tumor formation and metastasis (Van Dycke et al., 2015; Hadadi et al., 2020). It was demonstrated that chronic jet lag accelerated formation of pancreatic cancer, ovarian cancer, lymphoma, and HCC in mice, as did genetic disruption of either Per1 and Per2, Cry1 and Cry2, or Bmal1 (Kettner et al., 2016). Although the mechanistic link between clock disruption and cancer remains an open

area of investigation, it is clear that the circadian clock holds an important tumor-suppressive role in many tissues.

The objective and experimental design of the dissertation project

The unexpected findings that blockade of individual classical oncogenic pathways in hepatocytes ironically promoted chemical carcinogenesis have prompted our laboratory to further explore the mechanisms behind these newly disclosed tumor-suppressive functions. It is interesting to note that, although each and every specific pathway has been extensively interrogated using multiple experimental approaches, how these pathways cross-talk and intertwine is poorly understood. One experimental approach to address this issue is to generate and characterize compound mutant mouse lines with two or more pathways deleted simultaneously. The findings from this elegant genetic approach make it clear that the outcomes of signaling interactions, particularly in liver cancer, cannot be simply predicted based on the results of individual pathway disruptions. They often suggest cell type-specific interactions of parallel signaling pathways in different tissues and organs in health and disease conditions. Therefore, characterization of compound mutant mice could reveal new functions and mechanisms of these “well-characterized” pathways, which could not otherwise be disclosed by dissecting individual pathways separately.

Given these considerations and based on previous data from this laboratory on dissecting the roles of Shp2 in liver tumorigenesis in mouse models, the goal of my PhD dissertation project was to determine the functional interaction of two classically oncogenic pathways in the liver, both in response to exogenous stressors

and at physiological steady-state. Based on the conflicting roles of NF-κB signaling in different models of liver damage and carcinogenesis, the question that I asked was how loss of Ikkβ in the Shp2-deficient liver, which develops relatively mild inflammation and cholestasis, would affect liver health. Another major goal was determining whether hepatocytes lacking both Ras/MAPK and NF-κB activity would be able to undergo compensatory proliferation and eventually form HCCs, given that multiple growth and survival pathways were disrupted.

For this purpose, I utilized the Albumin-Cre system to specifically remove floxed alleles of Shp2 and Ikkβ in the hepatocytes of mice. I then assessed the rates of tumorigenesis in the double-knockout (DKO) mice compared to each single knockout, and to wild-type mice, in a chemical carcinogen-induced model of hepatocellular carcinoma. I also examined the functional interaction of these pathways at physiological steady-state, without any exogenous injury or mutagen. I assessed several parameters of liver health in the knockout mice and performed transcriptomic analyses to identify further processes disrupted in the double knockout livers. Following the observations of enhanced tumor formation in double-knockout mice in the chemical carcinogenesis model, I also monitored the untreated cohort long-term to assess spontaneous tumorigenesis. This exploratory approach has unexpectedly disclosed a baseline function of Ras/MAPK and NF-κB in control of homeostasis in mammals. I report here that these two pathways work in concert to maintain multiple aspects of liver homeostasis. A particularly striking outcome of blocking basal Ras-ERK and NF-κB signaling is circadian clock dysregulation

followed by spontaneous HCC development. These findings reveal a new level of complexity in oncogenic signaling networks.

Materials and Methods

Mice

C57BL/6 mice were maintained in 12h light/dark cycles with standard chow and water *ad libitum.* Mice with hepatocyte-specific Shp2 deletion (Alb-Cre;$Shp2^{f/f}$, SKO) and were previously generated by G.S.F's group. $Ikk\beta^{f/f}$ (IKO) mice were previously generated by Michael Karin's group at UCSD. These lines were crossed to generate double-knockout mice (DKO, Alb-Cre;$Ikk\beta^{f/f}$;$Shp2^{f/f}$). Mice lacking the Alb-Cre transgene were used as wild-type controls (WT). All mouse husbandry and procedures were performed in compliance with protocols approved by the UCSD Institutional Animal Care and Use Committee (protocol S09108).

Genotyping was performed by PCR analysis of genomic DNA extracted from tail snips using the following primers (5'-3') to detect the presence of the transgene (Cre) or differences in length between wild-type and floxed alleles (Shp2, Ikkβ):

Cre forward: GCG CGG TCT GGC AGT AAA AAC TAT C;

Cre reverse: TTG ATA GCT GGC TGG TGG GTG ATG;

Shp2 forward: ACG TCA TGA TCC GCT GTC AG;

Shp2 reverse: ATG GGA GGG ACA GTG CAG TG;

IKKβ forward: CCT TGT CCT ATA GAA GCA CAA C;

IKKβ reverse: GTC ATT TCC ACA GCC CTG TGA.

Mouse livers and other tissue samples were collected during the same four-hour period each day (ZT 7-11) following humane euthanasia. For tumor initiation, mice were intraperitoneally injected with 25 mg/kg diethylnitrosamine (DEN; N0258, Sigma-Aldrich) at postnatal day 15. Tumor loads were assessed at 2, 5, and 8

months of age by measuring maximal tumor size, number of visible tumors on the liver surface, and the liver/body weight percentage.

Histology and immunostaining

Liver samples harvested from mice were fixed in Z-Fix (175, Anatech) and paraffin-embedded. Hematoxylin and Eosin staining was performed by the UCSD Histology Core. Identification of tumor type (HCA or HCC) was determined by morphological assessment in consultation with an expert pathologist, Dr. Nissi Varki. Hepatocyte proliferation was assessed by costaining for Ki67 (eBioscience, 47569880) and HNF4a (Santa Cruz Biotechnologies, 8987). Detection of macrophages was performed by staining paraffin sections for F4/80 (eBioscience, *14-4801-81).* Picro-Sirius Red staining for detection of fibrosis was performed according to kit instructions (American MasterTech, STPSR).

Primary hepatocyte isolation and culture

Hepatocytes were isolated by the two-step perfusion method. Briefly, mice were humanely euthanized and livers were immediately perfused with perfusion buffer (HBSS without calcium and magnesium, HEPES, EGTA), then with digestion buffer (HBSS with calcium and magnesium, HEPES, collagenase H (11074059001, Sigma)). Digested livers were suspended in cold PBS, then centrifuged three times at 50g for three minutes to obtain a pure hepatocyte fraction.

Immediately after isolation, hepatocytes were plated on collagen-coated (C8919, Sigma) plates in Williams' Media E (W1878, Sigma) supplemented with 10%

FBS and Pen/Strep (15140, Gibco). For signaling experiments, hepatocytes were serum-starved, then stimulated with mouse recombinant IL-6 (BioLegend, 575702), TNFa (BioLegend, 575202), or mouse recombinant HGF (Sigma, SRP3300) before harvesting in RIPA.

Immunoblotting

Lysates from whole liver or isolated hepatocytes were prepared in RIPA (10mM Tris-HCl, 1mM EDTA, 1% Triton X-100, 0.1% sodium deoxycholate, 0.1% SDS, 140 mM NaCl) with protease inhibitors and phosphatase inhibitors. SDS-PAGE and immunoblotting were performed according to standard procedures using the antibodies listed in Table 0.1. Briefly, protein lysate concentrations were normalized using Bradford reagent and a BSA standard curve, then denatured in SDS-PAGE loading buffer. Lysates were run on 8-12% SDS-PAGE gels, based on the size of the target protein, then transferred in buffer containing 20% methanol onto nitrocellulose membranes. Membranes were blocked for 1 hour at room temperature in TBST containing 5% nonfat dry milk. Primary antibody incubations were performed overnight at 4°C, using antibodies diluted in TBST with 3% BSA. After washing, secondary antibody incubation was performed for 1 hour at room temperature. Blots were developed with ECL or ECL Plus (Thermo Fisher Scientific, 32209, 32134) and imaged using the BioRad ChemiDoc imaging system.

Serum Biochemistry

Serum was collected from 2-month-old male mice and immediately flash-

frozen. Serum AST and ALT were measured using commercially available kits (Sekisui), according to the kinetic measurement method.

Total bile acid analysis

Serum bile acids were diluted measured using a commercially available kit (Abcam, ab239702) according to kit instructions. Liver total bile acids were extracted from 50mg liver and homogenized in 1 ml of 70% room-temperature ethanol. The suspension was incubated for 3 hours at 50°C, then clarified by centrifugation at 10,000 rpm for 10 minutes at room temperature. The supernatant was used for analysis of bile acid levels.

Immune cell isolation and flow cytometric analysis

Spleens and liver-draining lymph nodes were collected from humanely euthanized mice between 8-12 weeks of age and homogenized through a 70um cell strainer, then further suspended using a 27-gauge needle. Liver nonparenchymal cells were isolated by two-step perfusion as described in “primary hepatocyte isolation and culture”. Hepatocytes were removed from the cell suspension by sequential centrifugation at 50g; the supernatants containing NPCs were centrifuged at 300g for 5 minutes to pellet the cells. Red blood cells were removed from NPCs, splenocytes, and lymph node suspensions by incubating in ACK lysis buffer for 5 minutes at room temperature. Cleared cells were pelleted by centrifugation at 500g for 5 minutes, then washed twice in phosphate-buffered saline (PBS).

Surface marker staining was performed as follows: First, viability staining was performed for 20 minutes on ice in PBS with Tonbo Ghost Dye UV450, with all samples protected from light through this and subsequent steps. Conjugated antibodies were added and cells were incubated 15-20 minutes on ice. See Table 0.2 for antibody panels used. Cells were washed 3 times in staining buffer (PBS with 5% FBS and 0.1% sodium azide).

Intracellular staining was performed using the Foxp3 Fix/Perm solution (BioLegend) according to manufacturer's instructions.

RNA Sequencing

Whole-liver samples or freshly isolated hepatocytes were immediately frozen. RNA was extracted from samples of whole liver using RNeasy Microarray Tissue Mini Kit (73304, Qiagen) or from isolated hepatocytes using RNeasy Plus Micro Kit (74034). Libraries were prepared using Illumina TruSeq v2 kit according to manufacturer's instructions. Sequencing was performed at UCSD Genomics Core on the HiSeq4000 platform. Raw data quality control was performed using fastqc, sequenced reads were mapped to the mm9 reference genome using STAR, and gene differential expression analysis was performed using Cuffdiff, with fragments per kilobase million (FPKM) values calculated. Gene set enrichment analysis (GSEA) using the preranked tool were used for pathway analysis. To compare different expression levels of pathway-related genes between KO and WT, we used the average FPKM in each group (n=3). Significantly expressed genes are determined with $|\log2FC| > 0.5$ and q-value < 0.05. Changes unique to DKO are found by

overlapping the significant genes in DKO vs. WT, DKO vs. IKO, and DKO vs. SKO. Heatmaps are made with R package gplots and bar plots with ggplot2.

TCGA analysis

The raw counts of TCGA hepatocellular carcinoma (LIHC) patient transcriptomic dataset was downloaded from Genomic Data Commons Data Portal (https://portal.gdc.cancer.gov/). This dataset includes 371 HCC patient samples and 50 adjacent normal liver tissues. The R package DESeq2 was used to normalize raw counts across all samples. Next, we divided all HCC samples into three groups: (1) circadian clock-normal, (2) circadian clock-mid, (3) circadian clock-dysregulated, based on whether circadian clock genes were dysregulated or not in these patient samples compared to non-tumor tissues. In detail, we checked expression of 7 core clock genes, including *CLOCK*, *ARNTL*, *PER1*, *PER2*, *PER3*, *CRY1*, and *CRY2*. For each gene, the mean and standard deviation (sd) of normalized values in non-tumor tissues were calculated. We set (mean-sd) as lower bound and (mean+sd) as upper bound, then we defined an HCC patient with this circadian clock gene as dysregulated if its normalized value was higher than the upper bound or lower than the lower bound. We repeated this process for all 7 circadian clock genes. Next, we assigned patients with at most 2 dysregulated circadian clock genes into “normal” group, patients with at least 5 dysregulated circadian clock genes into “dysregulated” group, and others into “mid” group. With sub-clustering of all HCC patients, we first performed differential expression analysis between “normal” and “dysregulated” groups using DESeq2. The genes with adjusted p value < 0.05 were defined as

differentially expressed. We specifically checked components from Ras/MAPK signaling pathway and NF-κB pathway, then made volcano plots with differentially expressed genes in pathways above. Next, in order to further verify whether activities of these two pathways were inhibited in dysregulated group, we collected downstream targets of Ras/MAPK pathway as well as NF-κB pathway from Msigdb gene sets HALLMARK_TNFA_SIGNALING_VIA_NFKB and BILD_HRAS_ONCOGENIC_SIGNATURE, respectively. The pathway activity was defined as the sum of rank-transformed normalized values of all genes in corresponding gene set. The boxplot was made using Wilcoxon rank sum test.

Survival analysis was performed using OncoLnc (http://www.oncolnc.org/), with “high” and “low” expression defined as the upper and lower quartiles of expression for each gene.

qRT-PCR

RNA from whole liver or from isolated hepatocytes was isolated using a standard phenol-chloroform extraction with Trizol reagent according to manufacturer’s protocol. cDNA was prepared using High-Capacity cDNA Reverse Transcription Kit (Life Technologies, 4368813). Quantitative reverse transcription was performed using PowerUP SYBR Green PCR Master Mix (Invitrogen, A25743) and the primers listed below on the Stratagene MX3005P. Ct values for each transcript were normalized to β-actin, and fold change was calculated using the $\Delta\,\Delta$Ct method. Primer sequences are listed in Table 0.3.

Statistical Analysis

Multiple comparisons were performed using one-way ANOVA with Tukey post-hoc analysis in GraphPad Prism. P<.05 was considered statistically significant. (*P<0.05; **P<0.01; ***P<0.001). Pooled data are presented as mean +/- standard deviation.

Table 0.1. Antibodies used for immunoblotting

Antibody name	**Manufacturer**	**Catalog Number**
Shp2	Santa Cruz Biotechnologies	Sc-280
Ikkβ	Cell Signaling Technology	8943
p-ERK1/2	Cell Signaling Technology	4695
ERK1/2	Cell Signaling Technology	4370
B-actin	Sigma	A5316
p-IκBα	Cell Signaling Technology	2859
p-p65	Cell Signaling Technology	3033
P65	Cell Signaling Technology	8242
Gapdh	Cell Signaling Technology	5174
p-Akt Ser473	Cell Signaling Technology	9272
Akt	Cell Signaling Technology	9271
p-Stat3	Cell Signaling Technology	9145
Stat3	Cell Signaling Technology	9139

Table 0.2. Antibody panels used for FACS analysis of immune cells

Fluorophore	Panel 1 (liver lymphocytes)	Panel 2 (liver myeloid cells)	Panel 3 (splenic lymphocytes)	Panel 4 (splenic myeloid cells)	Panel 5 (lymph nodes)
Aqua	L/D	L/D			
FITC	DX5	Ly6C		LY6C	
PE	NK1.1	CD68	NK1.1	CD11c	NK1.1
Percp-Cy5.5	CD45	CD45		CD3/CD19	
Pacific Blue	TCRb	F4/80	TCRb	F4/80	TCRb
APC	Foxp3	MHC II	Foxp3	MHCII	Foxp3
PE-Cy7	CD8		CD8		CD8
APC-Cy7	CD19		CD19	Ly6G	CD19
BV605	CD4	CD11b	CD4	CD11b	CD4
BV711		TCR b/B220			

Table 0.3. qPCR primer sequences

Primer name	Sequence (5'-3')
Col1a1 fwd	ATGGATTCCCGTTCGAGTACG
Col1a1 rev	TCAGCTGGATAGCGACATCG
Tgfb fwd	AGATTAAAATCAAGTGTGGAGCAAC
Tgfb rev	GTCCTTCCTAAAGTCAATGTACAGC
Ccl8 fwd	GTAGACCCCACACAGAAGTGG
Ccl8 rev	TTCCAGCTTTGGCTGTCTCTT
Ccl2 fwd	CCCAATGAGTAGGCTGGAGA
Ccl2 rev	TCTGGACCCATTCCTTCTTG
Ccr2 fwd	GGGCTGTGAGGCTCATCTTT
Ccr2 rev	TGCATGGCCTGGTCTAAGTG
Afp fwd	ATCGACCTCACCGGGAAGAT
Afp rev	GAGTTCACAGGGCTTGCTTCA
Igf2 fwd	GGGTCTTCCAACGGACTGG
Igf2 rev	CATTGGTACCACAAGGCCGAAG
Per2 fwd	CAGCTGCCCTCCCGGGATCT
Per2 rev	TCCTGGACATTGCATTGC
Per3 fwd	CCCTACGGTTGCTATCTTCAG
Per3 rev	CTTTCGTTTGTGCTTCTGCC
Cry1 fwd	CGCAGGTGTCGGTTATGAGC
Cry1 rev	ATAGACGCAGCGGATGGTGTCG
Cry2 fwd	GGTTCCTACTGCAATCTCTGG
Cry2 rev	GTCATATTCAAAGGTCAAACGGG
Bmal1 fwd	GCCCCACCGACCTACTCT
Bmal1 rev	CTTTGTCTGTGTCCATACTTTCTTG
Clock1 fwd	CATCAACTCAGCAGAGTCAACA
Clock1 rev	AGGCTGGGAAATCACCATCG
Dbp1 fwd	GGAACTGAAGCCTCAACCAAT C
Dbp1 rev	TCCGGCTCCAGTACTTCTCA

Table 0.3, continued. qPCR primer sequences

Primer name	Sequence (5'-3')
Aacs fwd	CGTGTGGTCGGCTATCTACC
Aacs rev	GCGGTCCAGGACACCATTTA
Fabp1 fwd	AGGGGGTGTCAGAAATCGTG
Fabp1 rev	CCCCCAGGGTGAACTCATTG
B-actin fwd	GGCACCACACCTTCTACAATG
B-actin rev	GGGGTGTTGAAGGTCTCAAAC
IL-6 fwd	TTCCATCCAGTTGCCTTCTT
IL-6 rev	ATTTCCACGATTTCCCAGAG
Tnfa fwd	GCCTCTTCTCATTCCTGCTT
Tnfa rev	CACTTGGTGGTTTGCTACGA
HGF fwd	AAATGAGAATGGTTCTTGGTG
HGF rev	CTGGCCTCTTCTATGGCT
PDGF-B fwd	TGTTCCAGATCTCGCGGAAC
PDGF-B rev	GCGGCCACACCAGGAAG
PDGF-D fwd	GACACTTTTGCGACTCCGC
PDGF-D rev	TGTGAGGTGATTGCTCTCATCTC

Chapter 1. Shp2 and Ikkβ cooperate to suppress liver damage and tumorigenesis

Although each of two pathways mediated by Shp2 and Ikkβ have been well characterized individually in carcinogenesis when over-activated, it is unclear how they intertwine to function physiologically at the ground state. Therefore, we sought to investigate the effect of dual blockade on these pathways on (1) liver physiology, particularly liver damage, and (2) malignant transformation and tumorigenic capacity of hepatocytes.

1.1 Shp2 and Ikkβ cooperatively suppress liver tumorigenesis

To interrogate pathway crosstalk, we generated a double knockout (DKO) mouse line with both Shp2 and Ikkβ deleted in hepatocytes by crossing *Shp2$^{f/f}$:Albumin-Cre* mice with the *Ikkβ$^{f/f}$* mouse line (Fig1.1A). Littermates lacking the *Albumin-Cre* transgene were used as WT controls for all experiments. Although Cre-mediated deletion in hepatocytes is highly efficient, it has been reported that livers can re-gain expression of β-Catenin after deletion, with approximately 50% of WT protein levels restored by 12 months of age (Wang et al., 2011). It seemed plausible that combined Ras/MAPK and NF-κB suppression might create a growth disadvantage, which might then lead to selection for hepatocytes that have escaped deletion. To ensure that both genes remained knocked out in the liver, we assessed protein levels of Shp2 and Ikkβ in liver tissue at 12 months of age, and confirmed that deficiency of both proteins was maintained long-term in liver tissue (Fig. 1.1B). The

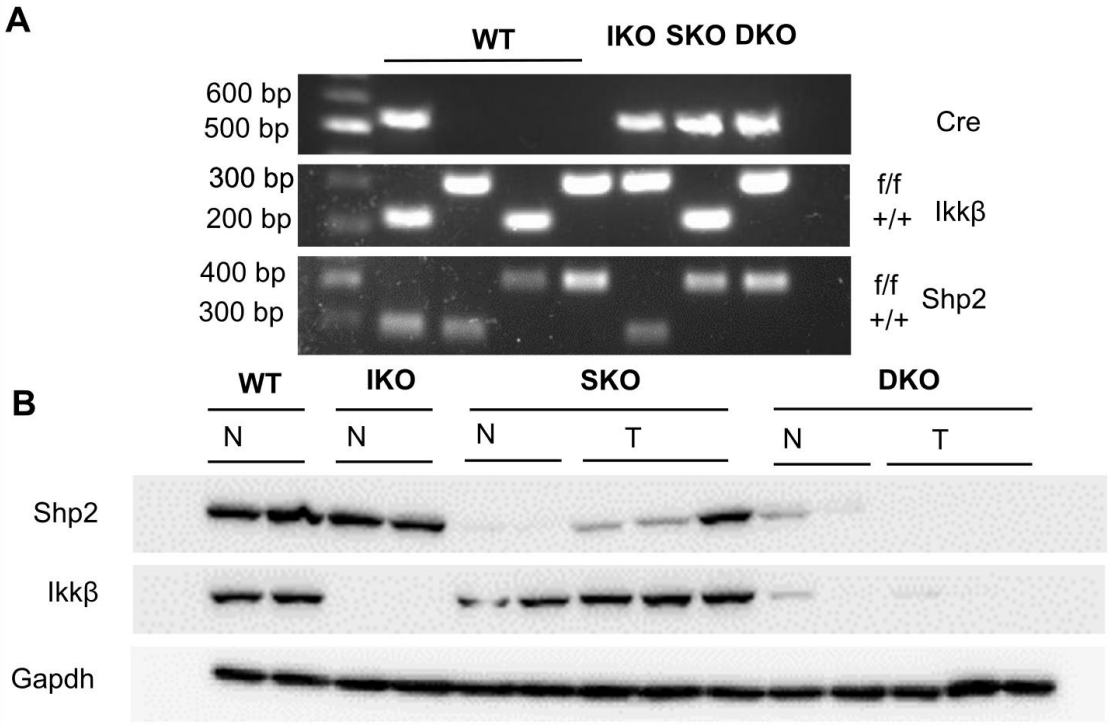

Figure 1.1 Generation of Shp2/Ikkβ DKO mouse line

A. PCR genotyping of Cre recombinase gene and of floxed (f) and wild-type (+) alleles of Shp2 and Ikkβ from genomic DNA isolated from tail snips of mice with the indicated genotype.
B. Representative immunoblot for Shp2 and IKKβ in whole liver lysates from 12-month old liver nontumor (N) and tumor (T) tissue.

DKO mice were born at Mendelian frequency with no obvious health problems noted in young pups, similar to the single Shp2 knockout (SKO) or Ikkβ knockout (IKO) in hepatocytes.

We first investigated the effects of combined pathway suppression on mouse susceptibility to diethylnitrosamine (DEN), which was shown to induce multiple mutations frequently detected in HCC patients, including *Hras* and *Braf* (Connor et al., 2018). Following DEN injection on postnatal day 15, we compared liver tumor loads in WT, SKO, IKO and DKO mice at 5 and 8 months (Fig.1.2, Fig. 1.3A,B). Although deleting either Ikkβ or Shp2 exacerbated DEN-induced HCC development relative to the WT mice, the DKO mice exhibited much more severe tumor burdens than IKO and SKO mice, as evaluated by numbers and maximal sizes of tumor nodules. As early as 5 months after DEN injection, the DKO mice developed numerous large tumors, when only a few small macroscopic nodules and microscopic lesions were detected in IKO and SKO mice (Fig. 1.2A, Fig.1.3A, Fig. 1.4A). The severe tumorigenic phenotype in DKO mice became more striking when examined at later stages (Fig. 1.2, Fig. 1.3B,C). The liver/body weight ratio of DKO was also significantly elevated at 5 and 8 months of age compared to all other genotypes, reflecting the severe tumor burden (Fig. 1.3C). Histopathological analysis of liver tissue sections identified the tumors as HCC (Fig. 1.4A,B). Thus, in the DEN model of liver tumorigenesis, signaling pathways mediated by Shp2 and Ikkβ work in concert to suppress carcinogenesis. This stands in contrast to the Shp2/Stat3 DKO model, in which each individual gene deletion promotes chemically-driven HCC, but combined deletion is neutralizing (Bard-Chapeau et al., 2011).

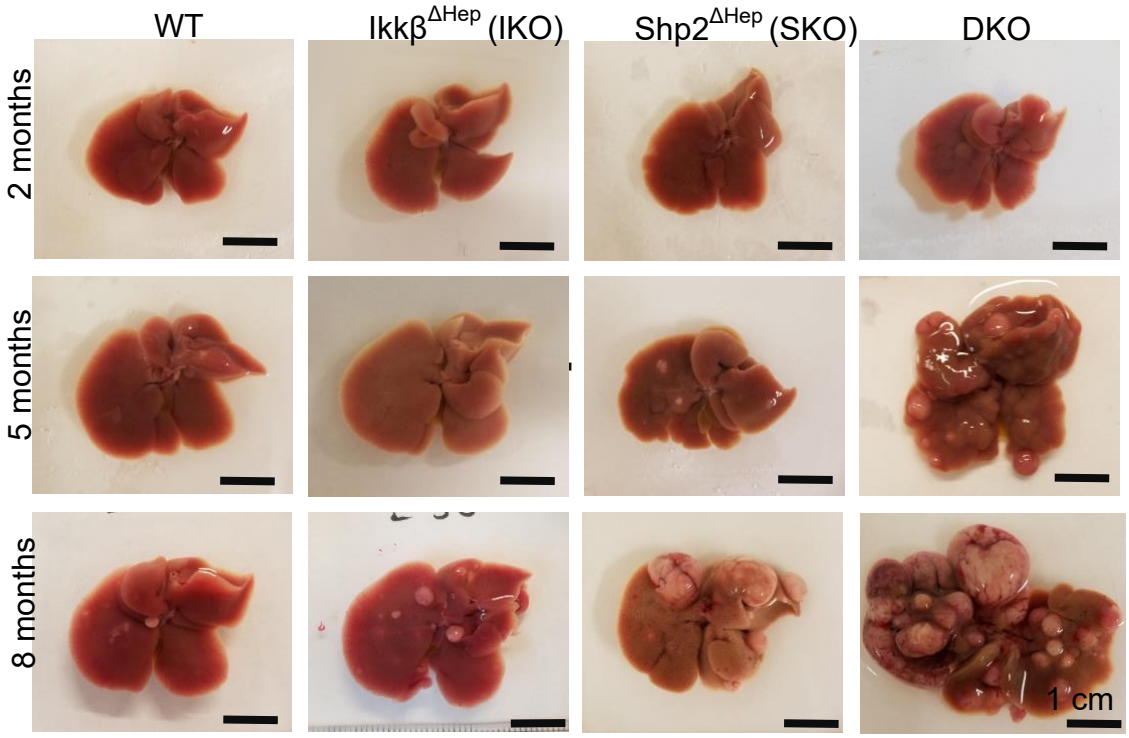

Figure 1.2 Dual deletion of Shp2 and Ikkβ accelerates chemically-induced liver carcinogenesis

Representative images of livers from DEN-treated male mice with the indicated genotype at 2, 5, and 8 months of age. Scale bar=1cm.

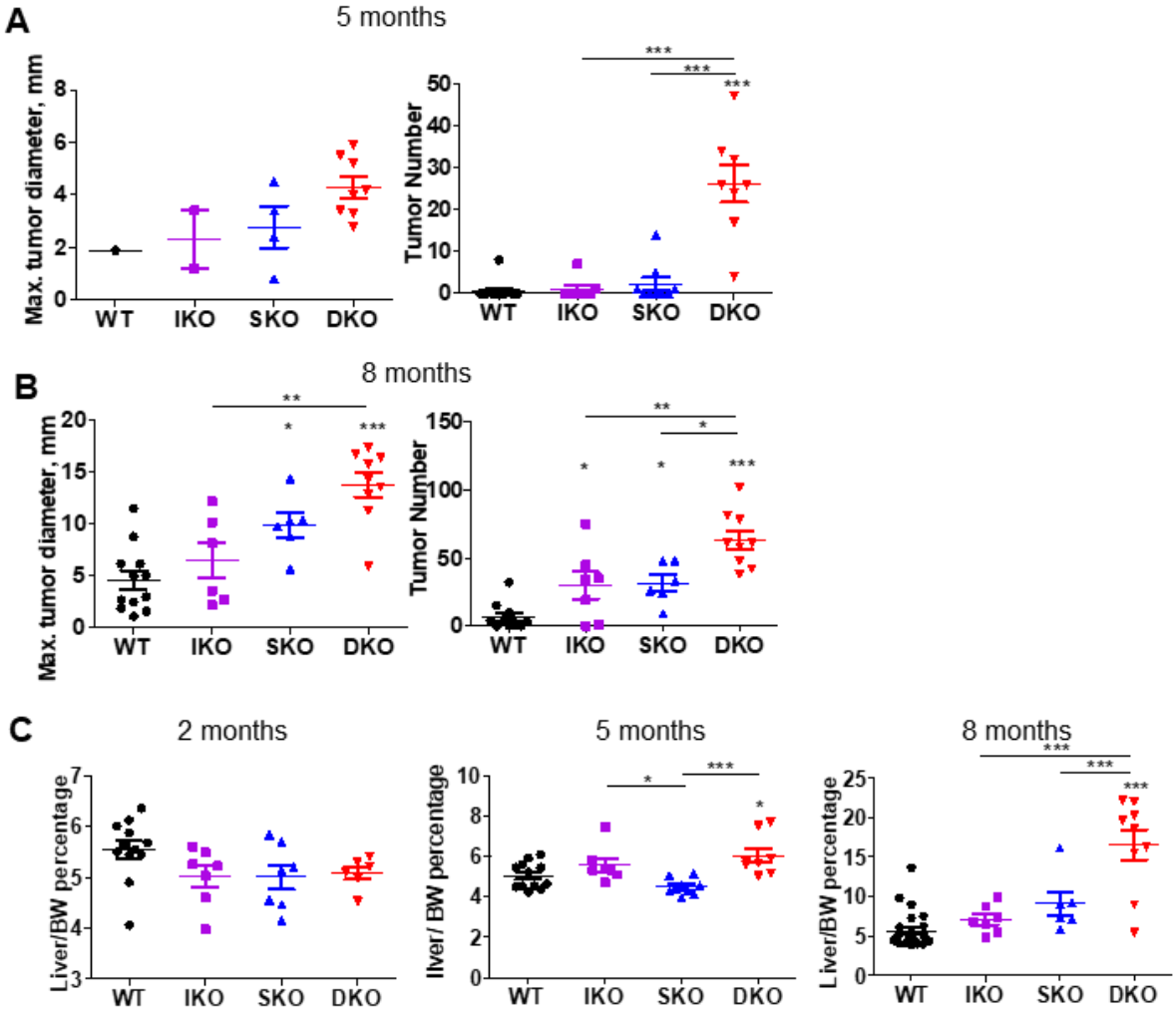

Figure 1.3 Quantification of tumor burden in livers of DEN-treated mice

A. Quantification of number of tumors per liver and maximal tumor size in DEN-treated mice at 5 months of age.
B. Quantification of number of tumors per liver and maximal tumor size in DEN-treated mice at 8 months of age.
C. Quantification of liver/body weight percentage in DEN-treated male mice at 2, 5, and 8 months of age.

n=6-12 mice/genotype for all time points.
Multiple comparisons were performed using one-way ANOVA with Tukey post-hoc analysis (*P<0.05; **P<0.01; ***P<0.001).

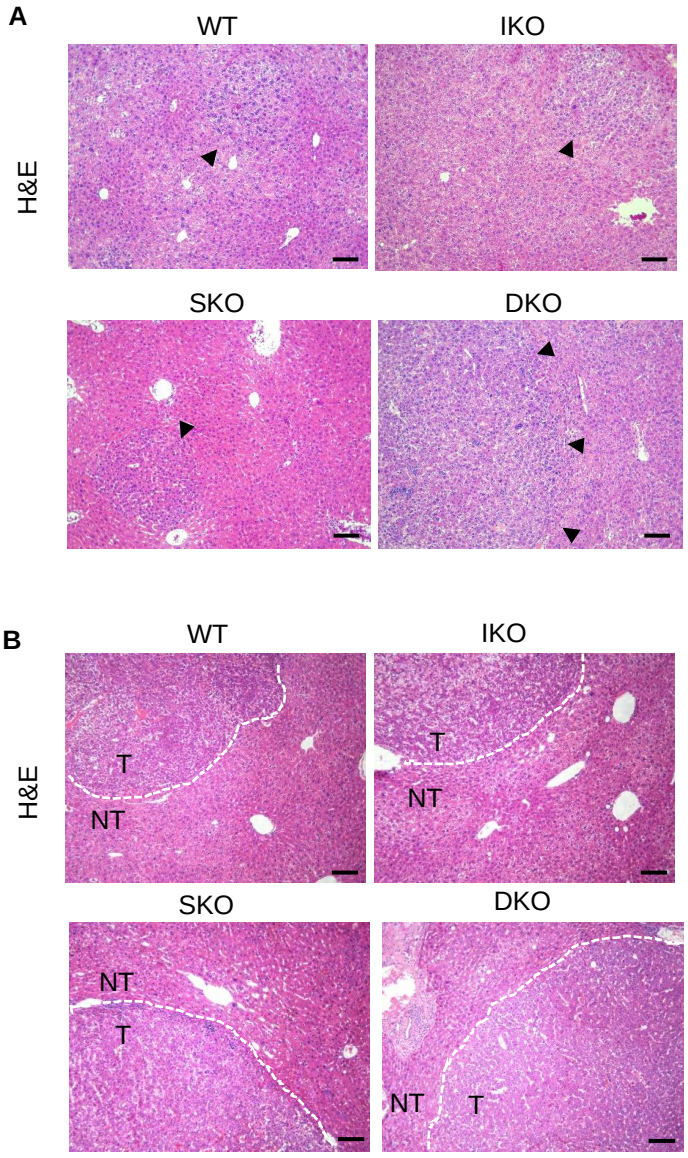

Figure 1.4 Histological determination of tumor type in DEN-treated mice

A. H&E staining from 5-month-old DEN-treated mice. Arrows indicate microscopic nodules or, in DKO, macroscopically visible tumor margins. Scale bar=100um.
B. H&E staining from 8-month-old DEN-treated mice. Dotted lines delineate tumor (T) and nontumor (NT) regions. Scale bar=100um.

Based on previous reports on IKO and SKO mice, it was not totally unexpected to detect more severe tumor phenotype in DEN-treated DKO mice (Bard-Chapeau et al., 2011; Maeda et al., 2005). However, it was unclear how the liver damage and eventual malignant transformation would be affected by dual knockout at physiological steady-state, without genotoxic insult. To this end, we maintained colonies of untreated WT, IKO, SKO, and DKO mice long-term, up to 12 months. Surprisingly, the DKO livers showed spontaneous tumors at 9 months of age, a time at which no tumor nodules were detected in WT, IKO or SKO mice (Fig. 1.5A, Fig. 1.7A). Given the relative resistance of the WT C57/BL6 strain to liver tumorigenesis, even with exogenous carcinogen, this represents unexpectedly rapid tumor development. At 12 months, 75% of DKO mice showed large liver tumors, whereas only 29% of SKO and no IKO mice showed small benign hepatocellular adenomas (HCA) (Fig. 1.5B, Fig. 1.6A) The spontaneously developed tumors in DKO liver were malignant, exhibiting typical HCC morphology (Fig. 1.7A,B). The tumor burden in DKO livers was also reflected in elevated liver/body weight percentage (Fig. 1.6C). These results indicate that concurrent inactivation of two pro-oncogenic pathways, Ras/MAPK and NF-κB, results in paradoxical emergence of spontaneous HCC.

1.2 Dual deletion of Shp2 and Ikkβ triggers severe hepatic damages

To probe the tumor-promoting mechanisms at play in DKO livers, we carefully examined liver phenotypes in young mice at the pre-cancer stage. The structure of DKO livers was macroscopically disrupted at 2 months of age, with irregular lobe edges and visible crevices (Fig. 1.8A). The IKO livers had no gross structural or

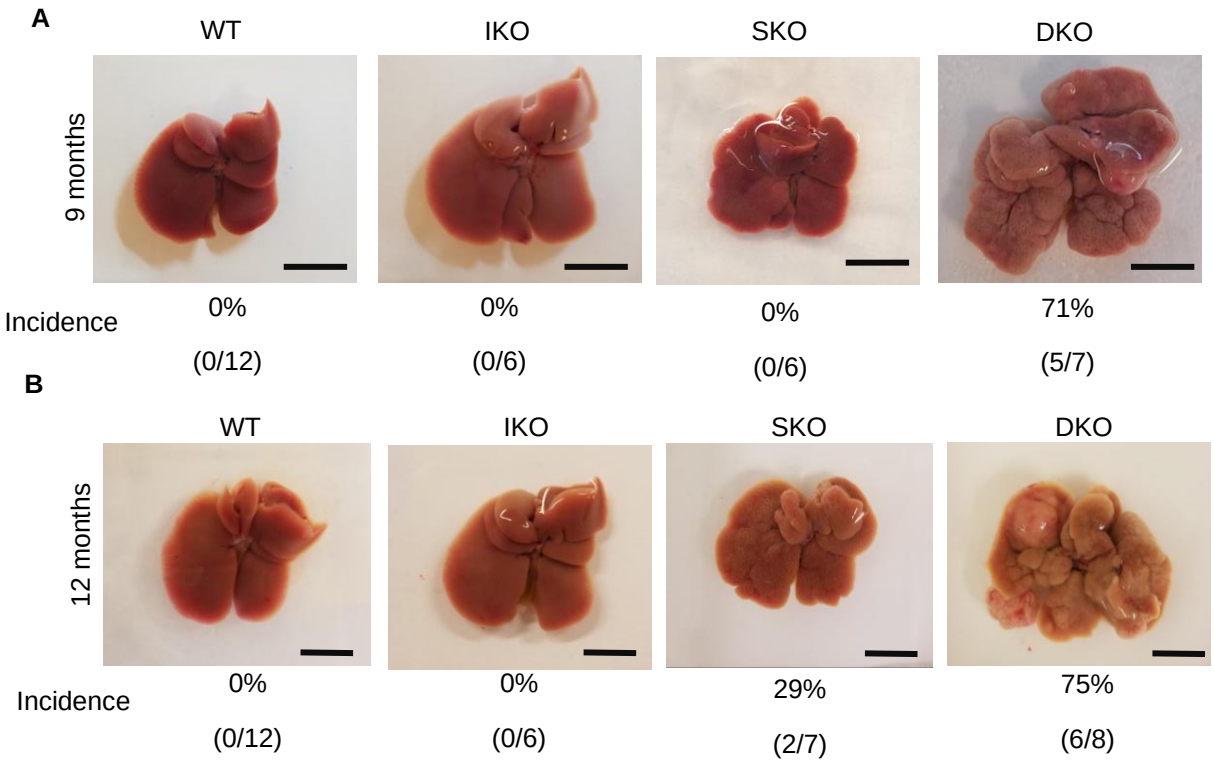

Figure 1.5 Dual deletion of Shp2 and Ikkβ induces spontaneous liver tumors

A. Representative images of livers from untreated male mice at 9 months of age, with tumor incidence listed below.
B. Representative images of livers from untreated male mice at 12 months of age, with tumor incidence listed below.

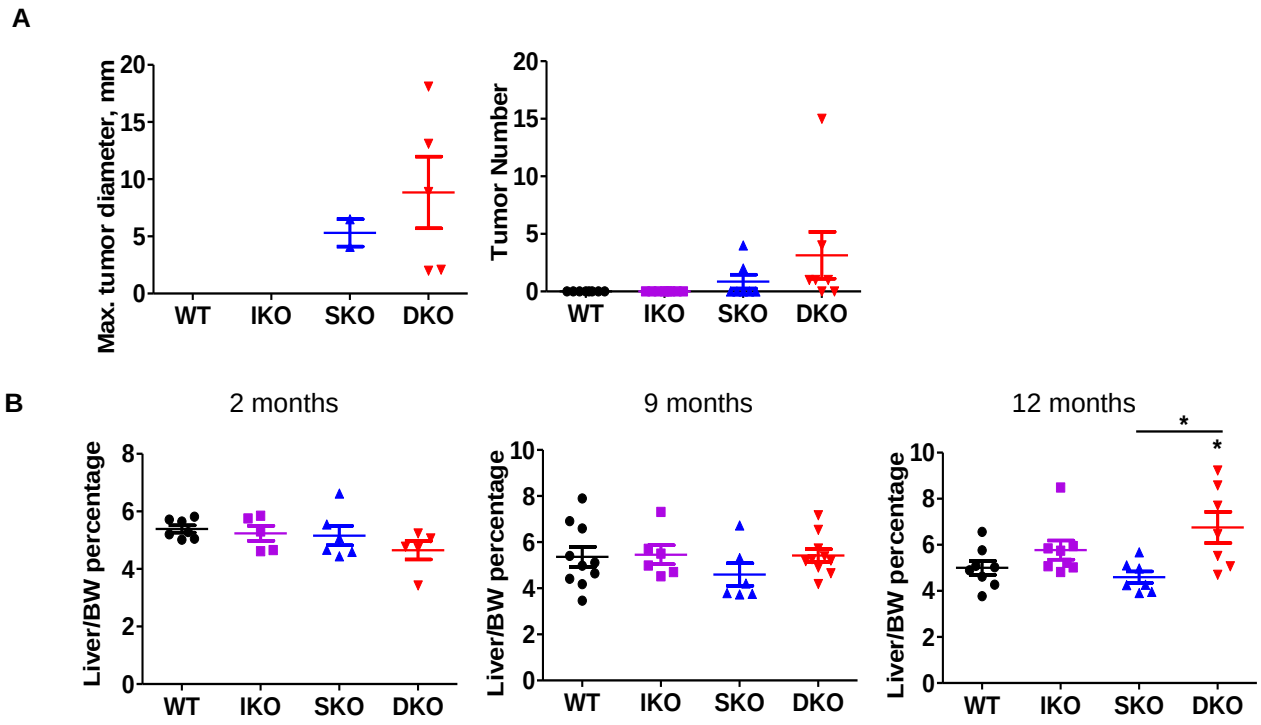

Figure 1.6 Quantification of spontaneous tumor burden

A. Tumor size and tumor number/liver in 12-month-old untreated male mice
B. Quantification of liver/body weight ratio in untreated mice of the indicated ages.

n=6-12 mice/genotype for all panels

Multiple comparisons were performed using one-way ANOVA with Tukey post-hoc analysis (*P<0.05; **P<0.01; ***P<0.001).

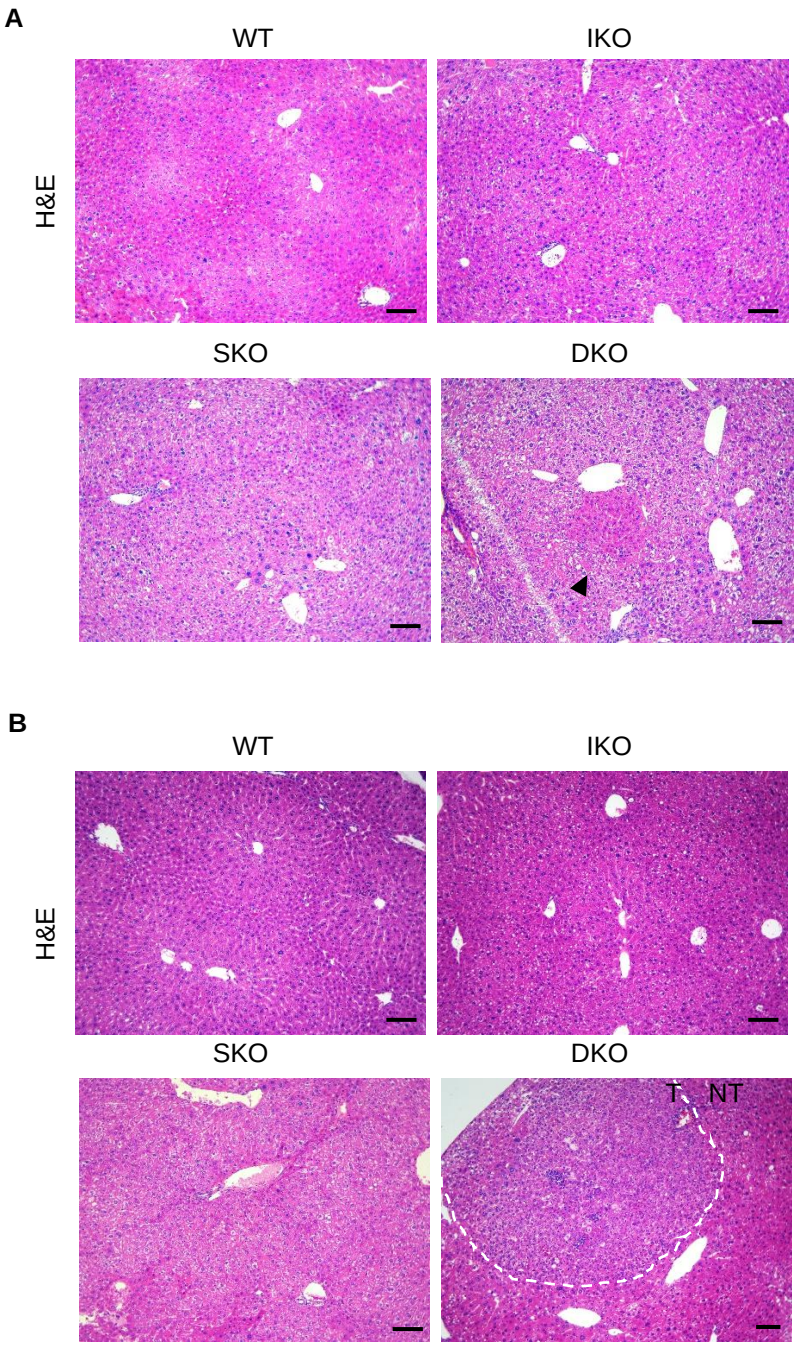

Figure 1.7 Histological determination of tumor type in DKO livers

A. H&E staining showing nontumor (NT) and tumor (T) (if present) areas in livers from 9-month-old untreated mice.
B. H&E staining showing nontumor (NT) and tumor (T) (if present) areas in livers from 12-month-old untreated mice. Scale bar=100um.

developmental defects (Fig. 1.8A,B). SKO livers displayed mild inflammatory cell infiltrates around portal triads at early ages, which were markedly worsened in DKO mice (Fig. 1.8B). Similarly, mild periportal fibrosis in SKO livers was dramatically worsened, with much more extensive fibrosis seen in DKO by Picro-Sirius Red staining (Fig. 1.9A). Consistent with the anatomical lesions, qRT-PCR detected progressively increased levels of fibrosis-related *Col1α1* and *Tgfβ* mRNAs in IKO, SKO and DKO livers at the early time point (Fig. 1.9B). Serum AST and ALT levels were also slightly elevated in single KO, and further in double KO mice (Fig. 1.10A). The SKO mice displayed modestly elevated bile acids (BA) levels in serum and liver (Fig. 1.10B), consistent with a role of Shp2 in control of BA biosynthesis (Li et al., 2014). Of note, while deleting Ikkβ alone did not alter BA levels, both the intrahepatic and serum BA amounts were markedly elevated in DKO mice (Fig. 1.10B).

Another striking phenotype in the DKO mice is the enlarged spleen and liver-draining lymph nodes, which occurred both in DEN-treated and -untreated mice (Fig. 1.11A,B,C). Of note, splenomegaly occurred prior to tumorigenesis. To determine whether enlargement of these organs was due to increased populations of a particular immune subset, we performed flow cytometric analysis of major immune cell sub-populations in the liver, spleen and lymph node (Fig. 1.12, Fig. 1.13, Fig. 1.14). We detected lowered CD4/CD8 cell ratios and NKT percentages in SKO and DKO livers relative to WT and IKO livers. Treg cells were elevated in SKO but not in DKO liver (Fig. 1.14). One caveat to these results is the difficulty in completely digesting fibrotic regions of the DKO liver, which may have precluded identification of

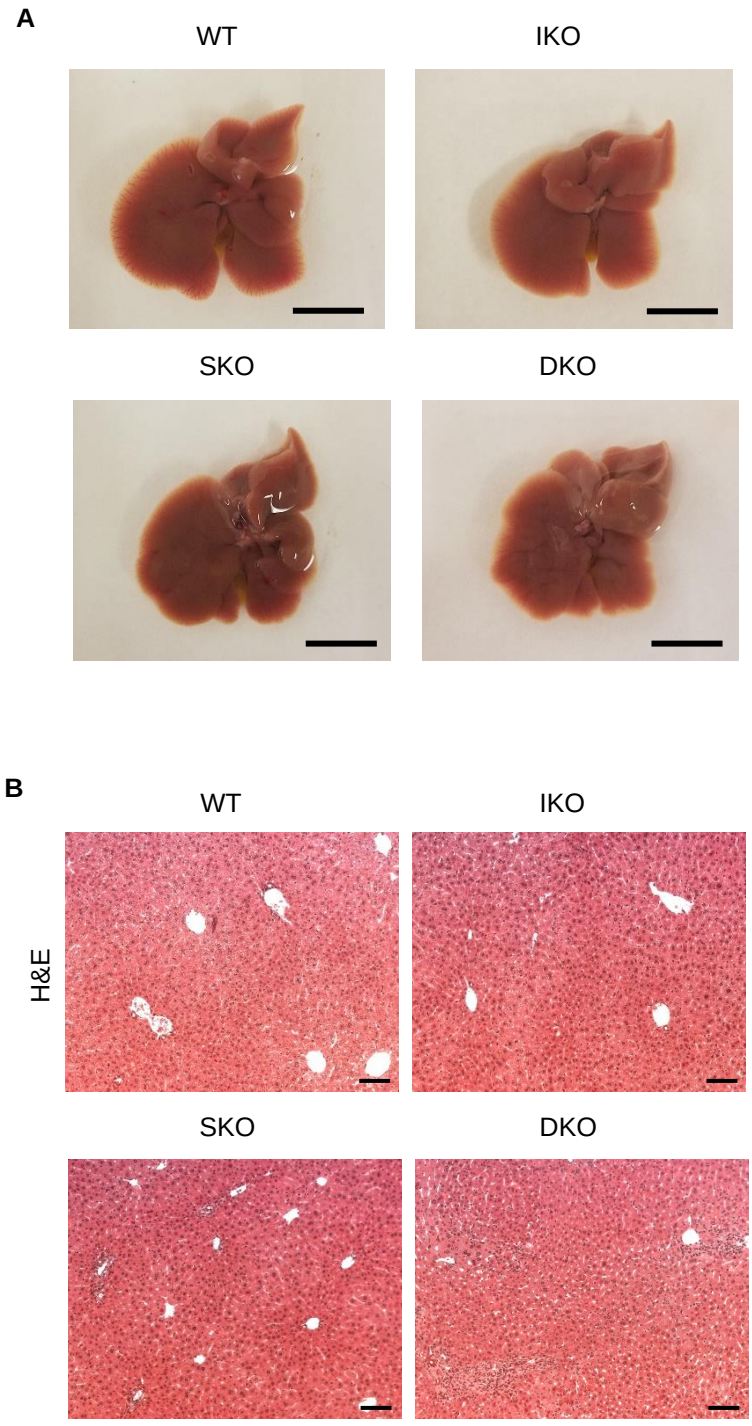

Figure 1.8 DKO mice exhibit macroscopic and microscopic indicators of liver damage at early age

A. Representative images of livers from 2-month-old untreated male mice. Scale bar=1cm.
B. H&E staining of sections from 2 month livers. Scale bar=100um.

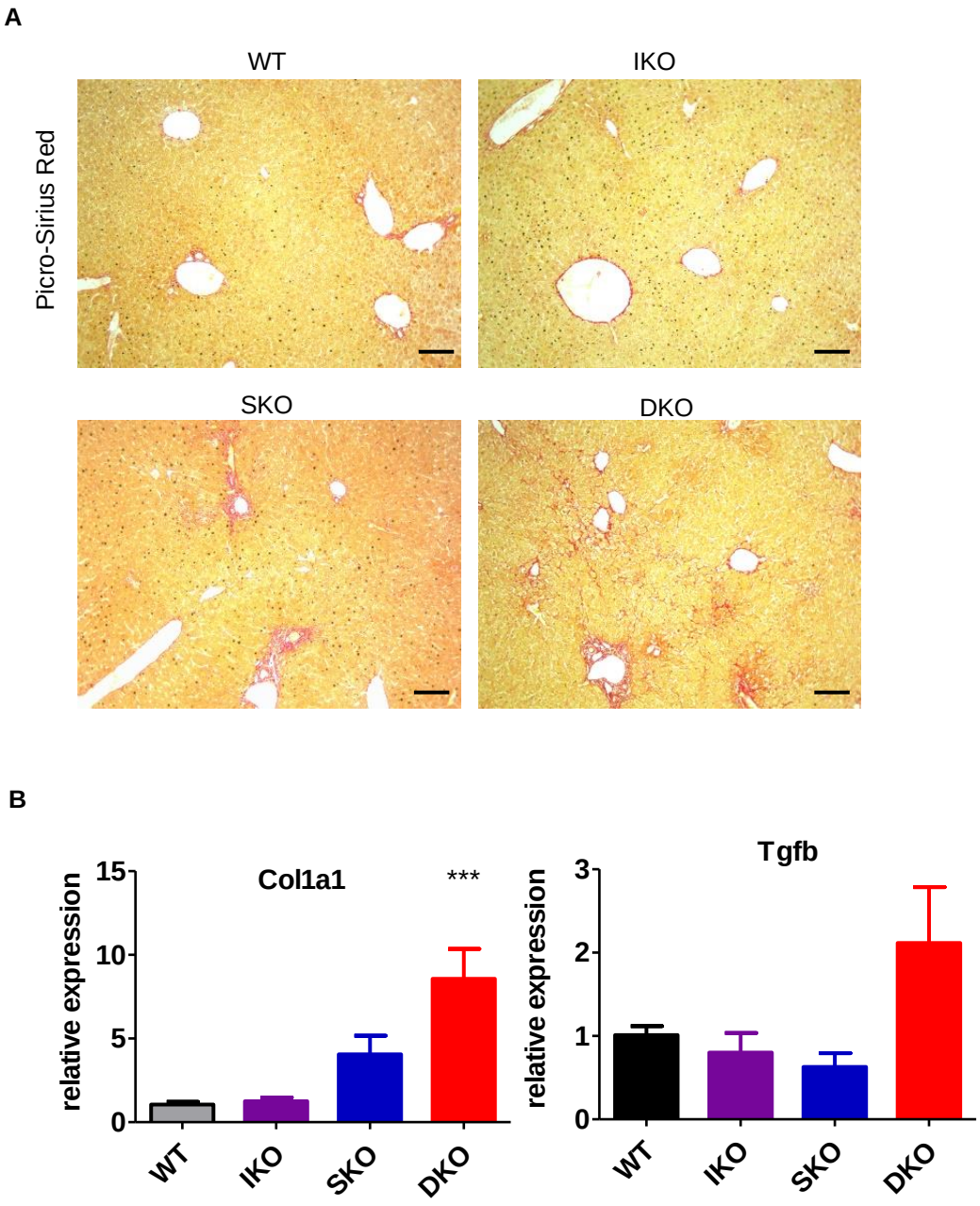

Figure 1.9 DKO livers develop fibrosis at an early age

A. Representative images of Picro-Sirius Red staining to detect fibrosis in liver sections from 2-month-old untreated male mice.
B. mRNA levels of fibrosis-associated genes in whole-liver lysates from 2-month-old mice (n=3/genotype).

Multiple comparisons were performed using one-way ANOVA with Tukey post-hoc analysis (*P<0.05; **P<0.01; ***P<0.001).

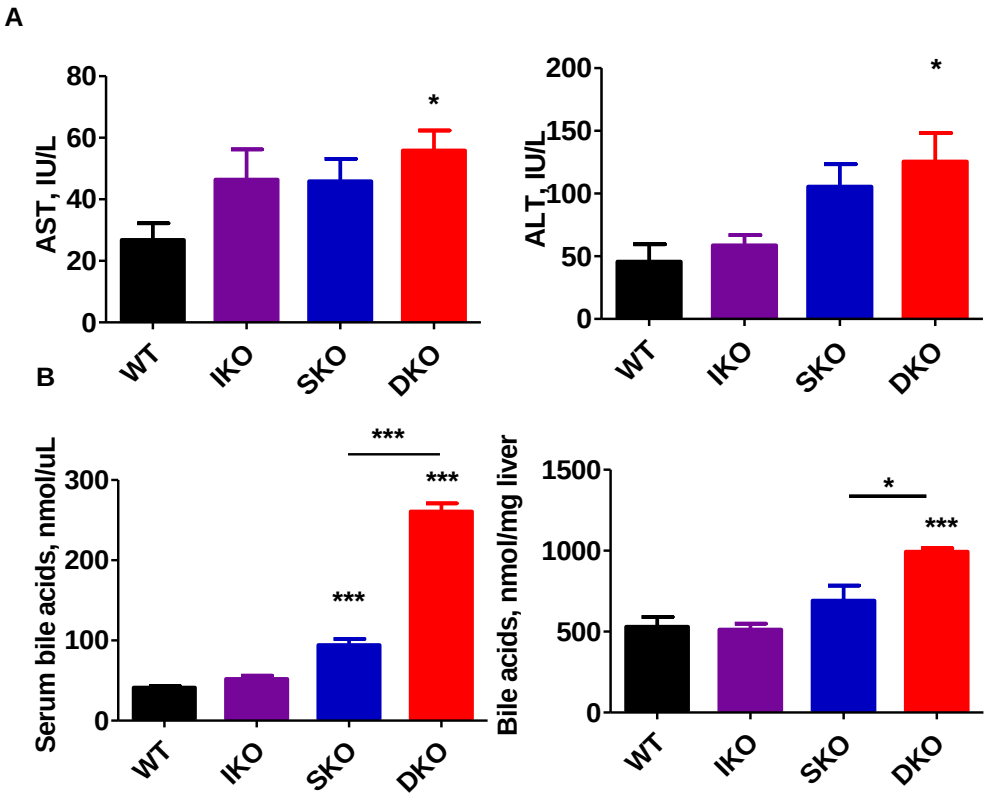

Figure 1.10 Elevated transaminases and bile acid levels in DKO mice

A. Serum aspartate transaminase (AST, left) and alanine transaminase (ALT, right) levels in serum from 2-month-old untreated male mice (n=3-5/genotype).
B. Total serum bile acids, left, and total intrahepatic bile acids, right, in 2-month-old male mice. (n=4-5/genotype)

Multiple comparisons were performed using one-way ANOVA with Tukey post-hoc analysis (*P<0.05; **P<0.01; ***P<0.001).

immune changes that localize to damaged regions.

In our analysis of other organs, we did not observe significant or biased changes in the spleen of DKO mice, with only lower DCs detected in IKO and a trend towards decreased monocytes in SKO spleens (Fig. 1.12). Similar trends were detected in the lymph nodes, with slightly higher ratios of B and NKT cells in DKO mice (Fig. 1.13). Thus, the enlarged spleen apparently resulted from portal hypertension due to liver injuries rather than a specific immune response in peripheral organs.

1.3 DKO mice develop immune changes and metabolic dysregulation

Following the morphological dissection, we performed RNA-seq analysis of the 2-month-old livers, and compared the WT liver transcriptome with that of IKO, SKO or DKO mice (Fig.1.15, Fig. 1.16A,B,C). The gene expression heatmap showed relatively fewer significant transcriptomic changes in the IKO/WT than the SKO/WT comparison, consistent with the respective liver damage and tumor phenotypes (Fig. 1.15). Gene set enrichment analysis (GSEA) of gene ontology (GO) terms revealed changes in immune response pathways in both IKO and SKO liver, with IKO livers showing more positive immune enrichment and the SKO livers also exhibiting positive enrichment of cell-cycle related terms (Fig. 1.16A,B). The DKO liver appeared to have most of the changes detected in IKO and SKO; however, the DKO/WT comparison also revealed more prominent changes in cell cycle progression and metabolic pathways (Fig. 1.16C). The DKO liver was characterized

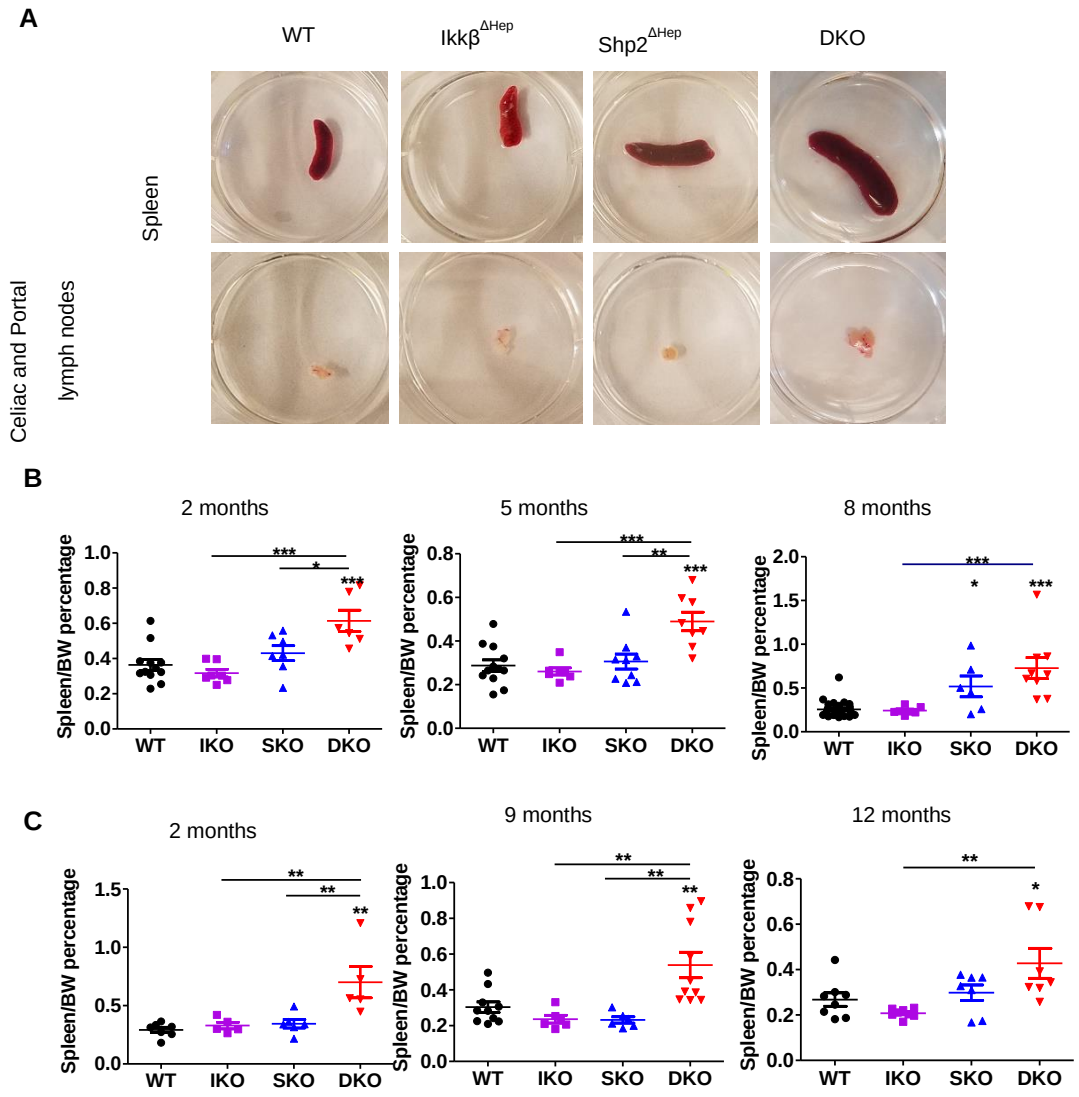

Figure 1.11 Early splenomegaly in the DKO model

A. Representative images of spleens and liver-adjacent lymph nodes from 2-month-old untreated male mice.
B. Spleen/body weight ratio of DEN-treated male mice at indicated ages (n=6-12 mice/genotype).
C. Spleen/body weight ratio of untreated male mice at indicated ages (n=6-12 mice/genotype).

Multiple comparisons were performed using one-way ANOVA with Tukey post-hoc analysis (*P<0.05; **P<0.01; ***P<0.001).

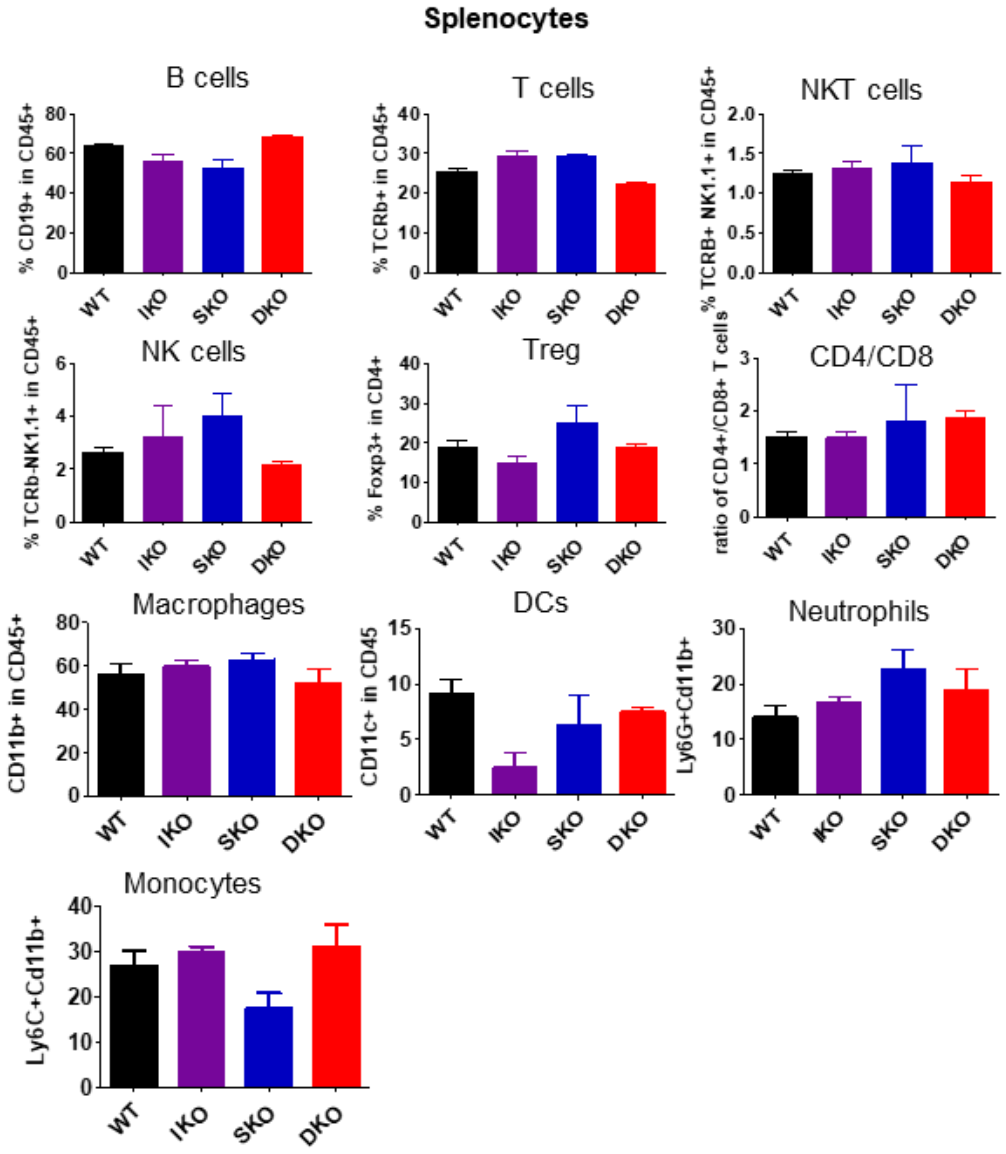

Figure 1.12 Immune populations in spleens of knockout mice.

Summary of flow cytometric analyses of indicated immune populations in spleens of 8-12-week old untreated mice. T cells are the TCRβ+ population among CD45+ cells; CD4 cells are the CD4+ population among CD3+ cells; CD8 cells are the CD8+ population among CD3+ cells; regulatory T cells (Treg) are the Foxp3+ population among CD4+ cells; NKT cells are the TCRβ+ Nk1.1+ population in CD45+ cells; NK cells are the TCRβ- Nk1.1+ population in CD45+ cells; B cells are the CD19+ population in CD45+ cells, macrophages are the CD11b+ population in CD45+ cells; dendritic cells (DCs) are the CD11c+ population in CD45+ cells; neutrophils are the Ly6G+ population in CD11b+ cells, and monocytes are the Ly6C+ population in Cd11b+ cells. n=3-5 mice/genotype.

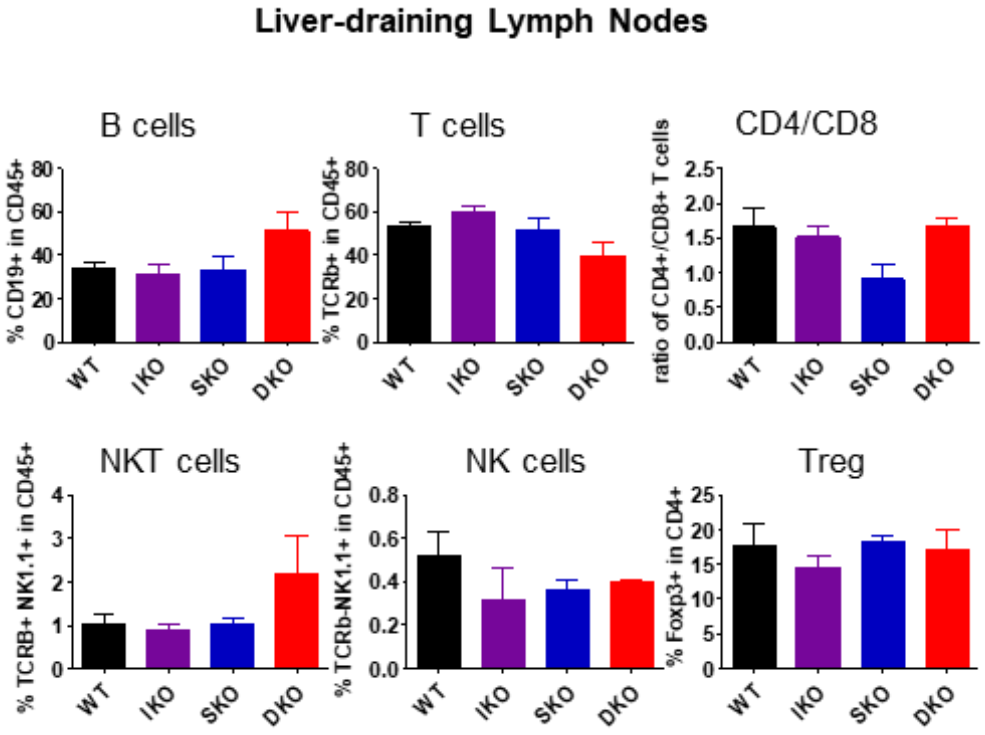

Figure 1.13 Immune populations in liver-draining lymph nodes

Summary of flow cytometric analyses of indicated immune populations in liver-draining lymph nodes from 8-12-week old untreated mice. T cells are the TCRβ+ population among CD45+ cells; CD4 cells are the CD4+ population among CD3+ cells; CD8 cells are the CD8+ population among CD3+ cells; regulatory T cells (Treg) are the Foxp3+ population among CD4+ cells; NKT cells are the TCRβ+ Nk1.1+ population in CD45+ cells; NK cells are the TCRβ- Nk1.1+ population in CD45+ cells; and B cells are the CD19+ population in CD45+ cells. n=3-5 mice/genotype.

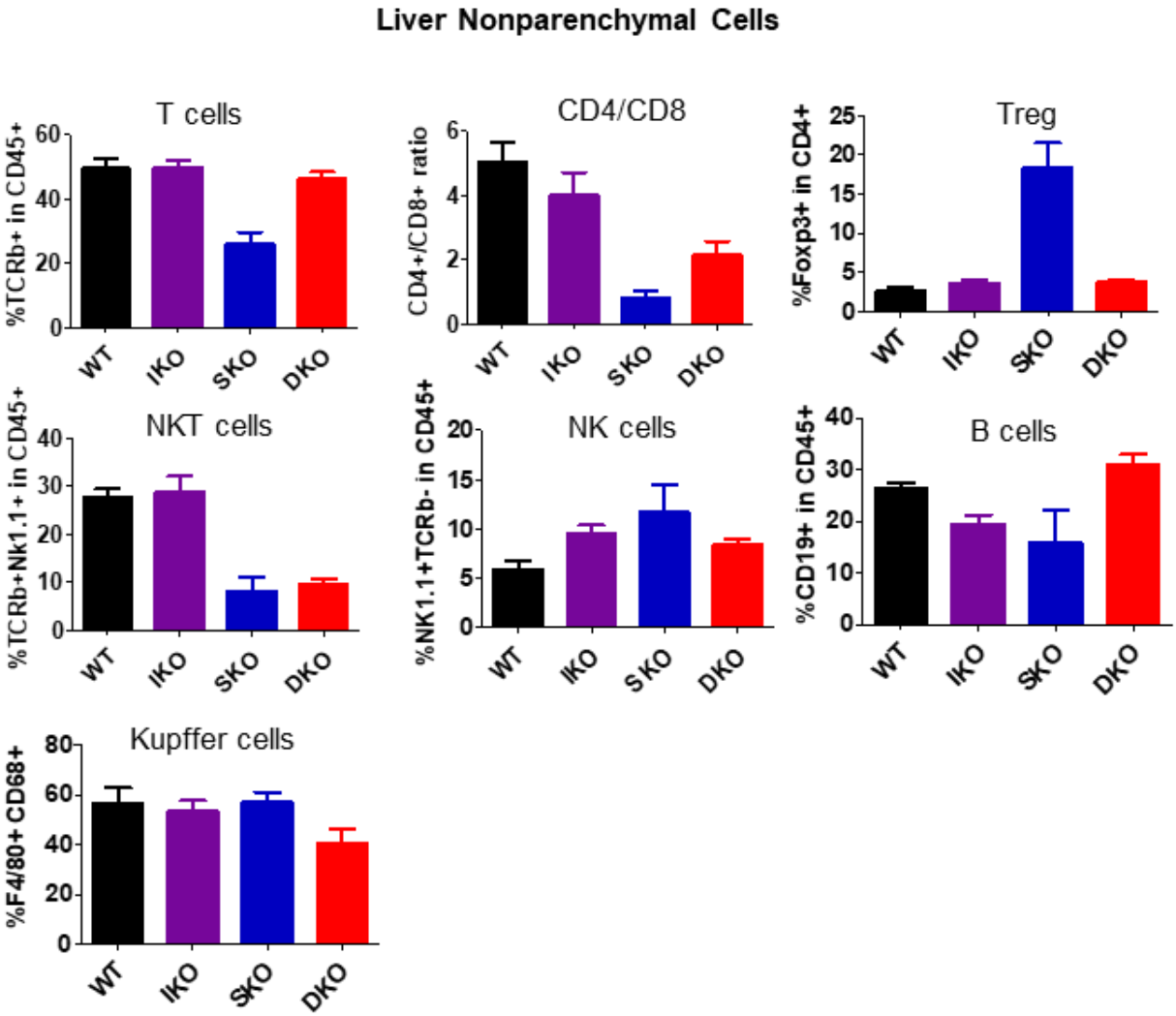

Figure 1.14 Immune populations in knockout livers

Summary of flow cytometric analyses of indicated immune populations in nonparenchymal cells isolated from livers of 8-12-week old untreated mice. Immune subtype were determined as follows: T cells are the TCRβ+ population among CD45+ cells; CD4 cells are the CD4+ population among CD3+ cells; CD8 cells are the CD8+ population among CD3+ cells; regulatory T cells (Treg) are the Foxp3+ population among CD4+ cells; NKT cells are the TCRβ+ Nk1.1+ population in CD45+ cells; NK cells are the TCRβ- Nk1.1+ population in CD45+ cells; B cells are the CD19+ population in CD45+ cells, and Kupffer cells are the F4/80+ population in CD68+ cells. n=3-5 mice/genotype.

by upregulation in cell cycle, cell division and chromosome segregation, with reduced homeostatic processes and cytokine responses as might be reasonably anticipated with both Ikkβ and Shp2 deleted. However, this analytical approach was unable to differentiate which processes were unique to DKO livers.

We then looked at changes specific to DKO, relative to WT, IKO and SKO livers by determining to which gene sets the 258 DKO-unique upregulated genes belonged (Fig.1.17A). These upregulated genes were involved in extracellular matrix deposition, and various immune-related pathways such as myeloid and leukocyte activation (Fig. 1.17B). In support of this, previous GSEA analysis had identified enrichment of several immune processes in the DKO live compared to WT (Fig. 1.18A). Indeed, several transcripts relating to macrophage recruitment were upregulated in DKO livers (Fig. 1.18B). In particular, the mRNAs for the macrophage-recruiting cytokine *Ccl2* and its cognate receptor *Ccr2* were significantly upregulated in the DKO liver tissue only. Additionally, expression of the monocyte chemoattracant *Ccl8* showed a trend towards upregulation in DKO. Immunostaining for the macrophage marker F4/80 also demonstrated increased macrophage presence in DKO livers (Fig. 1.18C). We speculate that these immune alterations were not detected in flow cytometry experiments due to the difficulty in liberating these cells from fibrotic regions prevalent in the DKO liver; indeed, the F4/80+ cells tended to concentrate around portal triads (Fig. 1.18C). Therefore, the immunostaining and RNA-Seq data revealed a previously undetected inflammatory microenvironment in DKO livers.

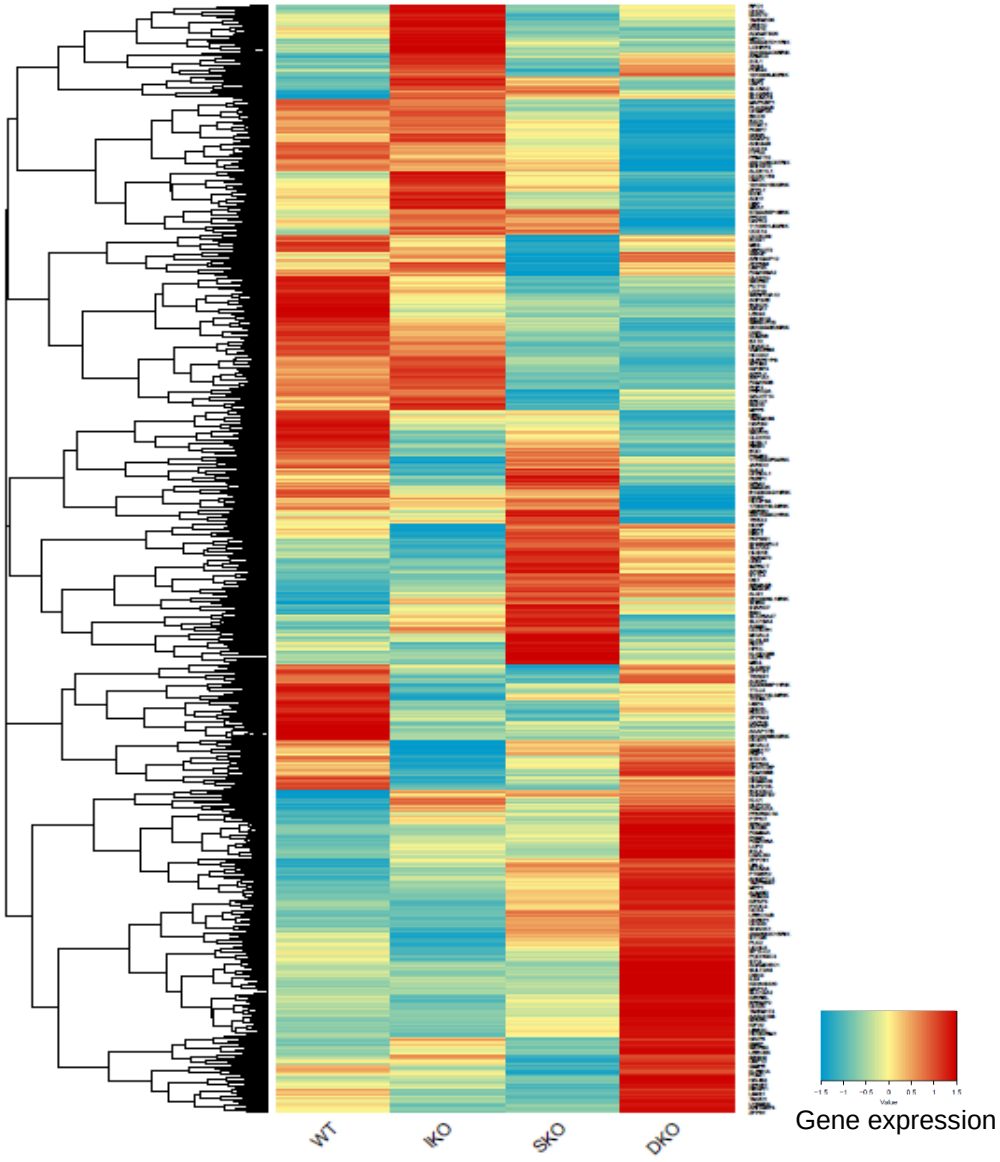

Figure 1.15 Heatmap of gene expression in knockout livers

Heatmap of gene expression levels in WT, IKO, SKO, and DKO livers, generated from RNA-Sequencing (n=3/genotype).

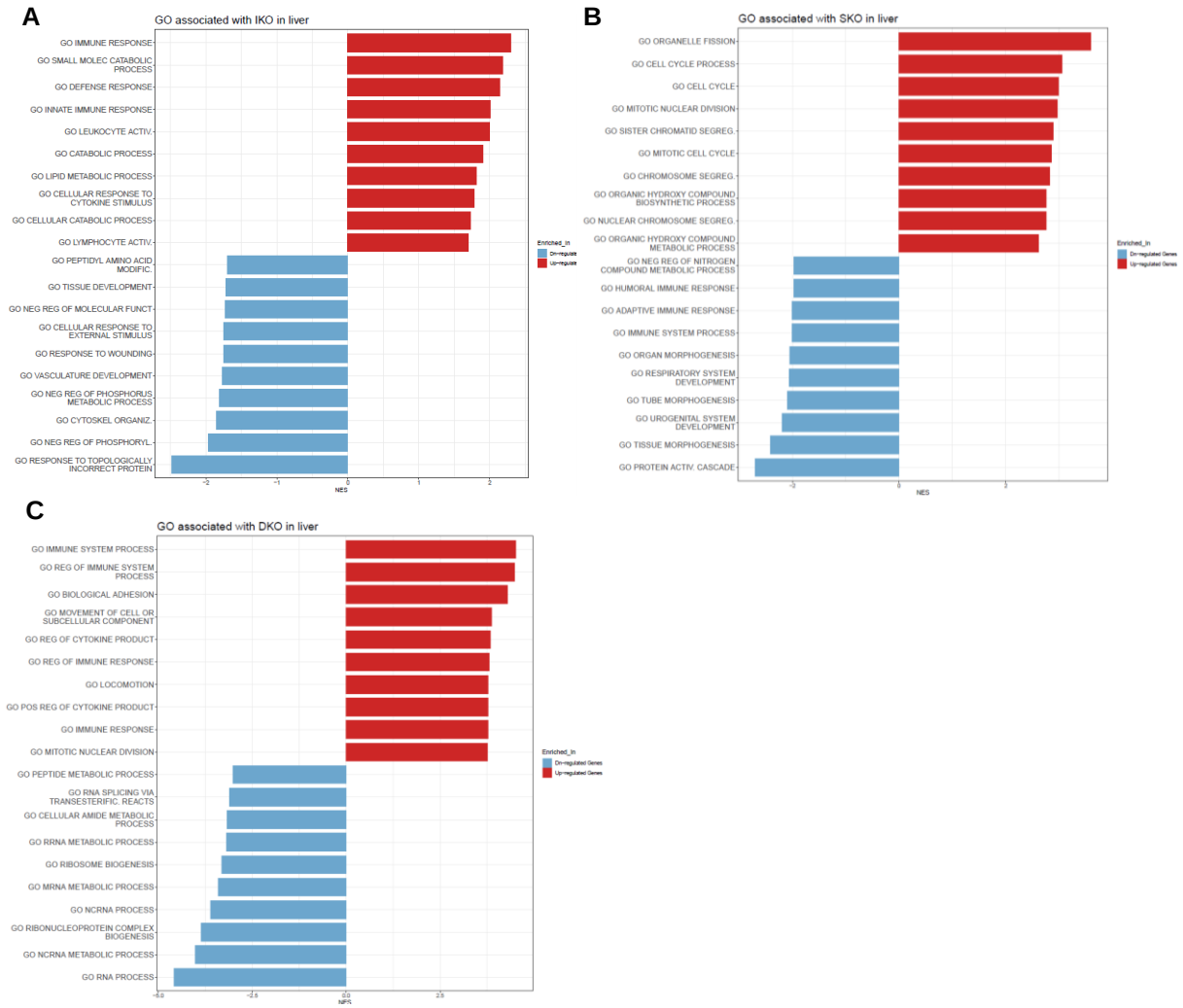

Figure 1.16 Gene set enrichment analysis of knockout livers

A. Top ten positive-and negatively- enriched pathways in IKO livers compared to WT, using GO-BP terms.
B. Top ten positive-and negatively- enriched pathways in SKO livers compared to WT, using GO-BP terms.
C. Top ten positive-and negatively- enriched pathways in DKO livers compared to WT, using GO-BP terms.

NES, normalized enrichment score.

A

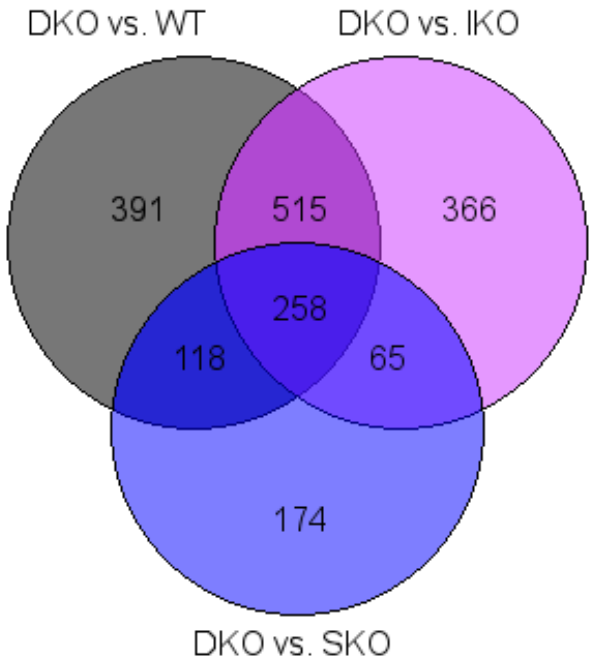

B

Gene Set Name	p-value	FDR
GO_CELL_ACTIVATION	2.88E-22	2.88E-18
GO_COLLAGEN_CONTAINING_EXTRACELLULAR_MATRIX	1.09E-20	5.45E-17
GO_EXTRACELLULAR_STRUCTURE_ORGANIZATION	2.87E-20	9.56E-17
GO_MYELOID_LEUKOCYTE_ACTIVATION	4.09E-20	1.02E-16
GO_EXTRACELLULAR_MATRIX	8.22E-20	1.64E-16
GO_SECRETORY_GRANULE	1.36E-19	2.27E-16
GO_BIOLOGICAL_ADHESION	2.51E-18	3.59E-15
GO_REGULATION_OF_IMMUNE_SYSTEM_PROCESS	1.54E-17	1.93E-14
GO_SECRETION	1.81E-17	2.02E-14
GO_SECRETORY_VESICLE	2.82E-17	2.82E-14

Figure 1.17 Identification of upregulated genes and processes unique to the DKO liver

A. Overlap of genes upregulated in DKO vs. indicated genotype from RNA-Seq analysis of 2-month-old livers. The center of the Venn diagram represents genes that are upregulated in DKO livers compared to all other genotypes.
B. Gene set enrichment analysis of the 258 genes upregulated in DKO livers compared to all other genotypes.

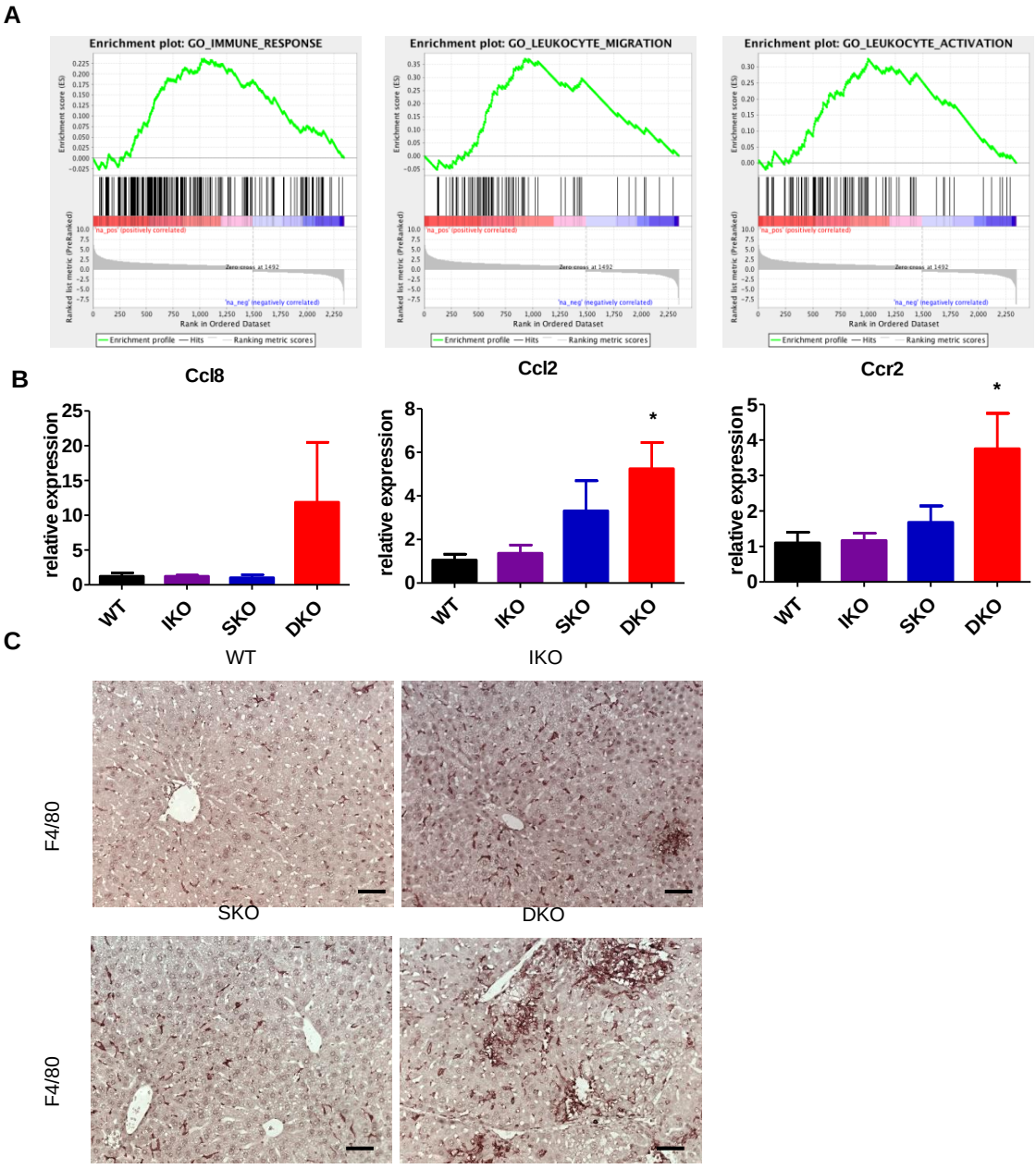

Figure 1.18 Inflammatory changes in DKO livers at young age

A. Enrichment plots of immune-related gene sets for DKO vs WT livers.
B. Expression of mRNAs associated with macrophage recruitment in 2-month-old livers (n=3-5/genotype).
C. Representative immunostaining for the macrophage marker F4/80 in 2-month-old liver sections. Scale bar=100um.

Multiple comparisons were performed using one-way ANOVA with Tukey post-hoc analysis (*P<0.05; **P<0.01; ***P<0.001).

Also noted in the DKO liver were altered metabolic pathways (Fig. 1.16C). As before, we probed the gene-set segregation of DKO-specific downregulated transcripts, and found that perturbed metabolic gene sets included metabolism of lipids and amino acids, transport of metabolic components, and oxidative processes (Fig. 1.19A,B). Enrichment plots of select metabolic pathways are shown in Fig. 1.20A. We examined changes in several metabolic pathways in more detail, using heatmaps of pathway components; this revealed distinct patterns of gene expression in each single knockout, with the DKO again most profoundly perturbed compared to WT(Fig. 1.20B). We then validated expression changes in select metabolic genes identified from the RNA-Seq results; indeed, the fatty acid metabolic genes *Aacs* and *Fabp* were downregulated in DKO liver (Fig. 1.20C). Together, these results suggest that removal of both Ikkβ and Shp2 caused more severe hepatic damages and metabolic changes relative to the two single gene knockouts, showing additive effects of dual gene deletion. These changes collectively made up a tumor-promoting microenvironment in DKO livers, contributing to more severe HCC development induced by DEN.

Chapter 1 is adapted from material that has been submitted for publication: Hanley, Kaisa L.; Lin, Xiaoxue; Liang, Yan; Yang, Meixiang; Karin, Michael; Fu, Wenxian; and Feng, Gen-Sheng. “Concurrent Disruption of Ras/MAPK and NF-κB Pathways Induces Circadian Deregulation and Hepatocarcinogenesis”. The dissertation author was the primary investigator and author of this paper.

A

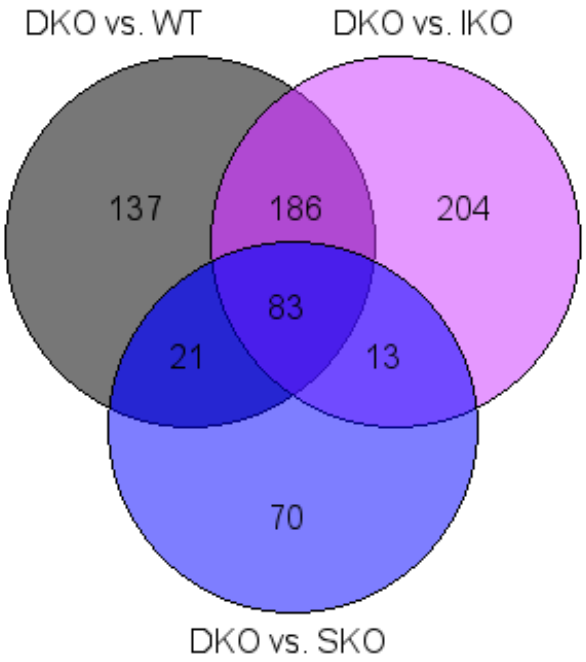

B

Gene Set Name	# Genes in Overlap (k)	p-value	FDR
GO_LIPID_METABOLIC_PROCESS	12	2.03E-07	1.50E-03
GO_MONOCARBOXYLIC_ACID_METABOLIC_PROCESS	8	4.67E-07	1.72E-03
GO_FATTY_ACID_METABOLIC_PROCESS	6	2.19E-06	5.36E-03
GO_CELLULAR_LIPID_METABOLIC_PROCESS	9	5.44E-06	8.67E-03
GO_ORGANIC_ACID_METABOLIC_PROCESS	9	6.39E-06	8.67E-03
GO_ORGANIC_ANION_TRANSPORT	7	7.07E-06	8.67E-03
GO_RESPONSE_TO_TOXIC_SUBSTANCE	7	1.12E-05	1.04E-02
GO_OXIDATION_REDUCTION_PROCESS	9	1.13E-05	1.04E-02
GO_RESPONSE_TO_DRUG	9	1.66E-05	1.36E-02
GO_RESPONSE_TO_OXYGEN_CONTAINING_COMPOUND	11	2.00E-05	1.47E-02

Figure 1.19 Identification of downregulated genes and processes unique to the DKO liver

A. Left, overlap of genes downregulated in DKO vs. indicated genotype from RNA-Seq analysis of 2-month-old livers. The center of the Venn diagram represents genes that are downregulated in DKO livers compared to all other genotypes.
B. Gene set enrichment of the 83 genes downregulated in DKO livers compared to all other genotypes.

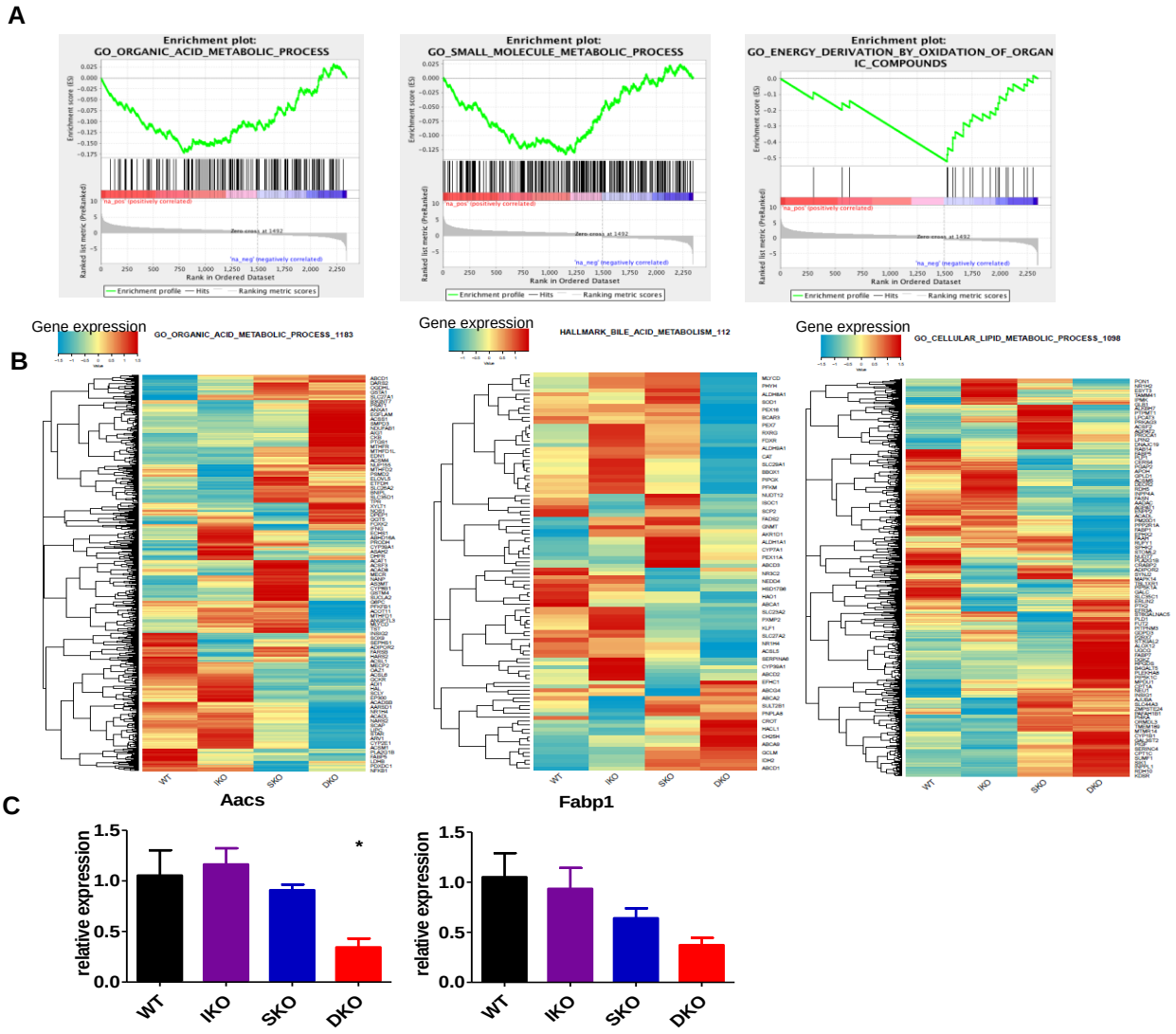

Figure 1.20 Multiple metabolic disruptions occur in DKO livers

A. Enrichment plots of metabolic processes in DKO liver compared to WT.
B. Heatmaps of select metabolic pathway gene expression in 2-month-old livers (n=3/genotype).
C. mRNA levels of lipid metabolic enzymes in whole-liver lysates from 2-month-old male mice (n=3-5/genotype).

Multiple comparisons were performed using one-way ANOVA with Tukey post-hoc analysis (*P<0.05; **P<0.01; ***P<0.001).

Chapter 2. Combined Ras/MAPK and NF-κB suppression cause accelerated hepatocyte proliferation and circadian deregulation

As described above, severe hepatic injuries, altered inflammatory/immune responses and disordered metabolic pathways constituted a tumor-conducive microenvironment in DKO liver, which illustrated its augmented susceptibility to chemical carcinogen. However, these environmental factors were apparently not sufficient to drive spontaneous HCC development without hepatocyte-intrinsic oncogenic changes. To identify the driver(s), we performed RNA-seq analysis with isolated hepatocytes, which would allow us to parse out hepatocyte-specific changes triggered by the targeted gene deletion (Fig. 2.1).

2.1 Cell cycle related genes are upregulated in DKO hepatocytes

Comparison of the transcriptomes (Fig. 2.2) revealed higher ROS levels, disordered metabolic pathways and reduced cell proliferation in IKO hepatocytes (Fig. 2.2A), while SKO hepatocytes displayed changes in innate immunity and interferon response, and epigenetic regulators (Fig. 2.2B). Notably, comparing DKO hepatocytes with WT control disclosed significantly increased expression of genes involved in cell mitosis, chromosome segregation and antigen processing (Fig. 2.2C).

We then compared the transcriptomes of DKO hepatocytes against WT, IKO, and SKO groups to identify changes induced specifically by dual loss of Ikkβ and Shp2 (Fig. 2.2A). This analysis revealed unique upregulation of 148 genes in DKO hepatocytes only, the majority of which were integral pro-mitotic genes or part of cell

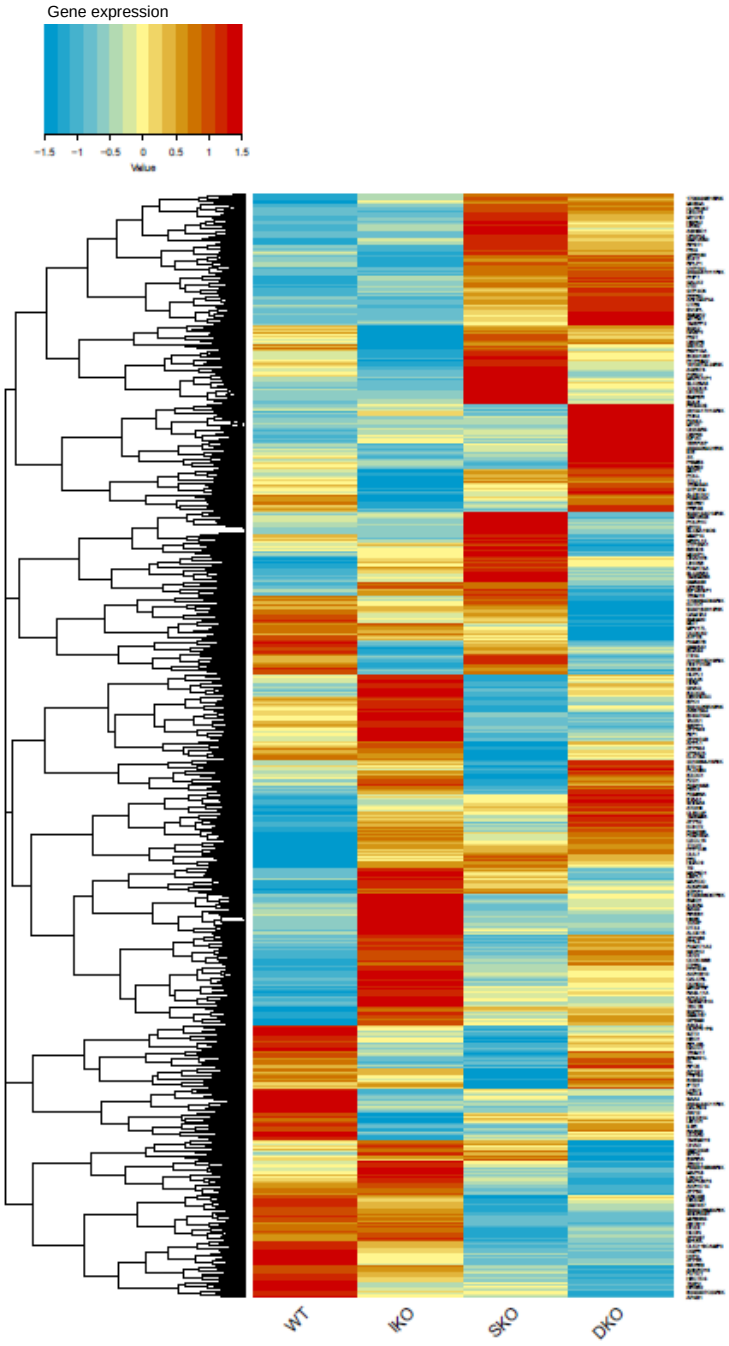

Figure 2.1 Heatmap of gene expression in knockout hepatocytes.

Heatmap of gene expression levels in hepatocytes isolated from WT, IKO, SKO, and DKO livers, generated from RNA-Sequencing (n=3/genotype).

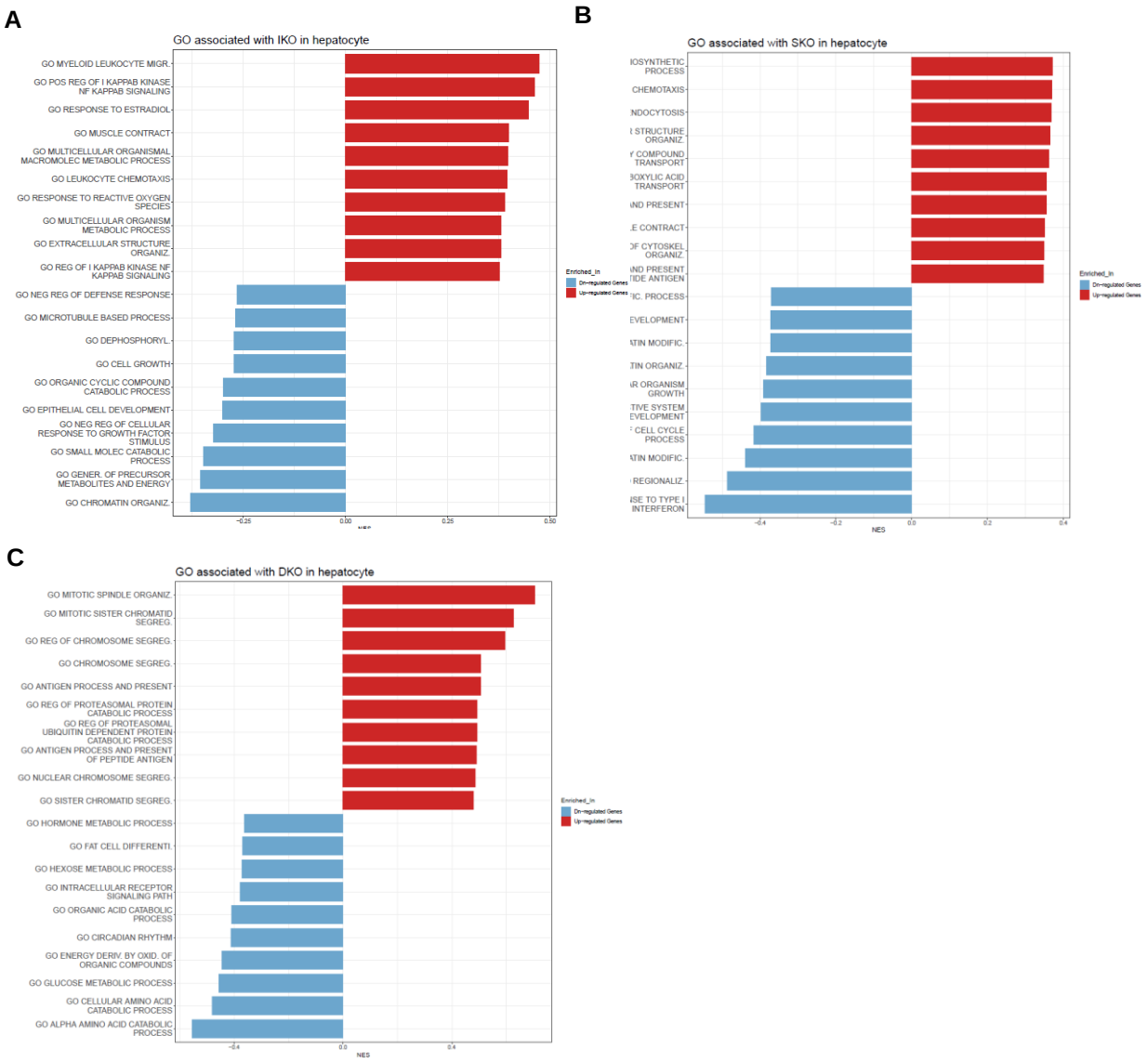

Figure 2.2 Gene set enrichment analysis of isolated hepatocytes

A. Top ten positive-and negatively- enriched pathways in IKO livers compared to WT, using GO-BP terms.
B. Top ten positive-and negatively- enriched pathways in SKO livers compared to WT, using GO-BP terms.
C. Top ten positive-and negatively- enriched pathways in DKO livers compared to WT, using GO-BP terms.

NES, normalized enrichment score.

A

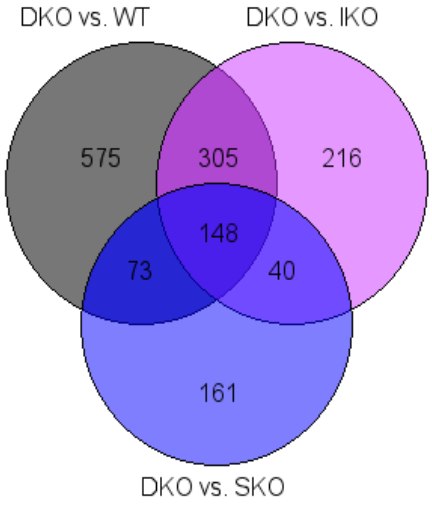

B

Gene Set Name	# Genes in Overlap	p-value	FDR
GO_CELL_CYCLE	61	5.82E-44	4.41E-40
GO_MITOTIC_CELL_CYCLE	49	5.97E-42	2.26E-38
GO_CELL_DIVISION	41	1.93E-41	4.87E-38
GO_CELL_CYCLE_PROCESS	52	1.95E-39	3.69E-36
GO_CHROMOSOME_SEGREGATION	32	5.24E-37	7.94E-34
GO_MITOTIC_NUCLEAR_DIVISION	30	2.49E-36	3.14E-33
GO_SISTER_CHROMATID_SEGREGATION	26	6.69E-34	7.24E-31
GO_ORGANELLE_FISSION	33	9.28E-34	8.78E-31
GO_NUCLEAR_CHROMOSOME_SEGREGATION	28	2.78E-33	2.34E-30
GO_MITOTIC_SISTER_CHROMATID_SEGREGATION	22	4.51E-29	3.42E-26

Figure 2.3 Identification of upregulated genes and processes unique to DKO hepatocytes

A. Overlap of genes upregulated in DKO vs. indicated genotype from RNA-Seq analysis of 2-month-old hepatocytes. The center of the Venn diagram represents genes that are upregulated in DKO hepatocytes compared to all other genotypes.
B. Gene set enrichment of the 148 genes upregulated in DKO hepatocytes compared to all other genotypes.

cycle-related pathways (Fig. 2.3A,B). This data indicates that the most distinguished feature of DKO hepatocytes is augmented cell cycle progression and cell division. Consistent with the RNA-seq data, immunostaining of liver sections detected significantly increased hepatocyte proliferation in mutant livers using antibodies for the proliferation marker Ki67 and the hepatocyte marker HNF4α (Fig. 2.4). qRT-PCR analysis showed marked upregulation of multiple growth factors, including HGF, IL-6, TNFα, PDGF-B, and PDGF-D, which were known to spur compensatory hepatocyte proliferation in damaged livers (Fig. 2.5).

Although several growth-promoting factors were upregulated at the transcript level, the downstream proliferative signaling induced by these factors mainly involves activation of NF-κB or Ras/ERK. To ensure that the observed proliferation was indeed proceeding despite suppression of these classically considered pro-growth pathways, we isolated hepatocytes from WT, IKO, SKO and DKO livers and examined the activation status of Ras/MAPK and NF-κB pathway components. Removal of Shp2 indeed blunted Erk phosphorylation and activation by HGF in both SKO and DKO hepatocytes (Fig. 2.6), and loss of Ikkβ suppressed p-IκBα and p-p65 levels following TNFα stimulation in IKO and DKO hepatocytes *in vitro* (Fig. 2.7). Following IL-6 stimulation, p-Erk and p-Akt levels were inhibited in SKO and DKO hepatocytes, with similarly increased p-Stat3 levels (Fig. 2.8) consistent with Shp2's role in suppressing Stat3 activation. As Stat3 activation had previously been implicated in chemical carcinogenesis in both IKO and SKO livers (Bard-Chapeau et al., 2011; He et al., 2010), we investigated whether Stat3 targets were enriched in

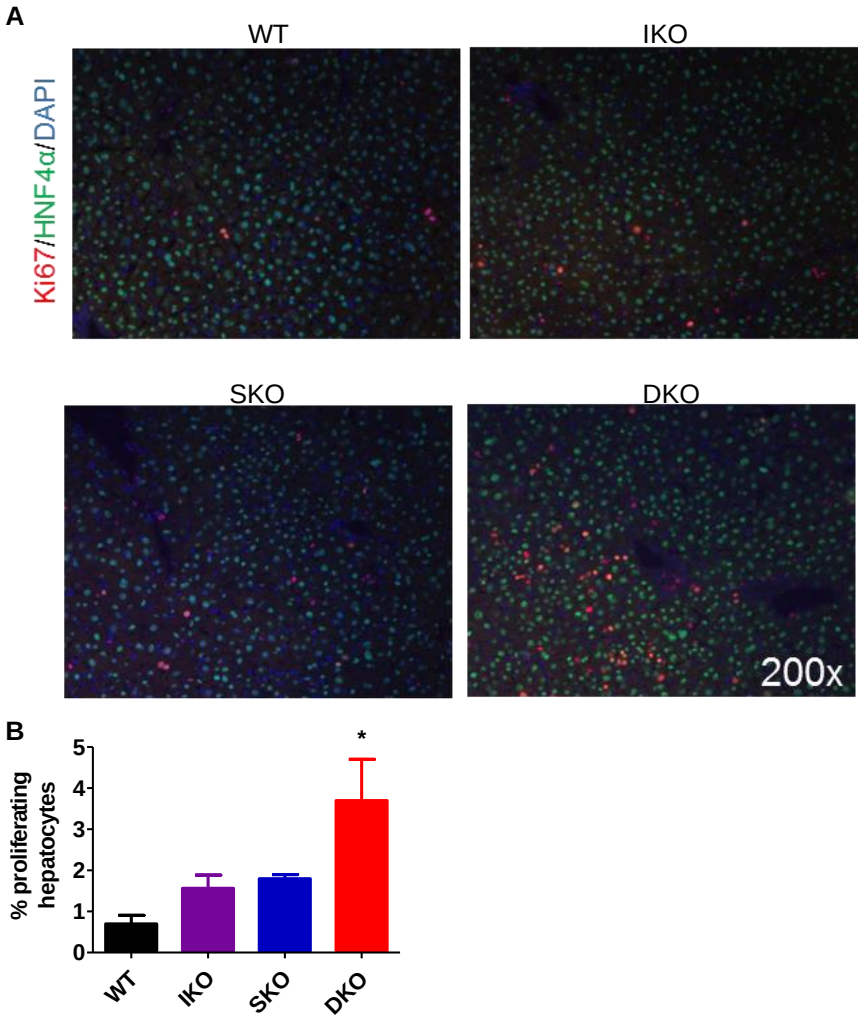

Figure 2.4 Co-immunofluorescence to detect proportion of proliferating hepatocytes *in vivo*

A. Co-immunofluorescence of the proliferation marker Ki67 and the hepatocyte marker HNF4α in sections of livers at 2 month of age.
B. Quantification of proliferating hepatocytes ($Ki67^+$ $HNF4\alpha^+$ cells).

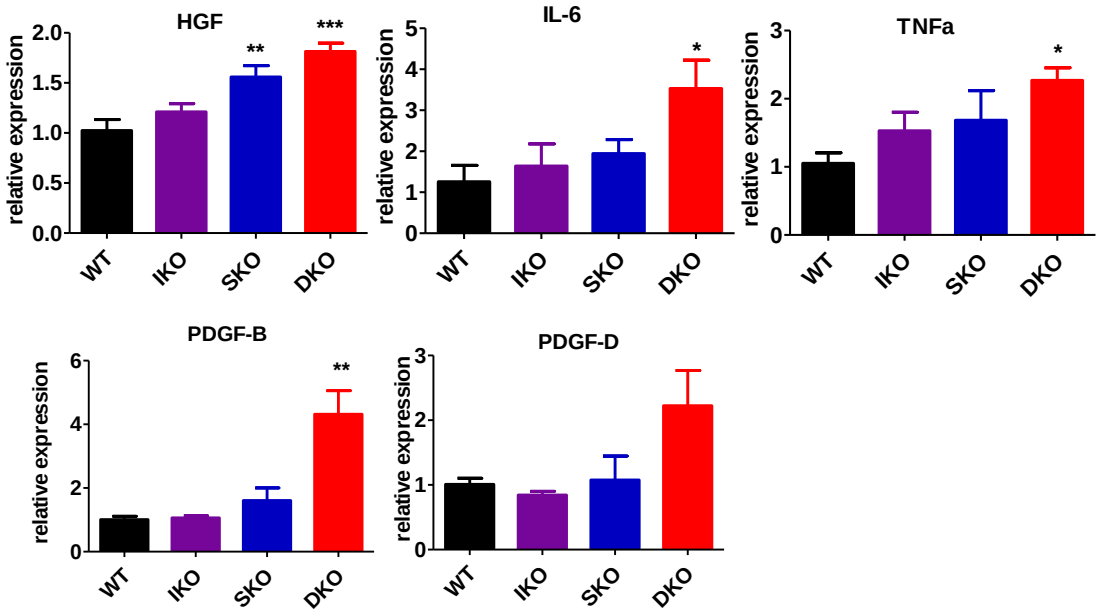

Figure 2.5 Expression of growth factors in knockout livers

mRNA expression of growth-stimulating factors in 2-month-old livers (n=3-5/genotype).
Multiple comparisons were performed using one-way ANOVA with Tukey post-hoc analysis (*P<0.05; **P<0.01; ***P<0.001).

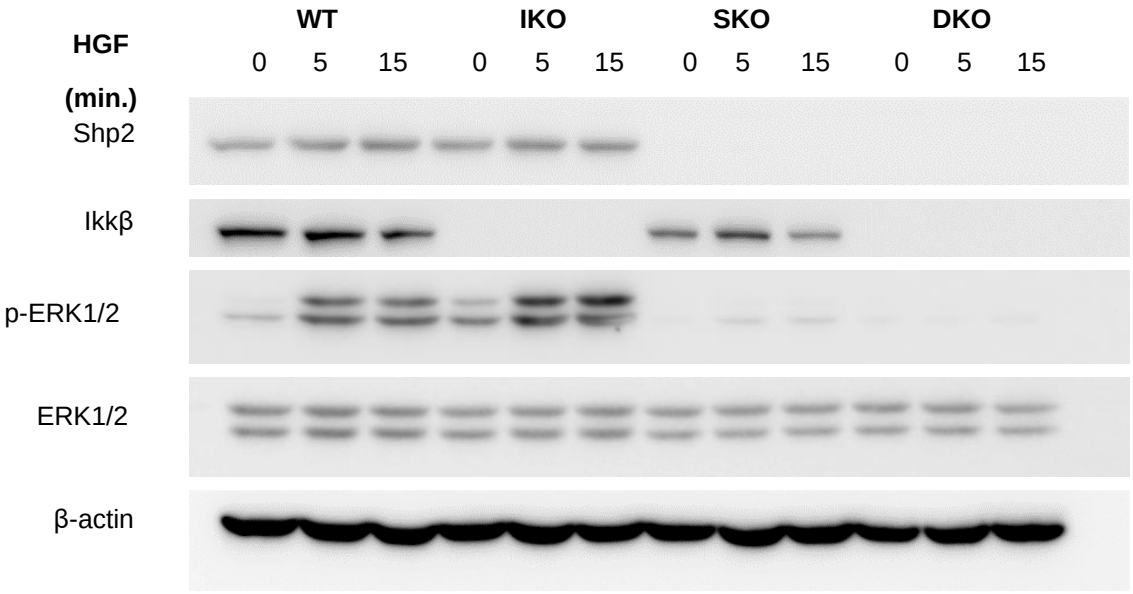

Figure 2.6 Signaling suppression of Ras/ERK pathway in SKO and DKO hepatocytes

Representative immunoblot of ERK activation, as assessed by levels of phosphorylated ERK, in isolated hepatocytes of indicated genotypes treated with 20 ng/ml mouse recombinant HGF.

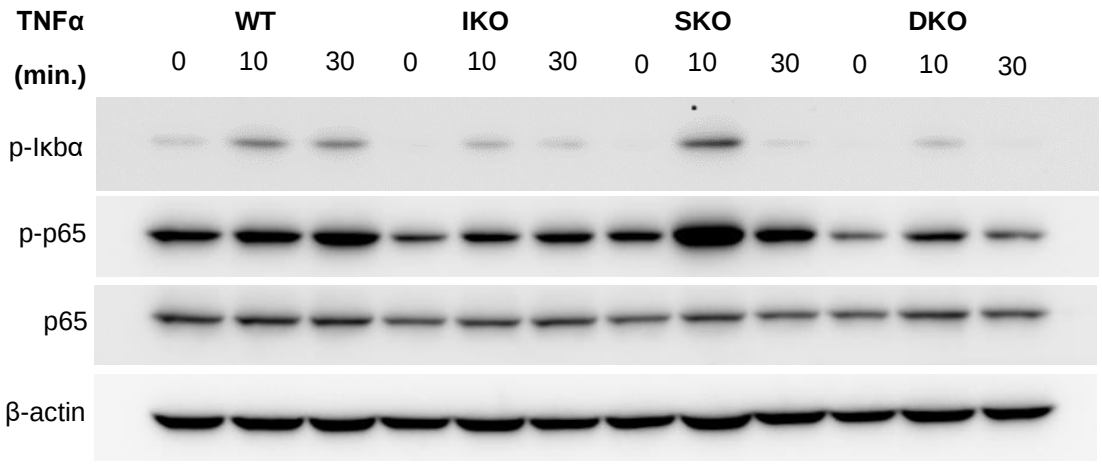

Figure 2.7 Signaling suppression of the NF-kB pathway in IKO and DKO hepatocytes

Representative immunoblot of NF-κB pathway constituents in isolated hepatocytes of the indicated genotype treated with 10 ng/ml mouse recombinant TNFα.

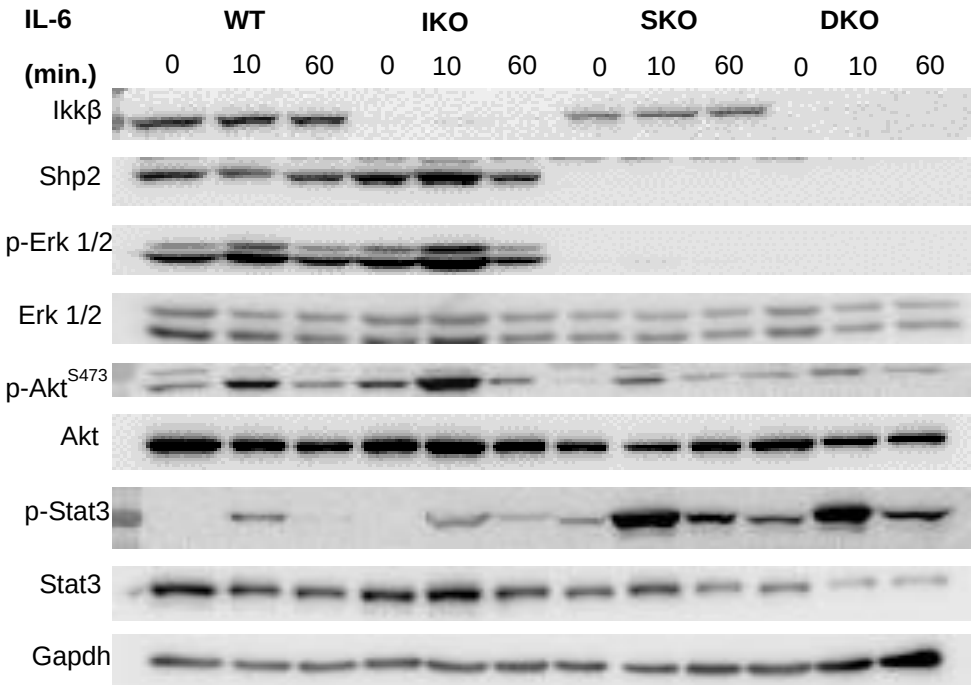

Figure 2.8 Disrupted signaling in response to IL-6 in SKO and DKO hepatocytes

Representative immunoblot of growth-promoting pathway members in isolated hepatocytes of the indicated genotype treated with 20ng/ml mouse recombinant IL-6.

either SKO or DKO models without DEN treatment. However, at this early stage, Stat3 target genes were not positively enriched in hepatocytes of any genotype (Table 2.1), making their involvement in proliferation and tumor initiation in the DKO model unlikely.

Therefore, both the Ras/MAPK and NF-κB pathways were indeed disrupted in hepatocytes deficient for Shp2 and Ikkβ. Furthermore, the expression of onco-fetal genes *Afp* and *Igf2* were upregulated in DKO livers in young mice at the pre-cancer stage, before detection of macroscopic tumors (Fig. 2.9). These results argue that the Ras/MAPK and NF-κB pathways are less critical for driving cell division than previously thought, and are actually dispensable for hepatocyte proliferation and transformation *in vivo*.

2.2. Clock genes are deregulated in DKO hepatocytes

While the accelerated proliferation was apparent in DKO hepatocytes, transcriptomic analysis of upregulated genes did not reveal increased activity of any alternative oncogenic pathways that might explain that phenomenon. Therefore, we then assessed the function of downregulated genes in DKO hepatocytes. IKO and SKO hepatocytes shared downregulation of cell division processes (Fig. 2.2A,B), while DKO hepatocytes demonstrated the metabolic changes already detected in whole liver (Fig. 2.2C). Intriguingly, despite being freshly isolated during the same time interval (ZT7-11), DKO hepatocytes also exhibited changes to circadian pathways. These results provided a potential explanation for the tumorigenic

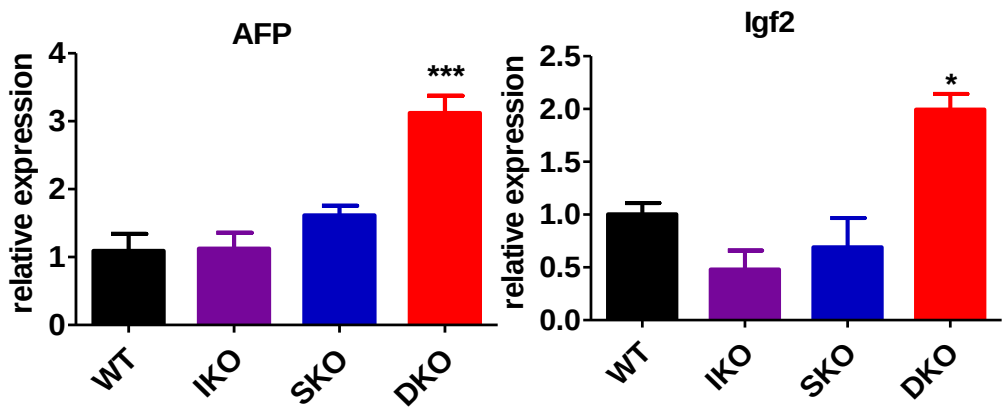

Figure 2.9 Early expression of onco-fetal genes in DKO livers

qPCR analysis of expression levels of onco-fetal mRNAs Afp and Igf2 in 2-month-old livers (n=3-5/genotype).
Multiple comparisons were performed using one-way ANOVA with Tukey post-hoc analysis (*P<0.05; **P<0.01; ***P<0.001).

phenotype of DKO mice due to the well-established link between circadian clock, accelerated cellular proliferation, and cancer (Masri and Sassone-Corsi, 2018).

To confirm that these processes were unique to the DKO hepatocytes, we interrogated the 90 genes that were downregulated in DKO hepatocytes only, as compared to WT, IKO and SKO (Fig. 2.10A). Interestingly, the most significant gene set changes were those involved in control of physiological homeostasis, the circadian clock and the response to light stimulus, as well as metabolic pathways (Fig. 2.10B). Specifically, we found that the expression of 13 circadian genes was dramatically inhibited in DKO hepatocytes, including inhibitory components Bhlhe40 (Dec1) and Bhlhe41 (Dec2); the transcription factor Klf10; core clock inhibitors Cry2, Per2, and Per3; clock-implicated nuclear receptor Rorc; Srebf1, Usp2 (ubiquitin specific peptidase 2), Tef (TF), Ccrn4l (deadenylase), Map2k6 (Erk kinase 6), Ciart (transcriptional repressor) (Fig. 2.11). Among them, the majority (10/13) were transcription factors that are negative or positive regulators of the clock system.

Consistent with the RNA-seq data, qRT-PCR analysis detected very low levels of mRNAs for *Per2, Per3, Cry1, Cry2* and *Dbp* in hepatocytes isolated from 2-month-old DKO mice (Fig. 2.12). Of note, these genes were expressed at similar or even higher levels in IKO and SKO hepatocytes than the WT (Fig. 2.11,2.12), suggesting that their drastic inhibition in DKO hepatocytes was not due to a simple additive effect of dual gene deletion. Rather, it was a specific defect in hepatocytes induced only by combined disruption of the two pathways. This is so far the most dramatic DKO-unique phenotype that affects circadian-related TFs so broadly. We further validated disrupted clock activity by examining enrichment of target genes for positive and

A

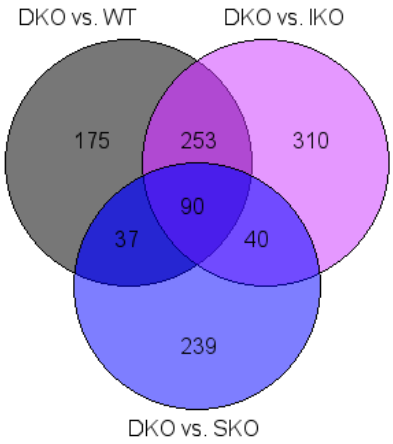

B

Gene Set Name	# Genes in Overlap	p-value	FDR
GO_CIRCADIAN_REGULATION_OF_GENE_EXPRESSION	9	6.60E-15	5.00E-11
GO_RHYTHMIC_PROCESS	13	2.22E-14	8.39E-11
GO_CIRCADIAN_RHYTHM	11	4.03E-13	1.02E-09
GO_REGULATION_OF_CIRCADIAN_RHYTHM	8	9.28E-11	1.76E-07
GO_PHOTOPERIODISM	5	4.89E-09	7.22E-06
GO_ENTRAINMENT_OF_CIRCADIAN_CLOCK	5	5.72E-09	7.22E-06
GO_LIPID_METABOLIC_PROCESS	15	7.06E-08	7.64E-05
GO_HOMEOSTATIC_PROCESS	17	1.22E-07	1.16E-04
GO_NEGATIVE_REGULATION_OF_TRANSCRIPTION_BY_RNA_POLYMERASE_II	12	1.63E-07	1.37E-04
GO_SMALL_MOLECULE_BIOSYNTHETIC_PROCESS	10	1.15E-06	8.72E-04

Figure 2.10 Identification of downregulated genes and processes unique to DKO hepatocytes

A. Overlap of genes downregulated in DKO vs. indicated genotype from RNA-Seq analysis of 2-month-old hepatocytes. The center of the Venn diagram represents genes that are downregulated in DKO hepatocytes compared to all other genotypes.
B. Gene set enrichment of the 90 genes upregulated in DKO hepatocytes compared to all other genotypes.

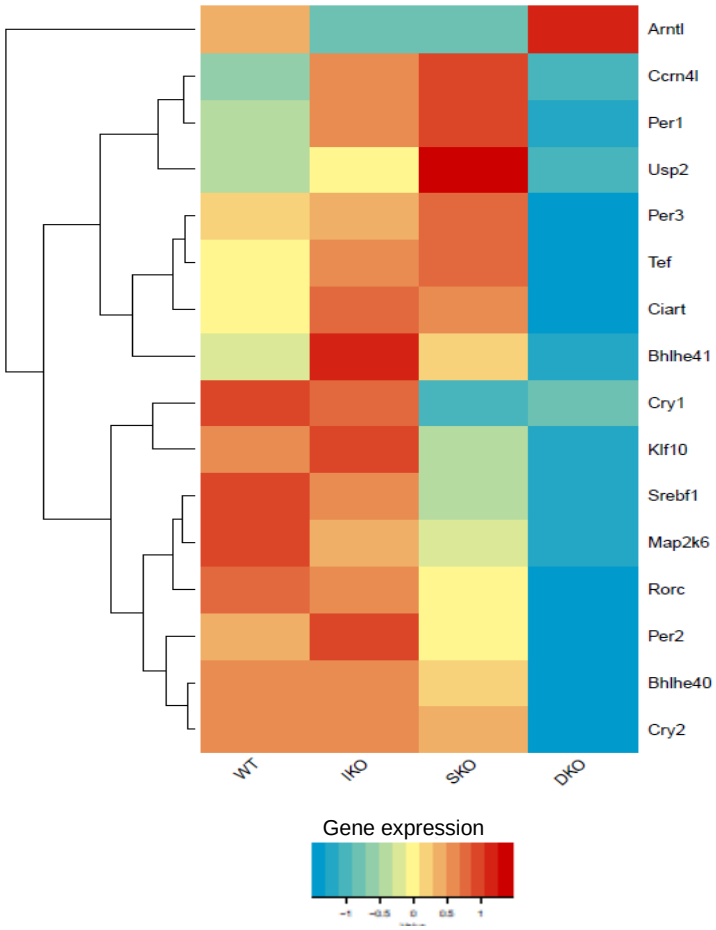

Figure 2.11 Circadian clock genes are dysregulated in DKO hepatocytes

Heatmap showing relative expression of differentially-expressed circadian genes identified from RNA-Seq analysis (n=3/genotype).

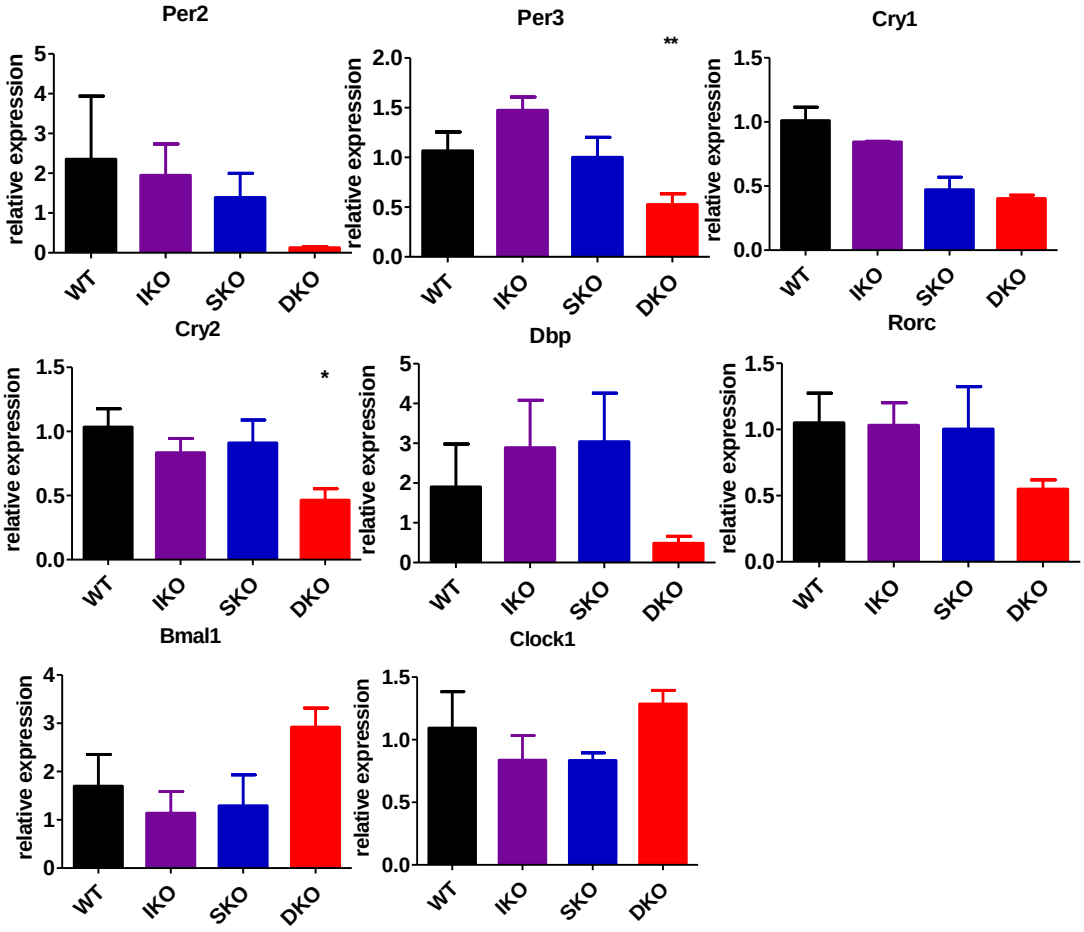

Figure 2.12 Validation of clock gene disruption in DKO hepatocytes

qPCR validation of circadian clock gene expression in isolated hepatocytes (n=3-5/genotype).
Multiple comparisons were performed using one-way ANOVA with Tukey post-hoc analysis (*P<0.05; **P<0.01; ***P<0.001).

negative clock regulators. Consistent with previous indications of clock dysfunction, we found that target genes of the negative clock regulators BHLHE40/Dec1 and BHLHE41/Dec2 were negatively enriched in DKO hepatocytes compared to IKO and SKO (Table 2.2). Target genes of the clock effector Arntl/Bmal1 were positively enriched in DKO, providing further evidence that clock regulation and output are disrupted in the DKO model (Table 2.1). Given that disruption of circadian rhythm or deletion of clock regulators in murine livers were reportedly sufficient to induce HCC (Kettner et al., 2016), we believe that circadian dysfunction is a key driver for spontaneous HCC development in DKO mice.

2.3 Disordered expression of circadian clock genes in human HCC

To explore relevance of the mouse data to human HCC, we analyzed 371 HCC patient samples and 50 adjacent normal liver tissues in a TCGA dataset. Based on expression levels of circadian clock genes in tumor tissues compared to non-tumor tissues, we divided HCC samples into three groups: (1) circadian clock-normal, (2) circadian clock-mid, (3) circadian clock-dysregulated. Specifically, we checked expression of 7 core clock genes, including *CLOCK*, *ARNTL*, *PER1*, *PER2*, *PER3*, *CRY1*, and *CRY2*. Patients with at most 2 dysregulated circadian genes were assigned into “normal” group, patients with at least 5 dysregulated clock genes into “dysregulated” group, others into “mid” group. With sub-clustering of all HCC patients, we performed differential expression analysis between “normal” and “dysregulated” groups using DESseq2. The genes with adjusted p value < 0.05 were defined as differentially expressed. We specifically checked components in Ras/MAPK pathway

or NF-κB pathway, and generated volcano plots with differentially expressed genes in the two pathways (Fig. 2.13A,B). This revealed that multiple constituents of each pathway were disrupted in patients with abnormal clock gene expression. Significantly lowered genes included Ras/MAPK genes *Raf1, Sos1,* as well *Mapk1* and *Map2k,* encoding ERK and MEK, respectively (Fig. 2.13B); notable downregulated NF-κB genes included *Nfkb1* and *Ikbkg*, which encodes Ikkγ/NEMO (Fig. 2.13A). Next, to verify whether activities of these two pathways were inhibited in the "clock-dysregulated" group, we collected downstream targets of Ras/MAPK and NF-κB pathways from Msigdb gene sets, respectively. The pathway activity was defined as the sum of rank-transformed normalized values of all genes in a corresponding gene set. These analyses revealed correlation of dysregulated circadian genes with downregulation in both Ras/MAPK and NF-κB pathways in HCC patients (Fig.2.14A,B).

Previous analyses of TCGA data identified a link between lower levels of a circadian "signature" and worse overall survival in multiple cancer types, including liver cancer. This signature was also found to correlate with disruption of other pathways; these associated pathways were highly tissue-specific (Liu et al., 2019). In liver cancer (LIHC cohort), a lower clock signature was linked to elevated proliferation and disruption of a wide range of metabolic pathways. To determine whether the changes induced by disruption of Ras/MAPK and NF-κB signaling produced a similar transcriptional signature to human clock-disrupted HCC, we assessed enrichment for these gene sets in our DKO model (Fig. 2.15). The majority of the clock-associated gene sets from human data were indeed altered in DKO hepatocytes compared to

A

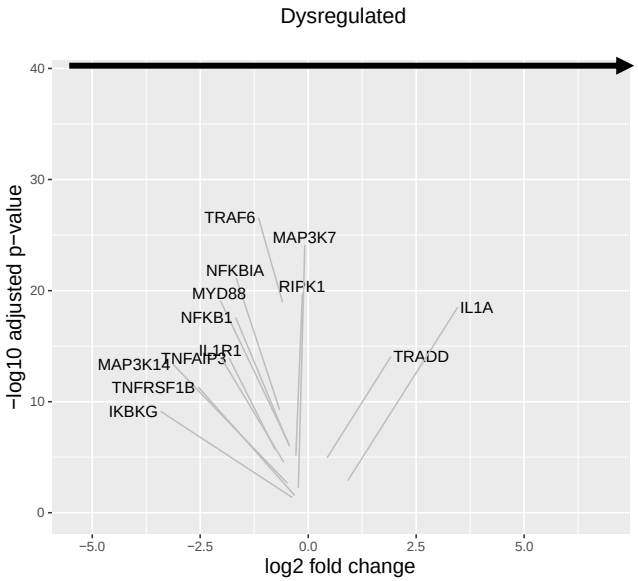

B

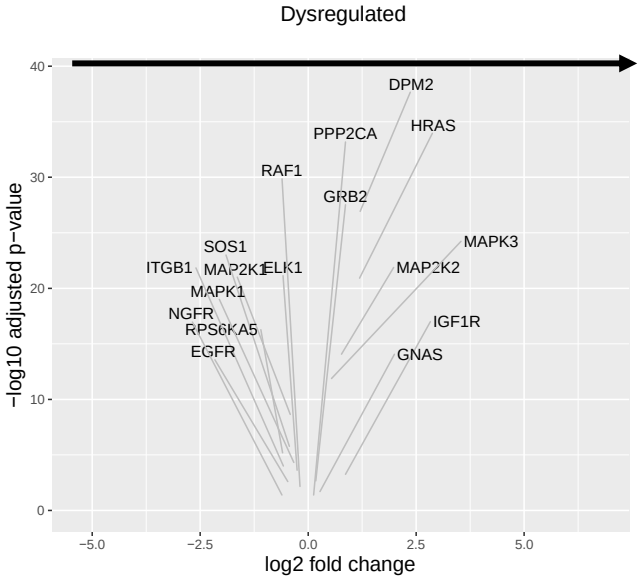

Figure 2.13. Clock gene dysregulation is associated with altered expression of NF-κB and Ras/MAPK pathway members in human HCC

A. Volcano plots of differentially expressed NF-κB pathway components in clock-dysregulated human HCCs (adjusted p<.05).
B. Volcano plots of differentially expressed Ras/MAPK pathway components in clock-dysregulated human HCCs (adjusted p<.05).

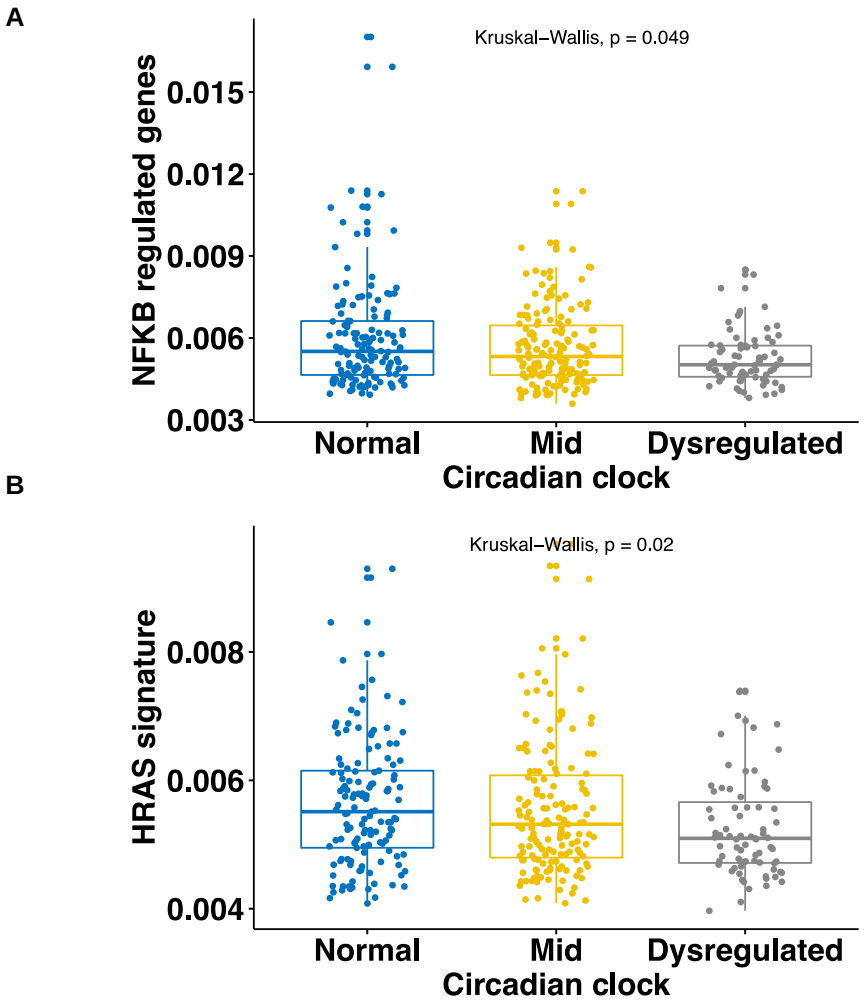

Figure 2.14 Circadian deregulation is associated with lower NF-κB and Ras/MAPK target gene expression in human HCC

A. NF-κB target gene expression profiles in human HCCs with Normal, Mid (<5 clock genes disrupted), or Dysregulated (>5 clock genes disrupted) circadian status.
B. HRas target gene expression profiles in human HCCs as classified above.

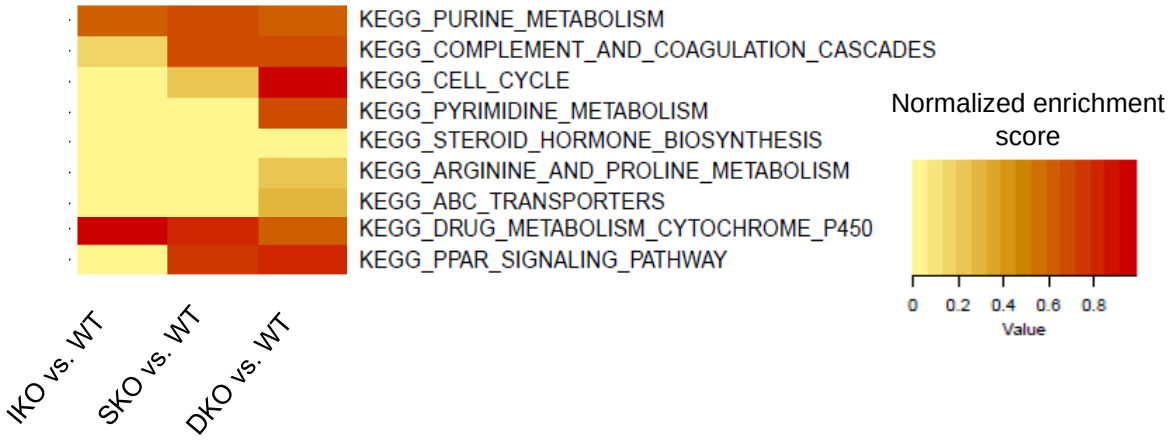

Figure 2.15 Transcriptional similarities between DKO mice and clock-disrupted human HCCs

Enrichment for KEGG pathways previously identified to correlate with disrupted circadian processes in human HCC. The expression of genes in these pathways was compared between WT and knockout hepatocytes isolated from 2-month-old livers. The differential expression was used to assess pathway enrichment in each genotype, shown in the heatmap above.

WT, with less enrichment seen in IKO or SKO hepatocytes. We then determined whether individual circadian genes downregulated in this mouse model were associated with prognosis of HCC patients. Indeed, lower quartile expression of *Per1, Rorc,* and *Cry2* was significantly associated with poorer overall survival (Fig. 2.16). Thus, impaired expression of individual clock genes was directly linked to disease progression and prognosis in human HCC. Together, these results demonstrate that this novel mechanism of HCC development unveiled in a compound mutant mouse model is indeed relevant to the pathogenesis of human HCC.

From these human and mice data, we propose a model in which NF-κB and Ras/MAPK signaling coordinately regulate the circadian clock. When both pathways are disrupted, clock disfunction contributes to a wide range of pathological changes, including disrupted bile acid homeostasis, altered lipid metabolism, and inflammation. This drives aberrant hepatocyte proliferation and transformation, as well as providing a tumor-promoting microenvironment. Together, these oncogenic changes drive spontaneous HCC formation. We believe it likely that some microenvironmental cues (i.e. elevated bile acids) feed back to further disrupt clock function. Additionally, Ras/MAPK and NF-κB pathways are also likely to directly contribute to the pathological changes seen in this model. For example, Shp2 has previously been shown to regulate intrahepatic bile acid levels, and loss of NF-κB signaling could sensitize hepatocytes to cholestatic damage by promoting apoptosis, which would also increase hepatic inflammation. This coordinate regulation of multiple homeostatic processes could help explain the tumor-suppressive role of basal NF-κB and Ras/MAPK signaling in the liver (Scheme 2.1).

Chapter 2 is adapted from material that has been submitted for publication: Hanley, Kaisa L.; Lin, Xiaoxue; Liang, Yan; Yang, Meixiang; Karin, Michael; Fu, Wenxian; and Feng, Gen-Sheng. “Concurrent Disruption of Ras/MAPK and NF-κB Pathways Induces Circadian Deregulation and Hepatocarcinogenesis”. The dissertation author was the primary investigator and author of this paper.

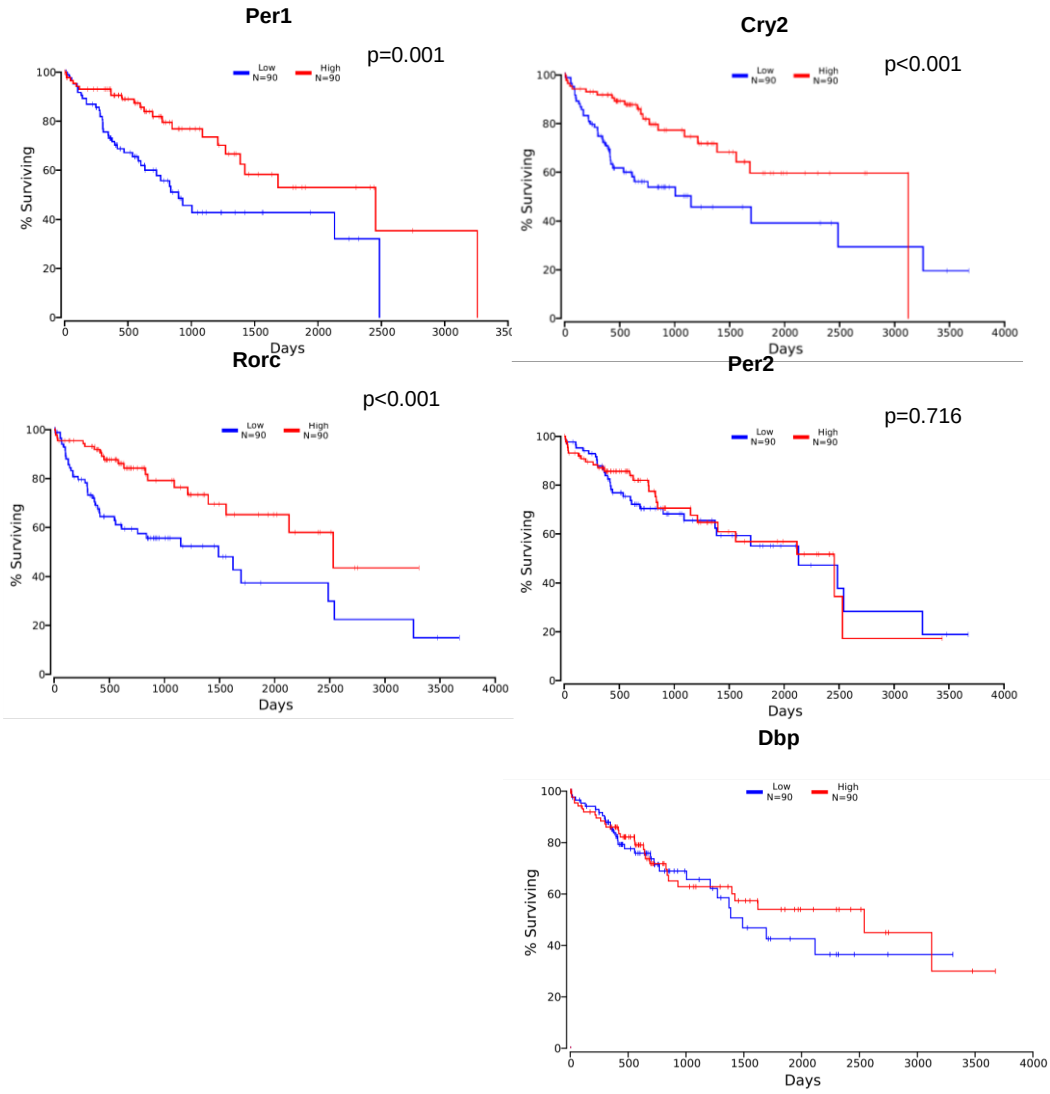

Figure 2.16 Lower expression of clock genes is associated with worse overall survival in human HCC

Association between clock gene expression and overall survival in HCC patients. TCGA-LIHC cohort data were analyzed and Kaplan-Meier plots were generated using OncoLnc; upper and lower quartiles of gene expression were used to determine “high” and “low” expression, respectively.

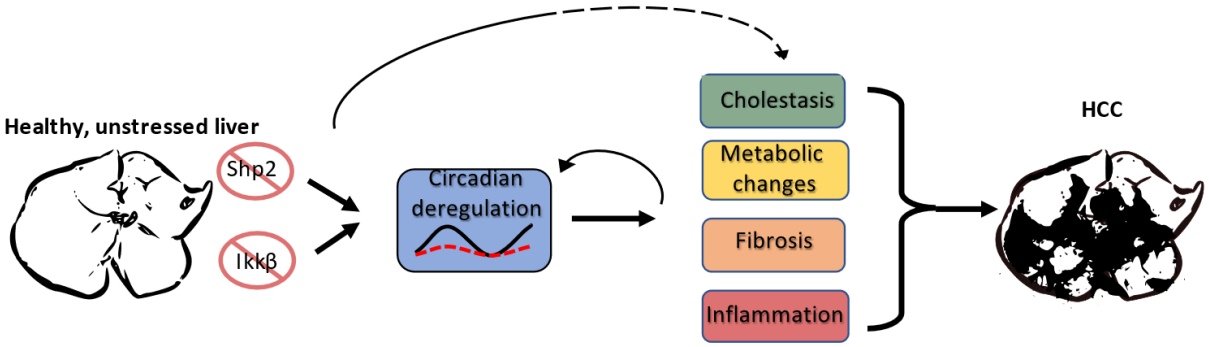

Scheme 2.1. A model to show spontaneous HCC development in the DKO mice.

Dual Shp2 and Ikkβ deletion triggers circadian dysregulation, as well as cholestasis, metabolic changes, fibrosis and inflammation, which are mutually enhancing and create both a tumor-promoting microenvironment and hepatocyte-intrinsic oncogenic changes that eventually result in HCC.

Table 2.1. Transcription factors with target genes positively enriched in indicated genotype comparison.

IKO vs. WT	SKO vs. WT	DKO vs. WT	DKO vs. IKO	DKO vs. SKO
AKNA	ATF3	AHR	AHR	ARNTL
BATF3	ATOH8	ATOH8	ARNTL	BCL6
BCL6	CEBPB	BCL6	ATF5	CENPA
BHLHE41	CPEB1	BCL6B	CEBPE	CLOCK
ELF4	CUX2	CENPT	E2F8	E2F8
ELK3	ELF3	E2F8	ELF3	EGR1
ERG	GATA6	ELF4	FOS	FOXM1
ETS1	KLF16	ELK3	FOSL2	FOXQ1
FLI1	KLF2	ETS1	FOXM1	ID2
FOXF1	KLF4	ETS2	GTF2IRD1	ID3
GLIS2	KLF6	FOXM1	HES1	JUN
HAND2	LHX6	HMGB2	ID3	KLF11
HMGB1	MYBL1	IKZF1	KLF6	NFIL3
ID1	MYC	KLF4	LHX6	NFXL1
IKZF1	NR4A2	KLF6	LITAF	NPAS2
JDP2	OLIG1	LHX6	MYBL1	ONECUT1
KLF2	PBX4	MAF	MYC	RFXANK
KLF6	PPARG	MYBL1	NFIL3	SOX13
LHX2	RELB	MYC	NPAS2	SP5
MAF	SALL1	MYEF2	OLIG1	STAT1
MEIS3	SNAI3	NFE2L2	PPARG	TBX3
NR1H5	SOX12	OLIG1	SOX12	TSC22D1
NR4A1	SOX4	PLEK	SOX4	ZBTB7C
PEG3	TCF24	PPARG	TBX3	ZFP36L1
PLEK	ZBTB44	SOX12	TCF24	ZFP652
POU2F2	ZFP28	SOX4	TSC22D1	ZFP951
RARG	ZFP354A	SPI1	ZBTB16	
SNAI2	ZFP950	TBX2	ZBTB42	
SP100		TBX3	ZFP36L2	
SPI1		TCF24	ZFP385A	
SPIC		TSC22D1		
STAT1		ZBTB42		
TBX2		ZEB2		
TBX20		ZFP334		
TCF21		ZFP385A		
TCF24		ZFP740		
TEAD2				
TFEC				
ZEB2				
ZFP9				

Table 2.2. Transcription factors with target genes negatively enriched in indicated genotype comparison.

IKO VS. WT	SKO VS. WT	DKO VS. WT	DKO VS. IKO	DKO VS. SKO
ARID5A	ARID5B	ARID5B	BACH1	ATF3
ARNTL	ARNTL	BACH1	BACH2	BHLHE40
CEBPE	BACH1	BACH2	BATF3	BHLHE41
FOXA2	BACH2	BHLHE40	BHLHE40	CEBPB
ID2	CLOCK	BHLHE41	BHLHE41	CEBPE
ID3	EGR1	CDIP1	D630045J12RIK	CPEB1
IKZF4	EPAS1	CSRNP1	DBP	CUX2
NFIL3	ETV5	CUX2	EPAS1	DBP
NPAS2	FOXA1	EPAS1	ESRRA	ELF3
NR0B2	FOXA2	ERF	ETV6	ERF
ONECUT1	FOXA3	ESR1	FOXF1	ESRRA
ZBTB16	FOXK1	ESRRA	HAND2	FOXO1
ZFP36L1	FOXP4	FOXA1	HLF	GM14403
ZKSCAN5	FOXQ1	FOXA3	HMGB1	HIVEP2
	GATA4	FOXQ1	HOPX	KLF1
	HHEX	GM14403	IRF2	KLF10
	HMGB1	HES6	IRF5	KLF13
	HNF1A	HLF	IRF7	MAFB
	HOPX	HMGB1	KLF10	MAFF
	ID2	HOPX	KLF13	MAFG
	IKZF4	IKZF4	MAFB	NR1D2
	IRF2	IRF2	MAFF	PBX4
	IRF5	IRF5	MYCL	RORC
	IRF6	IRF7	NFX1	SALL1
	IRF7	KLF1	NR0B2	SNAI3
	IRF9	KLF10	NR1D2	SREBF1
	KLF10	KLF12	NR1H5	TEF
	KLF12	MAFB	NR3C2	TSC22D3
	MLXIPL	MLX	NR4A1	ZFP276
	NCOR2	MLXIPL	POU6F1	ZFP629
	NFIL3	NR0B2	RLF	
	NPAS2	NR3C2	RORC	
	NR0B2	NR4A1	SOX5	
	ONECUT1	ONECUT1	SP140	
	PRDM2	PRDM2	SREBF1	
	RFXANK	RORC	STAT1	

Table 2.2, continued. Transcription factors with target genes negatively enriched in indicated genotype comparison.

IKO VS. WT	SKO VS. WT	DKO VS. WT	DKO VS. IKO	DKO VS. SKO
	SALL2	SOX5	TCF21	
	SOX13	SOX9	TEF	
	SOX9	SREBF1	TSC22D3	
	SREBF1	TEF	TSC22D4	
	STAT1	TSHZ2	TSHZ2	
	TCF7L1	XBP1	ZBTB48	
	THRB	ZBTB16	ZFP146	
	TSC22D4	ZBTB48	ZFP276	
	TSHZ2	ZFP27	ZFP612	
	XBP1	ZFP629	ZFP629	
	ZBTB16	ZKSCAN1	ZKSCAN1	
	ZBTB48	ZKSCAN7		
	ZBTB7C			
	ZFP180			
	ZFP27			
	ZFP36L1			
	ZFP445			
	ZFP513			
	ZFP707			
	ZKSCAN7			

Discussion

A large body of literature supports the critical roles of the Ras/MAPK and IKK/NF-κB signaling pathways in cancer (Karnoub and Weinberg, 2008; Papke and Der, 2017; Simanshu, Dhirendra K., Nissley, Dwight. V., McCormick, 2017; Taniguchi and Karin, 2018). However, it is important to note that these oncogenic functions occur when the pathways are activated constitutively or excessively. The baseline functions of these pathways under physiological conditions are less understood and their functional cross-talk has never been interrogated. Surprisingly, many groups reported that blocking these and other oncogenic pathways in the liver accelerated some models of HCC (Feng, 2012). However, many of these models required a separate initiator and/or driver for HCC, most frequently mutations induced by the carcinogen DEN (Awuah et al., 2012; Bard-Chapeau et al., 2011; Maeda et al., 2005; Takami et al., 2007).

In this study, we characterized a new compound mouse mutant with hepatocyte-specific ablation of both Shp2 and Ikkβ, which suppresses both the Ras/MAPK and IKK/NF-κB signaling pathways. These DKO mice were found to be highly susceptible to carcinogen-induced HCC development, developing a substantial tumor burden well before either single knockout line. More surprisingly, the DKO mice exhibited spontaneous and rapid HCC development without any exogenous challenge. This spontaneous HCC development occurred in a background of liver disease characterized by inflammation, cholestasis, and fibrosis. This suggests that basal levels of these pathways are required to maintain liver health and prevent tumorigenesis.

Shp2- and Ikkβ- mediated signaling work together to prevent liver damage and maintain physiological homeostasis

A major contributing factor to HCC development is a background of progressive liver disease. To understand how dual deletion of Shp2 and Ikkβ might create a tumor-promoting environment, we assessed early changes to liver health. At an early age, the DKO mice developed substantial liver damages, including fibrosis, inflammation, and cholestasis, as well as liver-damage-associated splenomegaly. They also showed varied metabolic disruptions, including lipid and amino acid metabolism, indicating that Shp2- and Ikkβ- mediated signaling networks are required to maintain multiple aspects of liver homeostasis. Despite the lack of severe phenotype of Ikkβ single-knockout mice, additional ablation of Ikkβ drastically increased the mild inflammation and fibrosis seen in Shp2-deficient livers. While the mechanism of these damages is likely multi-factorial, a substantial contributor is the dramatically elevated bile acid levels that occur in the DKO liver. This phenotype reveals a different role for NF-κB signaling in cholestatic liver disease than previous reports, in which NF-κB inhibition did not exacerbate cholestasis-driven hepatitis; instead, a tumor-suppressive role was attributed due to promotion of apoptosis of transformed hepatocytes (Pikarsky et al., 2004). In this model, NF-κB downregulation not only enhanced cholestatic liver disease, but also contributed to a suite of tumor-promoting inflammatory and metabolic processes. Due to the well-established link between clock function, liver metabolism, and bile acid homeostasis, we propose that

both the anti-apoptotic role, as well as the cooperative role in circadian regulation, of NF-κB may contribute to the extensive damage in the DKO liver.

Cooperative regulation of circadian clock function and prevention of hepatocarcinogenesis by Ras/MAPK and NF-κB pathways

Even with a tumor-promoting microenvironment, it was unexpected that hepatocytes lacking activation of NF-κB and Ras/MAPK pathways were able to proliferate and undergo malignant transformation, leading us to investigate which pathway(s) might drive these surprising phenotypes. Assessment of signaling pathway activation in primary hepatocytes confirmed that the activation of most growth-promoting pathways was indeed dampened in DKO hepatocytes. Although increased STAT3 activity was implicated in DEN-induced HCCs accelerated by either Ikkβ or Shp2 deletion from hepatocytes (Bard-Chapeau et al., 2011; He et al., 2010), we did not detect enrichment for STAT3 target genes in untreated livers from either single knockout, nor in DKO livers, suggesting an alternate mechanism of tumorigenesis in this model. While transcriptomic analyses of both whole liver and isolated hepatocytes from DKO mice consistently identified upregulation of pathways related to cell division and proliferation, we were unable to identify positive enrichment for any pathways that might drive the elevated proliferation and tumorigenesis seen in this model.

In contrast, transcriptomic analysis of genes uniquely downregulated in DKO hepatocytes identified severe disruption of core circadian control gene expression as the most prominent feature specific to DKO hepatocytes in 2-month-old mice, several

months prior to HCC appearance. In previous studies, circadian dysregulation due to ablation of clock regulators or effectors was also found sufficient to drive spontaneous HCC development in mice (Kettner et al., 2016). More broadly, disruption of circadian clock function is related with loss of cell cycle control, leading to uncontrolled proliferation and enhanced formation of multiple tumor types (Masri and Sassone-Corsi, 2018). Circadian dysfunction has also been shown to disrupt BA homeostasis (Ma et al., 2009), and aberrant BA production influenced the expression dynamics of clock genes in the liver (Govindarajan et al., 2016). Of note, the BA levels were strikingly high in the DKO liver (Fig. 1.4I). We speculate that BA dysregulation and circadian clock disruption form a mutually enhancing feedback loop (Scheme 2.1). This would then drive excessive hepatocyte proliferation and malignant transformation.

Unexpectedly, the initial trigger in DKO mice leading to this pathogenic downward spiral was the combined suppression of two well established oncogenic signaling pathways, Ras/MAPK and IKK/NF-κB. Thus, this study unveils an indispensable function of these pathways in maintaining circadian homeostasis in hepatocytes. Circadian disruption may explain the surprising finding that these pathways are dispensable for driving proliferation in DKO hepatocytes. In fact, blockade of these pathways, which are viewed as pro-oncogenic, ironically induces tumorigenesis.

Many aspects of liver damages, such as inflammation and fibrosis, displayed largely additive effects in DKO liver relative to IKO and SKO. In contrast, downregulation of circadian genes occurred suddenly and dramatically in the DKO

hepatocytes. Thus, a systemic disorder caused by disruption of an intricate signaling network, rather than disruption of two linear signaling cascades, can result in spontaneous hepatic tumorigenesis, a finding that appears to be consistent with the highly heterogenous nature of HCC-associated oncogenic mutations (Nault et al., 2017).

Relevance to human disease

Epidemiological links of chronic circadian disruption, such as shift work, to increased rates of human cancer, and mechanistic mouse studies further cementing the link between clock disfunction and increased carcinogenesis, lead the IARC to list circadian disruption as a probable carcinogen (Stewart and Wild, 2014). In multiple human cancers, bioinformatic analyses have revealed a link between disruption of a signature of clock genes and poorer prognosis (Liu et al., 2019). Consistent with the mouse results reported here, TCGA data analysis revealed that a similar mechanism of liver tumorigenesis may be at play in human HCC; namely, clock disruption is linked to lower levels of Ras/MAPK and NF-κB activity, as assessed by lower levels of pathway constituents as well as lower target gene expression in patients with abnormal expression of multiple clock genes. In human liver cancer, as in our DKO model, circadian dysfunction was also coupled to higher rates of proliferation and disruption of numerous metabolic processes (Liu et al., 2019), indicating a similar network of signaling changes. Therefore, this mouse model, in which dual Ras/MAPK and NF-κB disruption causes a suite of progressive liver damages, circadian

disfunction, and enhanced proliferation leading to HCC development, may provide insight into human HCC linked to clock disruption.

Future Directions

Circadian disruption was specific to the DKO model, suggesting Ras/MAPK and NF-κB cooperate to regulate the hepatocyte clock. However, the precise mechanism of this regulation is unclear. We have proposed that both direct regulation and microenvironmental effects are at play. Based on previous bidirectional links between circadian disruption and loss of bile acid homeostasis (Govindarajan et al., 2016; Ma et al., 2009), we believe that elevated bile acids in the DKO liver are at least partially caused by initial circadian disruption, and then feed back to cause more profound deregulation of the hepatocyte clock.

Preliminary attempts to test the effect of bile acids on the hepatocyte clock were performed using Bmal::luciferase reporter HCC cell lines, as well as primary hepatocytes, in an attempt to dissociate the microenvironmental vs. hepatocyte-intrinsic processes contributing to clock disruption. However, in our hands, both models failed to maintain the robust circadian oscillations seen *in vivo* over the time course required for our experiments. Therefore, our future inquiries into the mechanism of clock disruption in DKO hepatocytes will be performed *in vivo.*

To uncouple the direct vs. indirect contributors to clock regulation, we will induce acute disruption of Shp2 and Ikkβ from hepatocytes using AAV-Cre in double-floxed mice, and monitor the expression of clock genes at regular intervals by collecting livers every four hours over a 24-hour span. The magnitude of circadian

disruption after gene deletion, but before an inflammatory, cholestatic environment develops, will reflect the extent to which Ras/MAPK and NF-κB pathways directly regulate clock genes**.** We will also use the results of these studies to identify key peak/trough expression times for representative circadian genes in WT and KO livers, and focus on these time points in further analyses. This will allow us to more efficiently probe the details of clock disruption in multiple mutants and under different conditions while minimizing animal use.

To approach the question of direct vs. microenvironmental effects from a different direction, we might attempt to relieve the severity of microenvironmental changes in DKO mice, and repeat liver collections and clock gene measurements at the previously identified key time points. This would be achieved by reducing cholestasis through treatments such as ursodeoxycholic acid (UDCA), which has long been used to treat cholestatic patients (Paumgartner and Beuers, 2002), or a slightly modified molecule, *nor*UDCA, that has been particularly successful in reducing cholestasis in Mdr2-deficient mice (Halilbasic et al., 2009). We may also attempt to neutralize the liver inflammation through antioxidant treatments; however, with the continued presence of elevated bile acid levels, we may not be able to reduce inflammation enough to full detect any putative effects on the hepatocyte clock. With these approaches, relative changes in clock genes in treated vs. untreated DKO mice would then reflect the contribution of that specific environmental factor.

We will investigate why combined disruption of Ras/MAPK and NF-κB appears to be required for clock disruption, when suppression of a single pathway appears to

have little effect. The previously described time course experiments would also include single knockout mice, and may be able to reveal more subtle temporal variations in individual clock gene expression. It may be that each single knockout has a small effect on multiple clock genes, or a moderate (but previously undetected) effect on just one or two genes. Given the robust feedback mechanisms in control of clock rhythmicity, such subtle alterations might be tolerated in a single knockout, with only combined disruption sufficient to disrupt the clock.

Alternatively, as several of the clock genes disrupted in the DKO model are themselves transcription factors, coordinate or redundant regulation of these genes by Ras/MAPK targets and NF-κB could yield a substantial clock disruption only when both pathways are blocked. To investigate this, we will initiate bioinformatic analyses to identify specific TF binding on clock gene regulatory sequences. The presence of motifs for NF-κB transcription factors or Ras/MAPK downstream factors near core clock genes would indicate whether cooperative regulation, or functional regulatory redundancy, is a possibility. If this preliminary bioinformatic approach yields any candidate TFs relevant to either pathway that may bind near clock genes, we can then perform validation studies such as chromatin immunoprecipitation (ChIP). These experiments would help clarify how coordinate disruption of these pathways generates such broad clock gene expression changes.

Changes to the hepatocyte clock have recently been reported to induce rhythmic changes in other liver cell populations (Guan et al., 2020). To investigate whether hepatocyte clock disruption induces systemic circadian dysfunction, we will perform video-aided monitoring of activity levels and compare the level and timing of

peak activity between genotypes. We will also determine whether the circadian disruption in DKO hepatocytes, which is associated with metabolic changes, affects nutritional input. This can be simply achieved by monitoring food consumption by weight. Together, these analyses will reveal whether the hepatocyte clock disruption observed in this model has a wider physiological impact.

This work, and others, have demonstrated a link between circadian disruption and multiple aspects of liver disease, including cholestasis, steatosis, and even HCC. The previous link between disrupted clock function and disease has lead to interest in developing small molecule modulators of the circadian clock (He and Chen, 2016). However, many of these compounds target only a single component of the clock machinery and can have clock-disrupting effects such as period lengthening or shortening rather than maintaining or re-establishing appropriate circadian rhythmicity. Some molecules have shown clock-gene-inducing activity (He and Chen, 2016), but it is unclear if they would be sufficient to rescue profound clock disfunction, such as that seen in the DKO liver.

Time-restricted feeding (in humans, time-restricted eating) has gained attention as an effective weight-loss method (Cienfuegos et al., 2020). This approach, in which nutritional intake is limited to a relatively narrow (usually approximately 6 hour) window, has been shown to robustly entrain the liver clock independent of the SCN (Cienfuegos et al., 2020; Stokkan et al., 2001). Since this nutritional entrainment efficiently re-established circadian oscillation of multiple clock genes, it may be more effective than strategies targeting a single clock constituent.

Methods to re-establish circadian function, such as small-molecule stabilizers or time-restricted eating, may provide therapeutic benefit for liver disease. Based on mouse and human data presented here and elsewhere (Kettner et al., 2016; Liu et al., 2019), it may also provide benefit as an adjunct therapy in HCC cases. The physiological and transcriptional similarities between this DKO model and clock-disrupted human HCC make it an attractive option for preclinical assessment of such approaches.

Concluding remarks

While overactivation of the IKK/NF-κB and Ras/MAPK pathways have long been linked to tumor formation and progression, we demonstrate that, in combination, their basal activities have a potent tumor-suppressive effect. Their coordinate regulation is required for preventing liver damage, maintaining metabolic homeostasis, and controlling circadian function. Suppression of both pathways therefore induces a network of pathological changes that lead to spontaneous liver carcinogenesis. This demonstrates that these pathways have a cooperative role in maintaining liver health and serve as “gatekeepers” in preventing tumor development.

Due to the limited efficacy of monotherapy that targets one oncogenic pathway, it has been suggested that multiple oncogenic pathways need to be blocked to increase the efficacy of targeted cancer therapeutics (Zucman-Rossi et al., 2015). Given the phenotypes of liver damage and enhanced tumorigenesis in DKO mice, combination therapies targeting these oncogenic axes may fail to provide a therapeutic effect and may even worsen tumor progression or promote relapsed

tumor formation. With consideration to the background of severe liver disease in most HCC patients and the accelerated liver damage seen in DKO mice, this dual treatment might also exacerbate underlying liver disease. The data presented here raise a cautionary note regarding combinatorial therapies that cause simultaneous disruption of multiple oncogenic pathways.

References

Ahmed, T.A., Adamopoulos, C., Karoulia, Z., Wu, X., Sachidanandam, R., Aaronson, S.A., and Poulikakos, P.I. (2019). SHP2 Drives Adaptive Resistance to ERK Signaling Inhibition in Molecularly Defined Subsets of ERK-Dependent Tumors. Cell Rep. *26*, 65-78.e5.

Ally, A., Balasundaram, M., Carlsen, R., Chuah, E., Clarke, A., Dhalla, N., Holt, R.A., Jones, S.J.M., Lee, D., Ma, Y., et al. (2017). Comprehensive and Integrative Genomic Characterization of Hepatocellular Carcinoma. Cell *169*, 1327-1341.e23.

Araki, T., Nawa, H., and Neel, B.G. (2003). Tyrosyl Phosphorylation of Shp2 Is Required for Normal ERK Activation in Response to Some, but Not All, Growth Factors. J. Biol. Chem. *278*, 41677–41684.

Awuah, P.K., Rhieu, B.H., Singh, S., Misse, A., and Monga, S.P.S. (2012). β-Catenin loss in hepatocytes promotes hepatocellular cancer after diethylnitrosamine and phenobarbital administration to mice. PLoS One *7*, 1–9.

Bard-Chapeau, E. a., Li, S., Ding, J., Zhang, S.S., Zhu, H.H., Princen, F., Fang, D.D., Han, T., Bailly-Maitre, B., Poli, V., et al. (2011). Ptpn11/Shp2 Acts as a Tumor Suppressor in Hepatocellular Carcinogenesis. Cancer Cell *19*, 629–639.

Bard-Chapeau, E. a, Yuan, J., Droin, N., Long, S., Zhang, E.E., Nguyen, T. V, and Feng, G.-S. (2006). Concerted functions of Gab1 and Shp2 in liver regeneration and hepatoprotection. Mol. Cell. Biol. *26*, 4664–4674.

Bennett, A.M., Tang, T.L., Sugimoto, S., Walsh, C.T., and Neel, B.G. (1994). Protein-tyrosine-phosphatase SHPTP2 couples platelet-derived growth factor receptor β to Ras. Proc. Natl. Acad. Sci. U. S. A. *91*, 7335–7339.

Bos, J.L., Rehmann, H., and Wittinghofer, A. (2007). GEFs and GAPs: Critical Elements in the Control of Small G Proteins (DOI:10.1016/j.cell.2007.05.018). Cell *130*, 385.

Bray, F., Ferlay, J., Soerjomataram, I., Siegel, R.L., Torre, L.A., and Jemal, A. (2018). Global cancer statistics 2018: GLOBOCAN estimates of incidence and mortality worldwide for 36 cancers in 185 countries. CA. Cancer J. Clin. *68*, 394–424.

Bruix, J., Qin, S., Merle, P., Granito, A., Huang, Y.-H., Bodoky, G., Pracht, M., Yokosuka, O., Rosmorduc, O., Breder, V., et al. (2017). Regorafenib for patients with hepatocellular carcinoma who progressed on sorafenib treatment (RESORCE): a randomised, double-blind, placebo-controlled, phase 3 trial. Lancet *389*, 56–66.

Bunda, S., Burrell, K., Heir, P., Zeng, L., Alamsahebpour, A., Kano, Y., Raught, B., Zhang, Z.Y., Zadeh, G., and Ohh, M. (2015). Inhibition of SHP2-mediated dephosphorylation of Ras suppresses oncogenesis. Nat. Commun. *6*.

Chan, R.J., and Feng, G. (2007). PTPN11 is the first identified proto-oncogene that encodes a tyrosine phosphatase. Blood *109*, 862–868.

Cienfuegos, S., Gabel, K., Kalam, F., Ezpeleta, M., Wiseman, E., Pavlou, V., Lin, S., Oliveira, M.L., and Varady, K.A. (2020). Effects of 4- and 6-h Time-Restricted Feeding on Weight and Cardiometabolic Health: A Randomized Controlled Trial in Adults with Obesity. Cell Metab. *32*, 366-378.e3.

Connor, F., Rayner, T.F., Aitken, S.J., Feig, C., Lukk, M., Santoyo-Lopez, J., and Odom, D.T. (2018). Mutational landscape of a chemically-induced mouse model of liver cancer. J. Hepatol. *69*, 840–850.

Cox, A.D., and Der, C.J. (2010). Ras history: The saga continues. Small GTPases *1*, 2–27.

Cunnick, J.M., Mei, L., Doupnik, C.A., and Wu, J. (2001). Phosphotyrosines 627 and 659 of Gab1 Constitute a Bisphosphoryl Tyrosine-based Activation Motif (BTAM) Conferring Binding and Activation of SHP2. J. Biol. Chem. *276*, 24380–24387.

Dance, M., Montagner, A., Salles, J.P., Yart, A., and Raynal, P. (2008). The molecular functions of Shp2 in the Ras/Mitogen-activated protein kinase (ERK1/2) pathway. Cell. Signal. *20*, 453–459.

Das, M., Garlick, D.S., Greiner, D.L., and Davis, R.J. (2011). The role of JNK in the development of hepatocellular carcinoma. Genes Dev. *25*, 634–645.

Dhillon, A.S., Hagan, S., Rath, O., and Kolch, W. (2007). MAP kinase signalling pathways in cancer. Oncogene *26*, 3279–3290.

Dvorak, H.F. (1986). Tumors: wounds that do not heal. Similarities between tumor stroma generation and wound healing. N. Engl. J. Med. *315*, 1650–1659.

Van Dycke, K.C.G., Rodenburg, W., Van Oostrom, C.T.M., Van Kerkhof, L.W.M., Pennings, J.L.A., Roenneberg, T., Van Steeg, H., and Van Der Horst, G.T.J. (2015). Chronically Alternating Light Cycles Increase Breast Cancer Risk in Mice. Curr. Biol. *25*, 1932–1937.

Ehlken, H., Kondylis, V., Heinrichsdorff, J., Ochoa-Callejero, L., Roskams, T., and Pasparakis, M. (2011). Hepatocyte IKK2 protects Mdr2 -/- mice from chronic liver failure. PLoS One *6*.

Feng, G.S. (2012). Conflicting Roles of Molecules in Hepatocarcinogenesis:

Paradigm or Paradox. Cancer Cell *21*, 150–154.

Furcht, C.M., Buonato, J.M., and Lazzara, M.J. (2015). EGFR-activated Src family kinases maintain GAB1-SHP2 complexes distal from EGFR. Sci. Signal. *8*, 1–13.

Govindarajan, K., MacSharry, J., Casey, P.G., Shanahan, F., Joyce, S.A., and Gahan, C.G.M. (2016). Unconjugated bile acids influence expression of circadian genes: A potential mechanism for microbe-host crosstalk. PLoS One *11*, 1–13.

Greten, F.R., Eckmann, L., Greten, T.F., Park, J.M., Li, Z.W., Egan, L.J., Kagnoff, M.F., and Karin, M. (2004). IKKβ links inflammation and tumorigenesis in a mouse model of colitis-associated cancer. Cell *118*, 285–296.

Gu, H., and Neel, B.G. (2003). The “Gab” in signal transduction. Trends Cell Biol. *13*, 122–130.

Guan, D., Xiong, Y., Trinh, T.M., Xiao, Y., Hu, W., Jiang, C., Dierickx, P., Jang, C., Rabinowitz, J.D., and Lazar, M.A. (2020). The hepatocyte clock and feeding control chronophysiology of multiple liver cell types. Science (80-.). eaba8984.

Hadadi, E., Taylor, W., Li, X.M., Aslan, Y., Villote, M., Rivière, J., Duvallet, G., Auriau, C., Dulong, S., Raymond-Letron, I., et al. (2020). Chronic circadian disruption modulates breast cancer stemness and immune microenvironment to drive metastasis in mice. Nat. Commun. *11*, 1–17.

Halilbasic, E., Fiorotto, R., Fickert, P., Marschall, H.U., Moustafa, T., Spirli, C., Fuchsbichler, A., Gumhold, J., Silbert, D., Zatloukal, K., et al. (2009). Side chain structure determines unique physiologic and therapeutic properties of norUrsodeoxycholic acid in Mdr2-/-mice. Hepatology *49*, 1972–1981.

Hanafusa, H., Torii, S., Yasunaga, T., and Nishida, E. (2002). Sprouty1 and Sprouty2 provide a control mechanism for the Ras/MAPK signalling pathway. Nat. Cell Biol. *4*, 850–858.

Hanafusa, H., Torii, S., Yasunaga, T., Matsumoto, K., and Nishida, E. (2004). Shp2, an SH2-containing protein-tyrosine phosphatase, positively regulates receptor tyrosine kinase signaling by dephosphorylating and inactivating the inhibitor sprouty. J. Biol. Chem. *279*, 22992–22995.

Hanahan, D., and Weinberg, R. a. (2011). Hallmarks of cancer: The next generation. Cell *144*, 646–674.

Hanahan, D., and Weinberg, R.A. (2000). The Hallmarks of Cancer. *100*, 57–70.

Hayden, M.S., and Ghosh, S. (2012). NF-κB, the first quarter-century: Remarkable

progress and outstanding questions. Genes Dev. *26*, 203–234.

He, B., and Chen, Z. (2016). Molecular Targets for Small-Molecule Modulators of Circadian Clocks. Curr. Drug Metab. *17*, 503–512.

He, G., and Karin, M. (2011). NF-κB and STAT3- key players in liver inflammation and cancer. Cell Res. *21*, 159–168.

He, G., Yu, G.Y., Temkin, V., Ogata, H., Kuntzen, C., Sakurai, T., Sieghart, W., Peck-Radosavljevic, M., Leffert, H.L., and Karin, M. (2010). Hepatocyte IKKβ/NF-κB Inhibits Tumor Promotion and Progression by Preventing Oxidative Stress-Driven STAT3 Activation. Cancer Cell *17*, 286–297.

Hoesel, B., and Schmid, J.A. (2013). The complexity of NF-kB signaling in inflammation and cancer. Mol. Cancer *12*, 1–15.

Huang, Y., Wang, J., Cao, F., Jiang, H., Li, A., Li, J., Qiu, L., Shen, H., Chang, W., Zhou, C., et al. (2017). SHP2 associates with nuclear localization of STAT3: Significance in progression and prognosis of colorectal cancer. Sci. Rep. *7*, 1–10.

Karnoub, A.E., and Weinberg, R.A. (2008). Ras oncogenes: Split personalities. Nat. Rev. Mol. Cell Biol. *9*, 517–531.

Kawamoto, T., Noshiro, M., Sato, F., Maemura, K., Takeda, N., Nagai, R., Iwata, T., Fujimoto, K., Furukawa, M., Miyazaki, K., et al. (2004). A novel autofeedback loop of Dec1 transcription involved in circadian rhythm regulation. Biochem. Biophys. Res. Commun. *313*, 117–124.

Kettner, N.M., Voicu, H., Finegold, M.J., Coarfa, C., Sreekumar, A., Putluri, N., Katchy, C.A., Lee, C., Moore, D.D., and Fu, L. (2016). Circadian Homeostasis of Liver Metabolism Suppresses Hepatocarcinogenesis. Cancer Cell *30*, 909–924.

Koch, C.A., Anderson, D., Moran, M.F., Ellis, C., and Pawson, T. (1991). SH2 and SH3 domains: Elements that control interactions of cytoplasmic signaling proteins. Science (80-.). *252*, 668–674.

Koch, K.S., Maeda, S., He, G., Karin, M., and Leffert, H.L. (2009). Targeted deletion of hepatocyte Ikkβ confers growth advantages. Biochem. Biophys. Res. Commun. *380*, 349–354.

Kulik, L., and El-Serag, H.B. (2019). Epidemiology and Management of Hepatocellular Carcinoma. Gastroenterology *156*, 477–491.

Lamarche, M.J., Chan, H.M., Fekkes, P., Garcia-fortanet, J., Acker, M.G., Antonakos, B., Chen, C.H., Chen, Z., Cooke, V.G., Dobson, J.R., et al. (2016). Allosteric

inhibition of SHP2 phosphatase inhibits cancers driven by receptor tyrosine kinases. Nature *535*, 148–152.

Li, S., Hsu, D.D.F., Li, B., Luo, X., Alderson, N., Qiao, L., Ma, L., Zhu, H.H., He, Z., Suino-Powell, K., et al. (2014). Cytoplasmic tyrosine phosphatase shp2 coordinates hepatic regulation of bile acid and FGF15/19 signaling to repress bile acid synthesis. Cell Metab. *20*, 320–332.

Liu, J.J., Li, Y., Chen, W.S., Liang, Y., Wang, G., Zong, M., Kaneko, K., Xu, R., Karin, M., and Feng, G.-S. (2018). Shp2 Deletion in Hepatocytes Suppresses Hepatocarcinogenesis Driven by Oncogenic β-Catenin, PIK3CA and MET. J. Hepatol. *69*, 79–88.

Liu, T., Zhang, L., Joo, D., and Sun, S.C. (2017). NF-κB signaling in inflammation. Signal Transduct. Target. Ther. *2*.

Liu, Z., Yu, K., Zheng, J., Lin, H., Zhao, Q., Zhang, X., Feng, W., Wang, L., Xu, J., Xie, D., et al. (2019). Dysregulation, functional implications, and prognostic ability of the circadian clock across cancers. Cancer Med.

Llovet, J.M., Ricci, S., Mazzaferro, V., Hilgard, P., Gane, E., Blanc, J., Oliveira, A.C. De, Santoro, A., Raoul, J., Forner, A., et al. (2008). Sorafenib in Advanced Hepatocellular Carcinoma. N. Engl. J. Med. *359*, 378–390.

Luedde, T., Beraza, N., Kotsikoris, V., van Loo, G., Nenci, A., De Vos, R., Roskams, T., Trautwein, C., and Pasparakis, M. (2007). Deletion of NEMO/IKKγ in Liver Parenchymal Cells Causes Steatohepatitis and Hepatocellular Carcinoma. Cancer Cell *11*, 119–132.

Luedde, T., Heinrichsdorff, J., De Lorenzi, R., De Vos, R., Roskams, T., and Pasparakis, M. (2008). IKK1 and IKK2 cooperate to maintain bile duct integrity in the liver. Proc. Natl. Acad. Sci. U. S. A. *105*, 9733–9738.

Luo, J.L., Maeda, S., Hsu, L.C., Yagita, H., and Karin, M. (2004). Inhibition of NF-κB in cancer cells converts inflammation- induced tumor growth mediated by TNFα to TRAIL-mediated tumor regression. Cancer Cell *6*, 297–305.

Luo, X., Liao, R., Hanley, K.L., Zhu, H.H., Malo, K.N., Hernandez, C., Wei, X., Varki, N.M., Alderson, N., Chu, C., et al. (2016). Dual Shp2 and Pten Deficiencies Promote Non-alcoholic Steatohepatitis and Genesis of Liver Tumor-Initiating Cells. Cell Rep. *17*, 2979–2993.

Ma, K., Xiao, R., Tseng, H.T., Shan, L., Fu, L., and Moore, D.D. (2009). Circadian dysregulation disrupts bile acid homeostasis. PLoS One *4*.

Maeda, S., Kamata, H., Luo, J.L., Leffert, H., and Karin, M. (2005). IKKβ couples hepatocyte death to cytokine-driven compensatory proliferation that promotes

chemical hepatocarcinogenesis. Cell *121*, 977–990.

Marbach-Breitrück, E., Matz-Soja, M., Abraham, U., Schmidt-Heck, W., Sales, S., Rennert, C., Kern, M., Aleithe, S., Spormann, L., Thiel, C., et al. (2019). Tick-tock hedgehog-mutual crosstalk with liver circadian clock promotes liver steatosis. J. Hepatol. *70*, 1192–1202.

Masri, S., and Sassone-Corsi, P. (2018). The emerging link between cancer, metabolism, and circadian rhythms. Nat. Med. *24*, 1795–1803.

Matsuo, T., Yamaguchi, S., Mitsui, S., Emi, A., Shimoda, F., and Okamura, H. (2003). Control mechanism of the circadian clock for timing of cell division in vivo. Science (80-.). *302*, 255–259.

Meylan, E., Dooley, A.L., Feldser, D.M., Shen, L., Turk, E., Ouyang, C., and Jacks, T. (2009). Requirement for NF-B signalling in a mouse model of lung adenocarcinoma. Nature *462*, 104–107.

Miller, B.H., McDearmon, E.L., Panda, S., Hayes, K.R., Zhang, J., Andrews, J.L., Antoch, M.P., Walker, J.R., Esser, K.A., Hogenesch, J.B., et al. (2007). Circadian and CLOCK-controlled regulation of the mouse transcriptome and cell proliferation. Proc. Natl. Acad. Sci. U. S. A. *104*, 3342–3347.

Montagner, A., Yart, A., Dance, M., Perret, B., Salles, J.P., and Raynal, P. (2005). A novel role for Gab1 and SHP2 in epidermal growth factor-induced Ras activation. J. Biol. Chem. *280*, 5350–5360.

Nault, J.C., Paradis, V., Cherqui, D., Vilgrain, V., and Zucman-Rossi, J. (2017). Molecular classification of hepatocellular adenoma in clinical practice. J. Hepatol. *67*, 1074–1083.

Ohtani, T., Ishihara, K., Atsumi, T., Nishida, K., Kaneko, Y., Miyata, T., Itoh, S., Narimatsu, M., Maeda, H., Fukada, T., et al. (2000). Dissection of signaling cascades through gp130 in vivo: Reciprocal roles for STAT3- and SHP2-mediated signals in immune responses. Immunity *12*, 95–105.

Panda, S., Antoch, M.P., Miller, B.H., Su, A.I., Schook, A.B., Straume, M., Schultz, P.G., Kay, S.A., Takahashi, J.S., and Hogenesch, J.B. (2002). Coordinated transcription of key pathways in the mouse by the circadian clock. Cell *109*, 307–320.

Papke, B., and Der, C.J. (2017). Drugging RAS: Know the enemy. Science (80-.). *355*, 1158–1163.

Paumgartner, G., and Beuers, U. (2002). Ursodeoxycholic acid in cholestatic liver disease: Mechanisms of action and therapeutic use revisited. Hepatology *36*, 525–531.

Pawson, T. (1995). Protein modules and signalling networks. Nature *373*, 573–580.

Pikarsky, E., Porat, R.M., Stein, I., Abramovitch, R., Amit, S., Kasem, S., Gutkovich-Pyest, E., Urieli-Shoval, S., Galun, E., and Ben-Neriah, Y. (2004). NF-kappaB functions as a tumour promoter in inflammation-associated cancer. Nature *431*, 461–466.

Qu, C.K., Yu, W.M., Azzarelli, B., and Feng, G.S. (1999). Genetic evidence that Shp-2 tyrosine phosphatase is a signal enhancer of the epidermal growth factor receptor in mammals. Proc. Natl. Acad. Sci. U. S. A. *96*, 8528–8533.

Ruess, D.A., Heynen, G.J., Ciecielski, K.J., Ai, J., Berninger, A., Kabacaoglu, D., Görgülü, K., Dantes, Z., Wörmann, S.M., Diakopoulos, K.N., et al. (2018). Mutant KRAS-driven cancers depend on PTPN11/SHP2 phosphatase. Nat. Med. *24*, 954–960.

Sen, R., and Baltimore, D. (1986). Multiple nuclear factors interact with the immunoglobulin enhancer sequences. Cell *46*, 705–716.

Simanshu, Dhirendra K., Nissley, Dwight. V., McCormick, F. (2017). RAS Proteins and Their Regulators in Human Disease. Cell *170*, 17–33.

Slattery, M.L., Mullany, L.E., Sakoda, L., Samowitz, W.S., Wolff, R.K., Stevens, J.R., and Herrick, J.S. (2018). The NF-κB signalling pathway in colorectal cancer: associations between dysregulated gene and miRNA expression. J. Cancer Res. Clin. Oncol. *144*, 269–283.

Stewart, B.W., and Wild, C.P. (2014). IARC World Cancer Report 2014.

Stokkan, K.A., Yamazaki, S., Tei, H., Sakaki, Y., and Menaker, M. (2001). Entrainment of the circadian clock in the liver by feeding. Science (80-.). *291*, 490–493.

Sun, S. (2012). The noncanonical NF-kB pathway. Immunol. Rev. *246*, 125–140.

Tahara, Y., and Shibata, S. (2016). Circadian rhythms of liver physiology and disease: Experimental and clinical evidence. Nat. Rev. Gastroenterol. Hepatol. *13*, 217–226.

Takahashi, J.S. (2017). Transcriptional architecture of the mammalian circadian clock. Nat. Rev. Genet. *18*, 164–179.

Takami, T., Kaposi-Novak, P., Uchida, K., Gomez-Quiroz, L.E., Conner, E.A., Factor, V.M., and Thorgeirsson, S.S. (2007). Loss of hepatocyte growth factor/c-Met signaling pathway accelerates early stages of N-nitrosodiethylamine-induced hepatocarcinogenesis. Cancer Res. *67*, 9844–9851.

Tang, X., Liu, D., Shishodia, S., Ozburn, N., Behrens, C., Lee, J.J., Waun, K.H., Aggarwal, B.B., and Wistuba, I.I. (2006). Nuclear factor-κB (NF-κB) is frequently expressed in lung cancer and preneoplastic lesions. Cancer *107*, 2637–2646.

Taniguchi, K., and Karin, M. (2018). NF-B, inflammation, immunity and cancer: Coming of age. Nat. Rev. Immunol. *18*, 309–324.

Tartaglia, M., Mehler, E.L., Goldberg, R., Zampino, G., Brunner, H.G., Kremer, H., Van der Burgt, I., Crosby, A.H., Ion, A., Jeffery, S., et al. (2001). Mutations in PTPN11, encoding the protein tyrosine phosphatase SHP-2, cause Noonan syndrome. Nat. Genet. *29*, 465–468.

Tartaglia, M., Niemeyer, C.M., Song, X., Buechner, J., Jung, A., Hählen, K., Hasle, H., Licht, J.D., and Gelb, B.D. (2003). Somatic mutations in PTPN11 in juvenile myelomonocytic leukemia, myelodysplastic syndromes and acute myeloid leukemia. Nat. Genet. *34*, 148–151.

Vallabhapurapu, S., and Karin, M. (2009). Regulation and function of NF-κB transcription factors in the immune system. Annu. Rev. Immunol. *27*, 693–733.

Wang, E., Yeh, S.S.-H., Tsai, T.-F.T., Huang, H.-P.H., Jeng, Y.-M.Y., Lin, W.-H.W., Chen, W.-C., Yeh, K.-H., Chen, P.-J., and Chen, D.-S. (2011). Depletion of beta -catenin from mature hepatocytes of mice promotes expansion of hepatic progenitor cells and tumor development. Proc. Natl. Acad. Sci. *108*, 18384–18389.

Wang, Q., Yu, W., Chen, X., Birnbaum, M.J., Guzman, G., Wang, Q., Yu, W., Chen, X., Peng, X., Jeon, S., et al. (2016). Spontaneous Hepatocellular Carcinoma after the Combined Deletion of Akt Isoforms. Cancer Cell *29*, 523–535.

Wang, W., Abbruzzese, J.L., Evans, D.B., Larry, L., Cleary, K.R., and Chiao, P.J. (1999). The nuclear factor-κB RelA transcription factor is constitutively activated in human pancreatic adenocarcinoma cells. Clin. Cancer Res. *5*, 119–127.

Zhang, X.F., Tan, X., Zeng, G., Misse, A., Singh, S., Kim, Y., Klaunig, J.E., and Monga, S.P.S. (2010). Conditional β-catenin loss in mice promotes chemical hepatocarcinogenesis: Role of oxidative stress and platelet-derived growth factor receptor α/phosphoinositide 3-kinase signaling. Hepatology *52*, 954–965.

Zhu, H.H., Luo, X., Zhang, K., Cui, J., Zhao, H., Ji, Z., Zhou, Z., Yao, J., Zeng, L., Ji, K., et al. (2015). Shp2 and Pten have antagonistic roles in myeloproliferation but cooperate to promote erythropoiesis in mammals. Proc. Natl. Acad. Sci. U. S. A. *112*, 13342–13347.

Zucman-Rossi, J., Villanueva, A., Nault, J.C., and Llovet, J.M. (2015). Genetic Landscape and Biomarkers of Hepatocellular Carcinoma. Gastroenterology *149*, 1226-1239.e4.